An intramolecular bivalent degrader glues an intrinsic BRD4-DCAF16 interaction

Oliver Hsia[1,8], Matthias Hinterndorfer[2,8], Angus D. Cowan[1,8], Kentaro Iso[1,3], Tasuku Ishida[3], Ramasubramanian Sundaramoorthy[4], Mark A. Nakasone[1], Andrea Rukavina[2], Koraljka Husnjak[5], Martin Wegner[5], Alejandro Correa-Sáez[1], Conner Craigon[1], Chiara Maniaci [1,6], Andrea Testa[1,7], Manuel Kaulich[5], Ivan Dikic[5], Georg E. Winter[2#] and Alessio Ciulli[1#]

Affiliations

[1] Centre for Targeted Protein Degradation, School of Life Sciences, University of Dundee, Dundee, UK

[2] CeMM Research Center for Molecular Medicine of the Austrian Academy of Sciences, 1090 Vienna, Austria

[3] Tsukuba Research Laboratory, Eisai Co., Ltd., Ibaraki, Japan

[4] Centre for Gene Regulation and Expression, School of Life Sciences, University of Dundee, Dundee, UK

[5] Institute of Biochemistry II, Faculty of Medicine, Goethe University Frankfurt, D-60590 Frankfurt am Main, Germany

[6] Present address: Medical Research Council (MRC) Protein Phosphorylation and Ubiquitylation Unit, School of Life Sciences, University of Dundee, Dundee, UK

[7] Present address: Amphista Therapeutics Ltd., Granta Park, Cambridge, UK

[8] These authors contributed equally

[#]correspondence to gwinter@cemm.oeaw.ac.at and a.ciulli@dundee.ac.uk

Abstract

Targeted protein degradation is a drug modality represented by compounds that recruit a target to an E3 ubiquitin ligase to promote target ubiquitination and proteasomal degradation. Historically, the field distinguishes monovalent degraders from bifunctional degraders (PROTACs) that connect target and ligase via separate binding ligands joined via a linker[1-4]. Here, we elucidate the mechanism of action of a PROTAC-like degrader of the transcriptional coactivator BRD4, composed of a BRD4 ligand linked to a ligand for the E3 ligase $CRL4^{DCAF15}$. Using orthogonal CRISPR/Cas9 screens we identify the degrader activity is independent of DCAF15, and relies on a different CRL4 substrate receptor, DCAF16. We demonstrate an intrinsic affinity between BRD4 and DCAF16, which is dependent on the tandem bromodomains of BRD4 and further increased by the degrader without physically engaging DCAF16 in isolation. Structural characterization of the resulting ternary complex reveals both BRD4 bromodomains are bivalently engaged in cis by the degrader and are bound to DCAF16 through several interfacial BRD4-DCAF16 and degrader-DCAF16

contacts. Our findings demonstrate that intramolecularly bridging domains can confer glue-type stabilization of intrinsic target-E3 interactions, and we propose this as a general strategy to modulate the surface topology of target proteins to nucleate co-opting of E3 ligases or other cellular effector proteins for effective proximity-based pharmacology.

Main

Sulfonamide-based PROTACs degrade BRD4 independently of DCAF15

The cullin-4 RING ligase (CRL4) substrate receptor DCAF15 is responsible for the pharmacologic degradation of the mRNA splice factor RBM39 induced by the aryl sulfonamide molecular glues indisulam and E7820[5-9]. Efforts to leverage aryl sulfonamides as E3 binding ligands for PROTACs, however, have so far met with limited success[10-12]. We designed a heterobifunctional degrader harbouring an indisulam warhead linked to the BET bromodomain inhibitor JQ1 to target BRD4, a protein that is particularly amendable to degradation[13], and similarly failed to induce measurable BRD4 degradation (Extended Data Fig. 1a, b). However, a recent patent filing described PROTAC-like degraders consisting of the same BET bromodomain ligand tethered to E7820 with compound **1** (**1**; Fig. 1a) reported a potent BRD4 degrader (DC_{50} = 0.15 nM) showing pronounced growth inhibition in various cancer cell lines[14]. We synthesized **1** alongside an analogue with a chloro-substitution at the 3-position of the indole ring, as present in indisulam (compound **2**; Extended Data Fig. 1c) and assessed their BET protein degradation activities in HEK293 and HCT-116 cells. We observed potent BRD4 and BRD2 degradation (Fig. 1b, Extended Data Fig. 1d) and cytotoxicity (Extended Data Fig. 1e), with **2** exhibiting lower potency overall. We further found that the proteasome inhibitor MG132 and the neddylation inhibitor MLN4924 efficiently blocked degradation activity (Extended Data Fig. 1f, g), while MLN4924 treatment also prevented in-cell BRD4 ubiquitination (Fig. 1c). Therefore, **1** and **2** work via proteasomal degradation likely involving a cullin-RING ligase. In addition, competition with an excess concentration of JQ1 prevented BRD4 ubiquitination and degradation, showing that **1** engages BRD4 via its BET bromodomain ligand (Fig. 1c, Extended Data Fig. 1f). Surprisingly, similar competition experiments with the sulfonamide warhead E7820 failed to rescue BRD4 ubiquitination by compound **1** (Fig. 1c). Moreover, BRD4/BRD2 degradation in HCT-116 was unaffected by DCAF15 knockout or knockdown (Fig. 1d, Extended Data Fig. 1h-j), thus suggesting an unexpected DCAF15-independent mode of degradation.

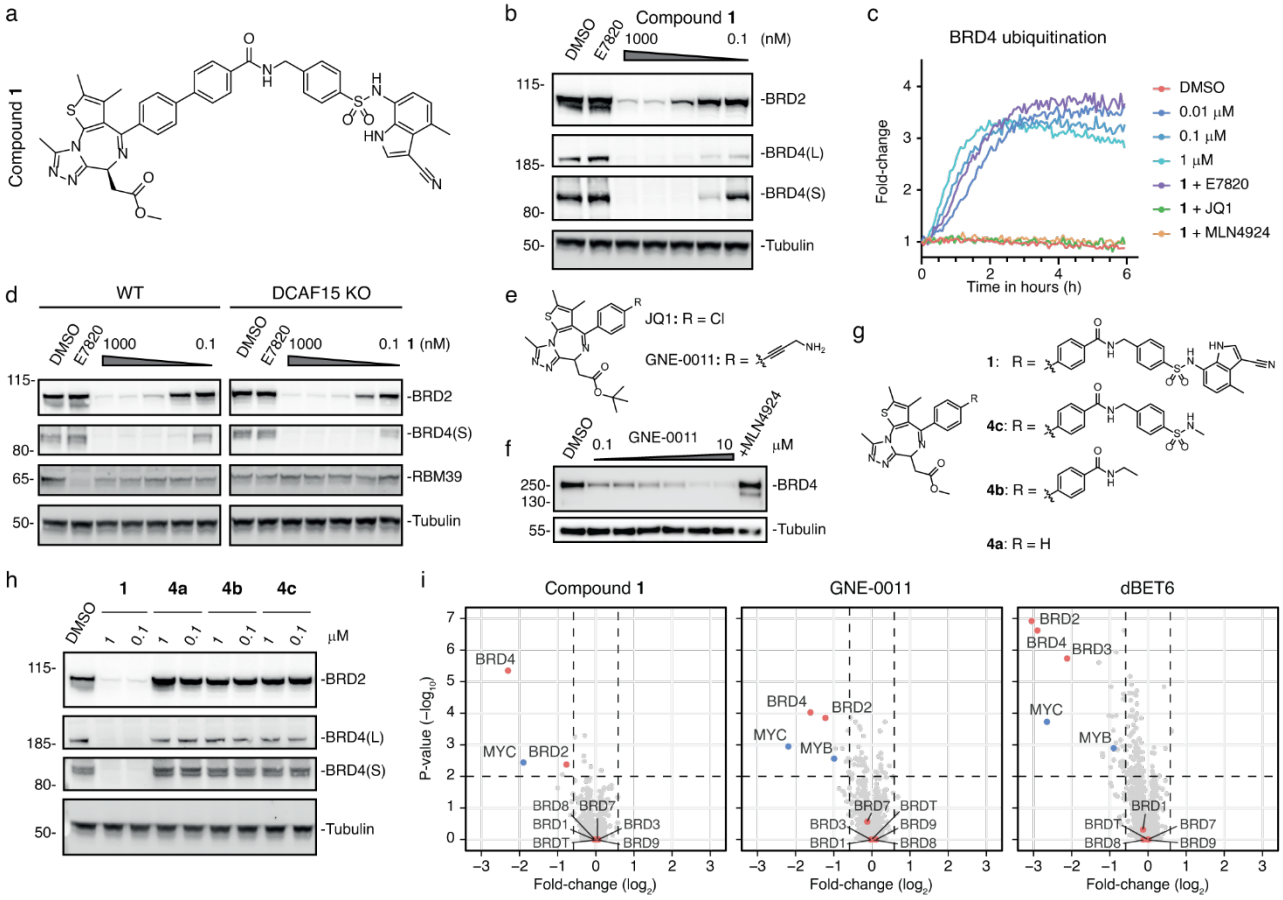

Fig. 1: Compound 1 and GNE-0011 degrade BDR2 and BRD4 independent of DCAF15.
a, Structure of sulfonamide-based PROTAC compound **1**. **b**, BET protein degradation activity of compound **1**. HEK293 cells were treated for 6 hours with DMSO, E7820 (1000 nM) or increasing concentrations of compound **1** and BET protein levels were assessed via immunoblot. Western blot representative of n = 3 independent experiments. **c**, NanoBRET kinetic ubiquitination assay. LgBiT-transfected HiBiT-BromoTag-BRD4 knock-in HEK293 cells were treated with compound **1** at indicated concentrations or at 10 nM following 1-hour pre-treatment with JQ1, E7820 (both 10 μM) or MLN4924 (1 μM). n = 4 biological repeats. **d**, DCAF15 independent protein degradation. HCT-116 WT and DCAF15 KO cells were treated with increasing concentrations of compound **1** for 6 h and BET protein levels were assessed via immunoblot. Western blots representative of n = 3 independent experiments. **e**, **f**, Structure (**e**) and degradation activity (**f**) of GNE-0011. KBM7 cells were treated for 16 h with the indicated concentrations of GNE-0011, with or without 30-min pre-treatment with MLN4924 (1μM), and BRD4 levels were assessed via immunoblot. **g**, **h**, Structures (**g**) and degradation activities (**h**) of compound **1** and truncations **4a-c**. HCT-116 were cells treated with the indicated compounds for 6 h. Western blot representative of n = 2 independent repeats. **i**, Whole proteome changes after compound treatment. Quantitative proteomics in KBM7 cells was performed after 6-hour treatment with DMSO, compound **1** (1 nM), GNE-0011 (1 μM), or dBET6 (10 nM). Volcano plots show fold-change and significance compared to DMSO. Data shown for n = 3 biological replicates.

Compound 1 and GNE-0011 are similar yet different BET degraders

Given this apparent DCAF15-independence, we next focused on testing the relevance of the sulfonamide warhead of **1** for its activity. We first synthesized a series of sulfonamide containing truncations that all lacked the BRD4-binding JQ1 warhead (compounds **3a-d**;

Extended Data Fig. 2a). Co-treatment of HCT-116 cells with an excess of E7820 or **3a-d** did not prevent BRD4 degradation by **1** (Extended Data Fig. 2b), indicating that the sulfonamide moiety is not required for the recruitment of an E3 ligase in a PROTAC-like manner. We therefore wondered whether JQ1, with some minor chemical modifications, may be sufficient to promote degradation. Interestingly, a recent patent filing[15,16] reported the monovalent BRD4 degrader GNE-0011, a JQ1-based compound with a propargylamine tail extending from the *para*-position of the phenyl ring (Fig. 1d, e). Based on its DCAF15-independent and apparent monovalent mode-of-action, we hypothesized that **1** may degrade BRD4 in a GNE-0011 like manner independently of its E7820 warhead. To test this hypothesis, we synthesized a series of compound **1** fragments (compounds **4a-c)**, harbouring progressively larger truncations of the sulfonamide warhead (Fig. 1g), however, none of these truncations promoted BRD4 degradation despite efficiently binding to BRD4 (Fig. 1h, Extended Data Fig. 1k). Together, these data indicate that the sulfonamide warhead of **1** is required for BRD4 degradation, but in a role independent of DCAF15 recruitment, a notion that would be consistent with a potential GNE-0011-like, monovalent mode of action.

Further supporting mechanistic similarity of both compounds, quantitative proteomics via isobaric tagging as well as in-cell HiBiT degradation assays revealed that **1** and GNE-0011 share the same specificity for BRD4 and BRD2, while BRD3 and other bromodomain-containing proteins are not degraded (Fig. 1i, Extended Data Fig. 1l). This specificity for BRD4/2 over BRD3 contrasts most other BET degraders[13], including the PROTAC dBET6[17], which equally degrade BRD2, BRD3 and BRD4 (Fig. 1i). This unique, shared target specificity as well as common dependency on proteasome activity and neddylation therefore suggested that despite their chemical differences, **1** and GNE-0011 might functionally converge on a shared mechanism of action, possibly involving the same cellular machinery.

Compound 1 and GNE-0011 recruit $CRL4^{DCAF16}$ for the degradation of BRD4

To systematically identify the factors involved in the degradation activity of compound **1** and GNE-0011, we set up a time-resolved, FACS-based CRISPR/Cas9 screen (Fig. 2a). We engineered a dual fluorescence BRD4 protein stability reporter, consisting of a BRD4-mTagBFP fusion and mCherry for normalization. We expressed this reporter in KBM7 cells harbouring a doxycycline (DOX) inducible Cas9 allele[18], transduced this cell line with a CRL-focused pooled sgRNA library[19] and induced Cas9 expression with DOX. We then triggered BRD4 degradation via treatment with **1**, GNE-0011 or MZ1[20] and used FACS to isolate cells with elevated ($BRD4^{HIGH}$) or decreased ($BRD4^{LOW}$) BRD4-BFP levels. In the DMSO control screen, we found 20S proteasome subunits, the COP9 signalosome, as well as the $CRL3^{SPOP}$ complex to potently regulate BRD4 stability, recapitulating the known endogenous BRD4 turnover machinery[21,22] (Fig. 2b). For MZ1, we identified subunits of the $CRL2^{VHL}$ complex, including the CUL2 backbone, the adapters ELOB and ELOC, and the substrate receptor VHL, consistent with the known engagement of VHL by MZ1[20,23,24] (Extended Data Fig. 3a). This confirmed that our time-resolved screens can identify genes required for steady-state as well as induced BRD4 degradation, independent of gene essentiality. Next, we focused on the genes required for BRD4 degradation by **1** and GNE-0011. In line with our previous observations, our screens found both compounds to work independent of DCAF15. Instead, we identified members of the $CRL4^{DCAF16}$ complex,

notably the CUL4A backbone, the adapters DDB1 and RBX1, as well as the substrate receptor DCAF16, to be required for BRD4 degradation by **1** and GNE-0011 (Fig. 2b). We additionally identified DCAF16 alongside the CUL4 associated ubiquitin-conjugating enzyme UBE2G1[25,26] as the top hits mediating resistance to compound **1** treatment in an orthogonal viability-based CRISPR screen (Fig. 2c).

In validation assays in KBM7 and HCT-116 cells, CRISPR-based knockout and siRNA-mediated knockdown of $CRL4^{DCAF16}$ complex members prevented degradation of BRD4-BFP as well as endogenous BRD2 and BRD4 by **1** and GNE-0011, (Fig. 2d, Extended Data Fig. 3b-f), while ectopic expression of sgRNA resistant DCAF16 in DCAF16 knockout cells restored degradation (Fig. 2e, Extended Data Fig. 3g). Finally, knockout of DCAF16 led to enhanced tolerance of KBM7 cells to **1** (67-fold IC_{50} increase) and GNE-0011 (4-fold IC_{50} increase), while DCAF16 perturbations did not affect degradation activity or cytotoxicity of dBET6 (Fig. 2d, f). Together, these data identify and validate the $CRL4^{DCAF16}$ complex as key factor for compound **1** and GNE-0011-mediated BET protein degradation and toxicity.

The shared dependence of **1** and GNE-0011 on DCAF16 was particularly intriguing because the indole-sulfonamide portion of **1** was strictly required for its degradation activity (Fig. 1g, h), while such a moiety is absent from GNE-0011. We therefore more closely interrogated the role of the compound **1** sulfonamide warhead. As expected, we observed dose-dependent binding of a FITC-labelled E7820 probe to recombinant DCAF15 (Fig. 2g), recapitulating the known interaction of E7820 with DCAF15[9]. In contrast, this probe showed no binding to DCAF16, demonstrating the lack of affinity between E7820 and DCAF16 and suggesting that **1** does not directly engage DCAF16 via its E7820 warhead. Instead, this moiety might be involved in coordinating the formation of a ternary complex with BRD4 and DCAF16, a role that might be similarly fulfilled by other moieties, such as the propargylamine handle, in GNE-0011.

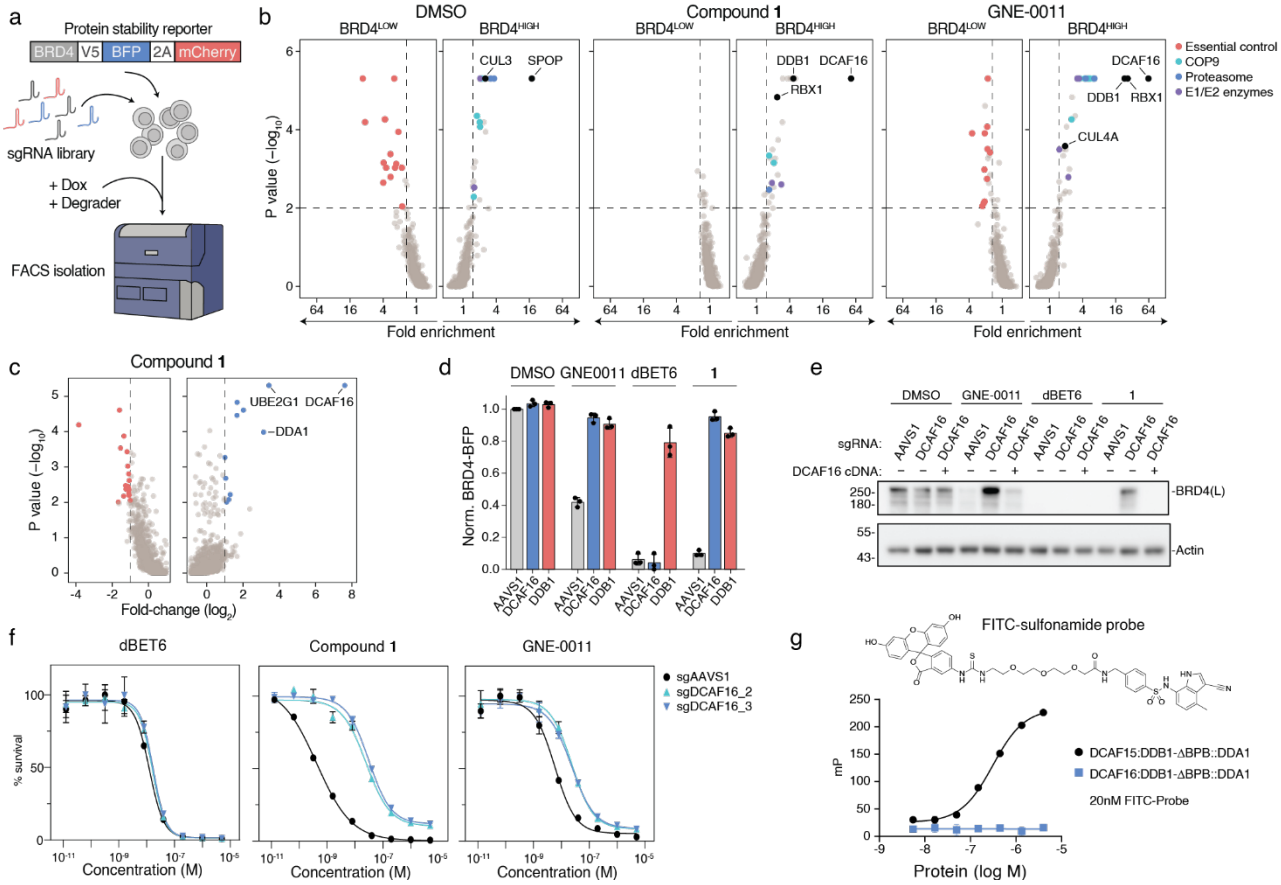

Fig. 2: Compound 1 and GNE-0011 recruit CRL4^{DCAF16} to induce degradation of BRD2/4.
a, Schematic representation of the FACS reporter system and CRISPR/Cas9 screen. KBM7 iCas9 cells expressing a BRD4-BFP protein stability reporter were transduced with a CRL-focused sgRNA library. After Cas9 induction via doxycycline, cells were treated with DMSO, 10 nM MZ1, 1 nM compound **1** or 1 μM GNE-0011 for 6 hours and sorted based on BRD4-BFP levels. **b**, KBM7 BRD4-reporter iCas9 CRISPR screen. Average gene-level fold-changes and p-values of BRD4^{HIGH} and BRD4^{LOW} cell populations compared to BRD4^{MID} fraction were calculated using MAGeCK[27]. Essential control genes (BRD4^{LOW}) and 20S proteasome subunits, COP9 signalosome subunits and E1 or E2 ubiquitin enzymes (BRD4^{HIGH}) inside the scoring window (p-value < 0.01, fold-change > 1.5) are highlighted. **c**, CRISPR/Cas9 viability screen. HCT-116 cells were transduced with Cas9 and a ubiquitin and NEDD8-system-focused sgRNA library and upon selection treated with compound **1** (58 nM; 4-fold IC_{50}) for 6 days. Average gene-level fold-changes and p-values compared to DMSO treated cells were calculated using MAGeCK. Genes showing > 2-fold enrichment or depletion and p-value < 0.01 are highlighted. **d**, Flow cytometric screen validation. KBM7 iCas9 BRD4-BFP reporter cells were transduced with the indicated sgRNAs and treated with DMSO, dBET6 (10 nM), GNE-0011 or compound 1 as above and BRD4-BFP levels were quantified. BRD4-BFP/mCherry ratio is normalized to DMSO treated sgAAVS1 cells. **e**, DCAF16 knockout/rescue. KBM7 iCas9 cells were lentivirally transduced with the indicated DCAF16-targeting or AAVS1 control sgRNAs, as well as a sgRNA resistant DCAF16 cDNA. After knockout of endogenous DCAF16, BRD4 expression levels were assessed via immunoblot. **f**, Viability assay. KBM7 iCas9 sgAAVS1 control or DCAF16 knockout cells were treated with increasing doses of dBET6, JQ1, GNE-0011 or compound **1** for 72 hours and vell viability was evaluated by CellTiterGlo assay. Dose-response curves fitted using non-linear regression. **g**, Fluorescence polarization (FP) binary binding assay. FITC-labelled sulfonamide probe (top) was titrated into DCAF15:DDB1ΔBPB:DDA1 or DCAF16:DDB1ΔBPB:DDA1. Data in **f**-**g** are shown as mean +/- s.d. (n = 3 technical replicates).

Compound 1 stabilizes an intrinsic interaction between BRD4 and DCAF16

Next, we focused on interrogating the possible formation of a ternary complex induced by **1.** We first performed size exclusion chromatography (SEC) to investigate potential interactions between the DCAF16:DDB1ΔBPB:DDA1 complex and $BRD4^{Tandem}$, a truncated BRD4 construct comprising the BD1 and BD2 bromodomains and the unstructured region connecting these domains. In isolation, DCAF16 or $BRD4^{Tandem}$ peaks did not shift upon addition of compound **1** (Extended Data Fig. 4a), however, when combining DCAF16 and $BRD4^{Tandem}$ in the presence of excess **1**, we observed formation of a higher molecular weight species, likely representing a ternary complex (Fig. 3a). Strikingly, we observed a similar but more diffuse left-shifted peak with DCAF16 and $BRD4^{Tandem}$ even in the absence of **1** (Fig. 3b), suggesting an intrinsic affinity between $BRD4^{Tandem}$ and DCAF16, that is stabilized by **1**. Since no complex was formed between DCAF16, compound **1** and isolated BRD4 BDs (Fig. 3b), this interaction likely involves both bromodomains tethered together by their endogenous linker.

In alphaLISA displacement assays, we found significantly enhanced affinity of **1** to $BRD4^{Tandem}$ in the presence of DCAF16 (IC_{50} = 12.8 nM), as compared to **1** and $BRD4^{Tandem}$ alone (IC_{50} = 462 nM; cooperativity (α) = 36; Fig. 3c, Extended Data Fig. 4b), further supporting a role of compound **1** in stabilizing the BRD4:DCAF16 complex. A similar, albeit significantly weaker positive cooperativity was observed for GNE-0011 (α = 1.6). In contrast, the presence of DCAF16 did not influence the affinity of either compound to isolated $BRD4^{BD1}$, further corroborating the requirement for the tandem bromodomain for complex formation. We finally performed a TR-FRET assay to investigate the interaction between a Cy5-labelled DCAF16:DDB1ΔBPB:DDA1 complex and His-tagged $BRD4^{Tandem}$. Consistent with the SEC and alphaLISA results, we observed a dose-dependent intrinsic BRD4:DCAF16 interaction (K_D = 1 μM) that was stabilized in the presence of **1** (K_D = 0.71 μM; Fig. 3d). Again, no such interaction was observed with individual bromodomains (Fig. 3d). Together, these orthogonal assays establish an intrinsic interaction between BRD4 and DCAF16, which is contingent on both bromodomains being present and tethered by their endogenous linker. Compound **1** and GNE-0011 stabilize this interaction, which might result in BRD4 ubiquitination and subsequent degradation.

To further explore this demarcation between individual bromodomains and $BRD4^{Tandem}$, we focused on cellular assays based on a dual fluorescence BRD4-BFP reporter. We generated a panel of KBM7 cell lines stably expressing either WT or truncated reporters (Fig. 3e, Extended Data Fig. 4c-f) and assessed the degradation of these constructs after treatment with **1**, GNE-0011 and dBET6 via flow cytometry. As expected, we observed potent degradation of WT BRD4(S) by all three degraders. This was independent of protein stretches outside the two bromodomains, as a serial deletion of the NPS, BID, ET and SEED regions did not affect degradation (Extended Data Fig. 4c, d) and the presence of a BRD4 bromodomain tandem was sufficient for degradation. While the isolated BD1 and BD2 bromodomains were potently degraded by dBET6, we observed no destabilization by GNE-0011 or **1** independent of subcellular localization (Fig. 3e, Extended Data Fig. 4e, f). Additionally, disruption of the JQ1 binding site in either bromodomain via single asparagine to phenylalanine changes (N144F or N433F, respectively) prevented degradation by GNE-0011 and **1**, whereas only the simultaneous mutation of both bromodomains disrupted

dBET6-based degradation (Fig. 3f). We furthermore utilized the BromoTag, a mutant BRD4^{BD2} L387A degron tag[28] , to evaluate the degradation of a BromoTag-MCM4 fusion. We observed potent degradation by the 'bumped' VHL-based PROTAC AGB1[28], while a similarly 'bumped' derivative of **1** (compound **5**) failed to induce any degradation (Extended Data Fig. 4g, h). Together, these data confirm that, unlike for most other BET degraders, a single BRD4 bromodomain is not sufficient to trigger degradation by GNE-0011 and compound **1**. Instead, both compounds require engagement of both acetyl-lysine binding pockets within a bromodomain tandem to induce degradation.

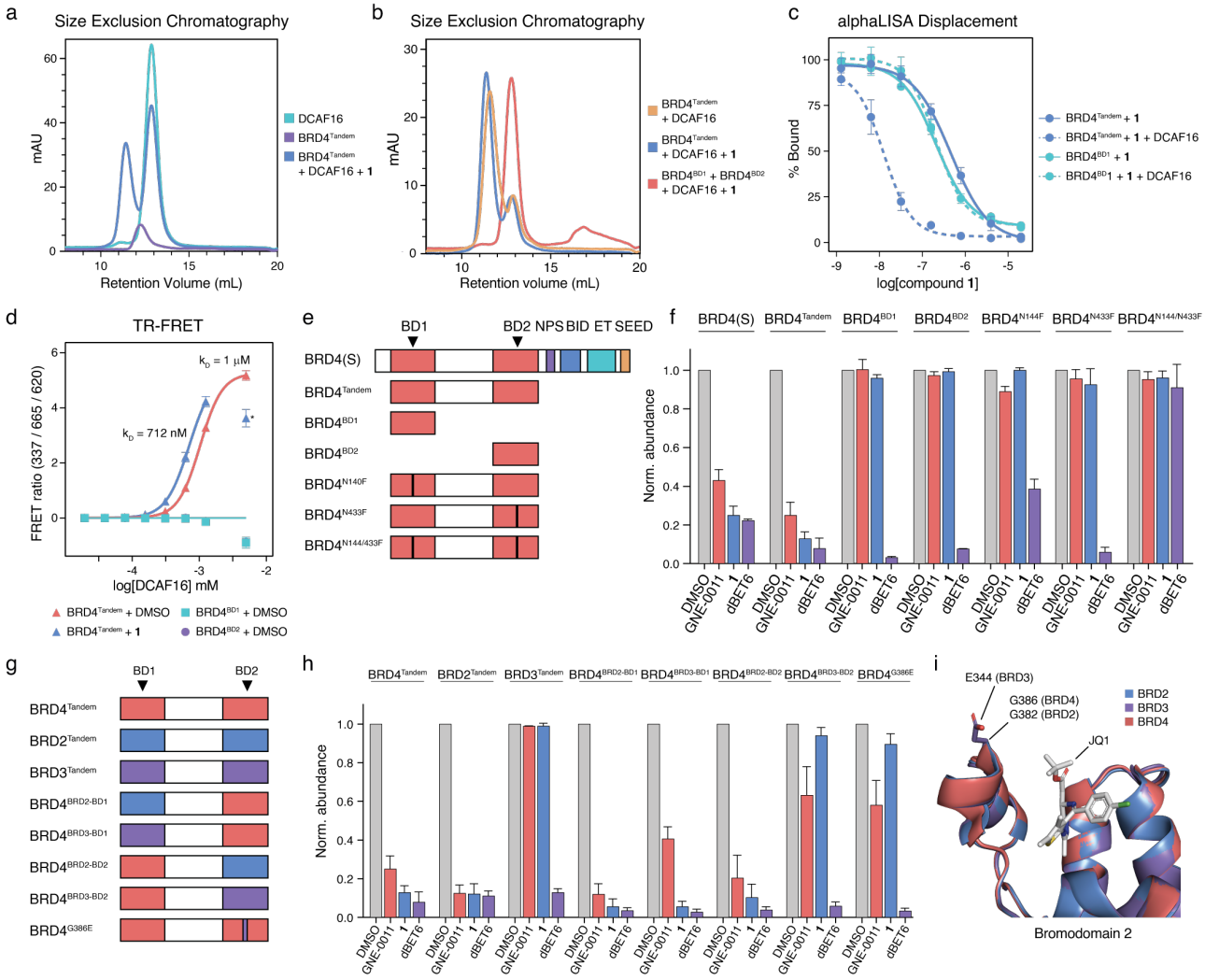

Fig. 3: Compound 1 enhances the intrinsic interaction between BRD4 tandem bromodomain region and DCAF16.

a, **b**, Size exclusion chromatography (SEC) UV chromatograms. DCAF16:DDB1ΔBPB:DDA1 and BRD4^{Tandem} alone or mixed at a 2:1 molar ratio in the presence of excess compound **1** (**a**), DCAF16:DDB1ΔBPB:DDA1 and BRD4^{Tandem} mixed at a 1:1 molar ratio in the absence or presence of excess compound **1** (**b**), as well as DCAF16:DDB1ΔBPB:DDA1 mixed with BRD4^{BD1} and BRD4^{BD2} at a molar ratio of 1:1:1 with excess compound **1** (**b**) were run on an S200 10/300 column. **c**, alphaLISA displacement assay. Competition of a biotinylated-JQ1 probe by compound **1** with His-BRD4^{Tandem} or His-BRD4^{BD1} in the presence or absence of DCAF16. Data shown are from n = 2 independent experiments each with 3 technical replicates, mean +/- s.d. **d**, TR-FRET proximity assay. 200 nM His-tagged BRD4 (BD1, BD2 or Tandem), bound to anti-His europium acceptor

beads, were incubated with increasing concentrations of Cy5-labelled DCAF16:DDB1ΔBPB:DDA1 complex and 1 μM compound **1** or DMSO. Data shown are from n = 2 independent experiments each with 2 technical replicates, mean +/- s.d. **e**-**h**, BRD4 protein stability reporter assay. BRD4(S) as well as BET protein truncations or mutants (**e**, **g**) fused to mTagBFP were ectopically expressed in KBM7 cells and protein stability after 6-hour treatment with DMSO, GNE-0011 (1 μM), compound **1** (1 nM) or dBET6 (10 nM) was quantified via flow cytometric evaluation of the mTagBFP/mCherry ratio (**f**, **h**). BD, bromodomain; NPS, N-terminal phosphorylation sites; BID, basic residue-enriched interaction domain; ET, extraterminal domain; SEED, Serine/Glutamic acid/Aspartic acid-rich region. Data shown are from n = 3 biological replicates, mean +/- s.d. **i**, Structural overlay of $BRD2^{BD2}$, $BRD3^{BD2}$ and $BRD4^{BD2}$, PDB codes 3ONI, 2OO1 and 6C7Q, respectively, along with JQ1 in the acetylated lysine binding pocket of $BRD2^{BD2}$. Residue E344 of BRD3, shown in stick representation, is a glycine residue at the equivalent position in BRD2 and BRD4.

Another feature that distinguishes **1** and GNE-0011 from many other BET protein degraders is their specificity for BRD2 and BRD4 over BRD3 (Fig. 1i, Extended Data Fig. 1l). We next employed the FACS-based protein stability assay to identify the features determining this specificity. Consistent with their effects on endogenous proteins, we observed potent degradation of BRD2, BRD3 and BRD4 tandem constructs by dBET6, whereas **1** and GNE-0011 selectively degraded $BRD2^{Tandem}$ and $BRD4^{Tandem}$ while not affecting $BRD3^{Tandem}$ (Fig. 3g, h). Next, we exchanged the linker from $BRD4^{Tandem}$ with the corresponding regions in BRD2 and BRD3, but observed no influence of the linker on degradation (Extended Data Fig. 4e, f). We also ruled out a role of the known SPOP degron in the conserved MotifA within the linker region (Extended Fig. 4e, f). Next, we swapped either BD1 or BD2 from $BRD4^{Tandem}$ with the corresponding domain from BRD2 or BRD3. While exchange of the first bromodomain had minimal influence on protein degradation, for BD2 only a swap with BRD2 was tolerated, while replacement by the $BRD3^{BD2}$ fully disrupted degradation by **1** (Fig. 3g, h). In sequence alignments, we identified five residues within BD2 that overlapped between BRD2 and BRD4 but differed from BRD3. Among these, residue 386/382 within the ZA loop in the vicinity of the JQ1 binding site encodes a glycine in BRD4 and BRD2, while the corresponding position 344 is a glutamate in BRD3. Upon structural alignment, we found this glutamate side chain to stick out of the bromodomain fold, thereby possibly interfering with ternary complex formation (Fig. 3i). Indeed, a G386E mutation in $BRD4^{Tandem}$ completely abrogated degradation by compound **1**, while not affecting degradation by dBET6 (Fig. 3h).

Compound 1 bivalently binds both bromodomains gluing BRD4 to DCAF16

To better understand the molecular mechanism underpinning **1**-induced BRD4 degradation, we solved the structure of the ternary complex formed between $BRD4^{Tandem}$, **1** and DCAF16:DDB1ΔBPB:DDA1 by cryo-electron microscopy at ~4 Å resolution (Fig. 4a). Despite co-purifying with DCAF16 and DDB1ΔBPB, we did not see density for DDA1, as was observed in another DDB1-substrate receptor structure from a recent publication[29]. While we were unable to confidently model DCAF16, we found its density to engage the central cleft between BPA and BPC of DDB1 in a binding mode distinct from other DCAF proteins and other CRL4 substrate receptors[7,29-31](Extended Data Fig. 5a). A web of density for DCAF16 runs from the binding cleft to the side surface of DDB1 BPC, where it folds into a helical bundle. Consistent with its role as CRL substrate receptor, this helical bundle of DCAF16 bridges the DDB1 adaptor protein with the neosubstrate BRD4. In contrast to

existing structures of BRD4 or other BET proteins which involve only truncated BD domains, we found both bromodomains simultaneously bound to DCAF16. Remarkably, sitting at the interface between DCAF16, BD1 and BD2, we observed a single continuous piece of density consistent with one molecule of **1** (Fig. 4b). The JQ1 moiety binds to BD2 while the E7820 moiety sits in the acetyl lysine pocket of BD1. The compound **1** aryl-sulfonamide overlays well with two other sulfonamide-containing BET inhibitors that have been crystallographically characterised bound to BD1[32,33] and the nitrogen atom of the cyano group occupies a position where a conserved water molecule is consistently observed in BET bromodomain crystal structures[34] (Extended Data Fig. 5b). Indeed, we found that E7820 and other aryl-sulfonamide derivatives exhibit weak binding to isolated bromodomains (Extended Data Fig. 5c, d).

The compound **1** linker region is sandwiched between the N-terminal end of BD2 αC, the ZA loop of BD1 close to αZ, and DCAF16, thus mediating numerous interactions at the interface. The two bromodomains share several intramolecular contacts in the ternary complex (Fig. 4c), including the sandwiching of M422 between W81 and P375 in the WPF shelves of BD1 and BD2, respectively (Fig. 4d). Furthermore, both BD1 and BD2 engage the surface of DCAF16 (Fig. 4e and f). Interestingly, we found G386 within the ZA loop of BD2 to be stacked against DCAF16, while the corresponding residue N93 in BD1 was solvent exposed, suggesting an explicit arrangement of both bromodomains. Indeed, BRD4 constructs harbouring either two copies of BD1 or BD2 were fully resistant to degradation (Extended Data Fig. 5e).

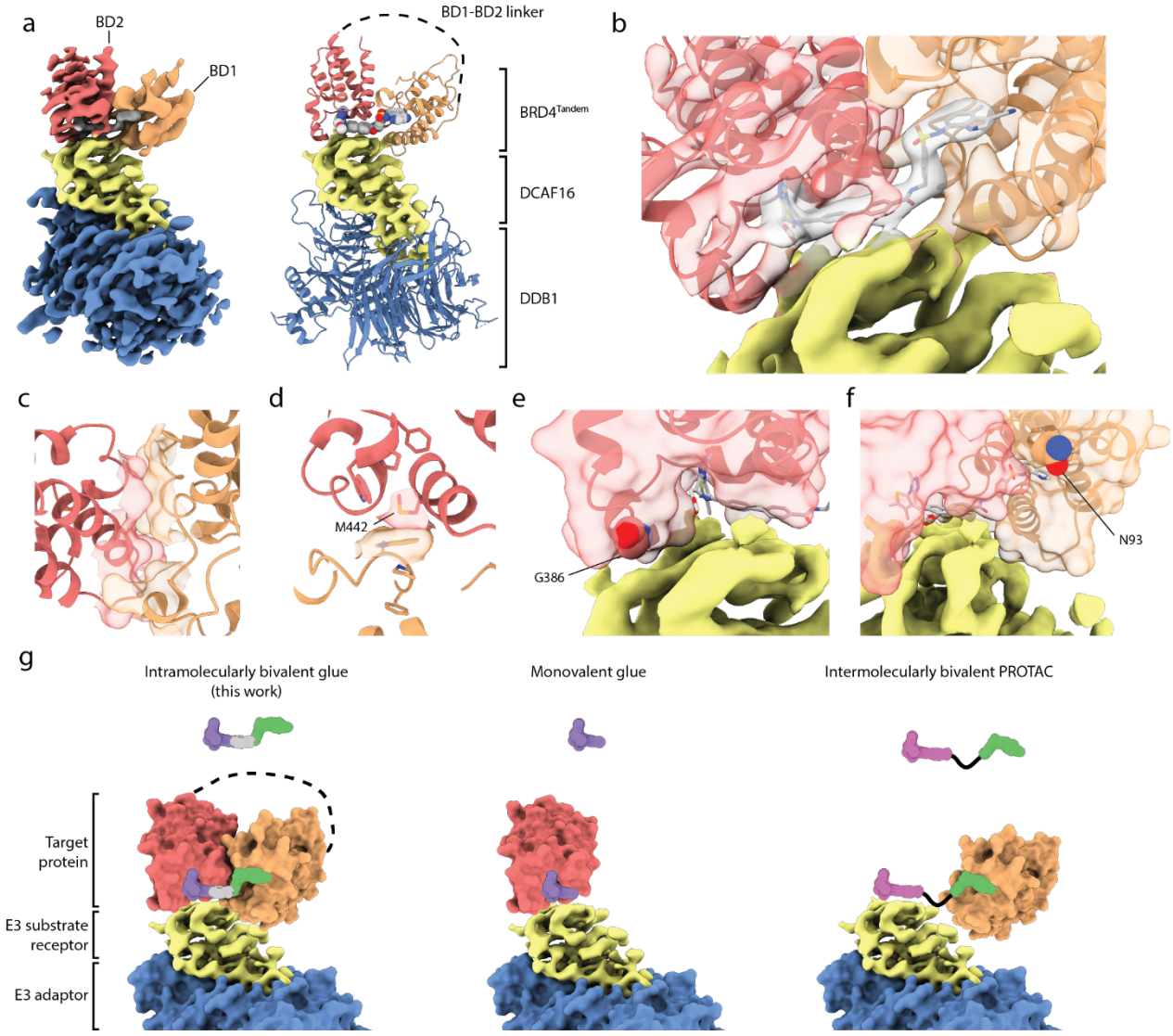

Fig. 4: Cryo-EM structure of the DCAF16:1:BRD4 ternary complex.
a, Electron density (left) and model (right) for the complex formed between DCAF16 (yellow), DDB1ΔBPB (blue), BRD4^{Tandem} (BD1 orange, BD2 red) and compound **1** (grey). **b**, Electron density at the DCAF16:BRD4:compound **1** interface. The JQ1 moiety binds to BD2 while the sulfonamide engages BD1. **c**, **d**, Detail views of BRD4 BD1 and BD2 intramolecular interaction surface (**c**) and M442 of BD2 bridging the WPF shelves of BD1 and BD2 (**d**). **e**, **f**, Intermolecular interaction surfaces between DCAF16 and BRD4 BD2 (**e**) and BD1 (**f**). G386 of BD2 and N93 of BD1 (spheres) face DCAF16 and solvent, respectively. For **b**-**f**, colours as in **a**. **g.** Schematic model of the different molecular recognition between intramolecularly bivalent glue as revealed in this work vs. traditional monovalent glues and bivalent PROTACs.

The ternary structure reveals a novel multivalent inter- and intramolecular interactions mediated by compound **1** that is unlike any reported to date. The indole-sulfonamide warhead of **1** neither binds directly to DCAF16 (in a PROTAC-like manner), nor does it mediate an interaction between BRD4 and DCAF16 (in a conventional glue-like manner). Instead, it binds to the adjacent bromodomain, linking the two domains and stabilizing their relative conformation in a bidentate fashion. Therefore, **1** is effectively binding the

bromodomains bivalently, but in contrast to known bivalent BET inhibitors[35,36], is also facilitating a multivalent gluing interaction between the two bromodomains and DCAF16. Thus, compound **1** serves as an intramolecular heterobifunctional binder that simultaneously stabilizes intermolecular and intramolecular protein-protein interaction surfaces to induce degradation (Fig. 4g).

Discussion

Most molecular glue degraders reported to date preferentially engage the E3 ligase at binary level, and then recruit target proteins. This notion underpins physiological regulatory circuits, such as the auxin-induced degradation of the IAA transcriptional repressor proteins in plant development[37] and is successfully leveraged therapeutically by monovalent molecular glue degraders such as lenalidomide and the related immunomodulatory drugs ("IMiDs") that induce the degradation of C2H2 zinc finger transcription factors (TFs) by binding to the E3 ligase CRBN and trigger ligase-TF interactions[38-42]. Such a mechanism, however, means that only targets that can be productively paired to a chemically accessible ligase can be actioned via this strategy. In contrast, very few glues to date have been developed from a given protein binder, and without relying on an independent E3 binding site as PROTACs do[43,44]. Here, we define the mode of action of compound **1** as involving intramolecular bivalent engagement of two sites on the target protein to nucleate a neomorphic drug-protein interface and stabilize an intrinsic target-E3 interaction. Hence, we reveal a new strategy, distinct from conventional bivalent PROTACs and monovalent glues, that enables development of glue degraders in a target-selective manner (Fig. 4g). Around 60-80% of all human proteins feature at least two distinct domains and are hence potentially accessible to the introduced mechanism of intramolecular, bivalent gluing[45,46].

Compound **1** activity depends on the $CRL4^{DCAF16}$ ligase complex, a surprising finding considering that **1** was chemically conceptualized as a PROTAC to recruit a different E3 ligase, DCAF15. Of note, DCAF16 was previously identified as the E3 ligase also involved in the degradation activity of BET PROTACs containing electrophilic fragments as E3 warheads[47]. Consistent with recent findings published during the preparation of our manuscript[48], we find the unrelated monovalent degrader GNE-0011 also depends on DCAF16. Here, we further establish that both **1** and GNE-0011 glue a hitherto unreported, intrinsic interaction between DCAF16 and BRD4, which reinforces the emerging concept that molecular glue degraders stabilize pre-existing, albeit often inconsequential E3 ligase-target interactions[49]. Our findings may also explain the eminent accessibility of BRD4 for chemically induced protein degradation, and offer a cautionary tale for the design and development of PROTACs using sub-specific E3 ligase binders such as E7820, thus possibly explaining the current challenges in expanding the PROTAC field to E3 ligases beyond CRBN and VHL[50].

Our findings have several implications for drug design that transcend TPD and reach into the wider scope of proximity-inducing pharmacology. Protein surfaces evolved on the edge of supramolecular self-assembly and show a general potential for intermolecular interactions to form interfaces[51]. Arguably, this tendency will be particularly pronounced for protein pairs characterized by a weak in vitro baseline affinity, priming such interfaces for drug-induced

stabilization that can prompt a functional consequence with enhanced specificity. Our work ushers in the enticing opportunity to productively glue by modulating protein conformation and surface topology via engaging multiple regions at the protein interface. This extends far beyond BRD4 to any multi-domain protein with ligandable domains, a property frequently found in gene-control proteins such as the transcriptional regulators CBP/P300, BAZ2A/B, or NSD2. DCAF16 has previously been shown to exclusively function in the nucleus[52], thus priming it to pursue targeted degradation of transcriptional regulators and chromatin factors. Compared to intermolecularly bivalent molecules, intramolecular bivalency may mitigate the hook effect due to avidity gained by binding to the same protein. Notably, avidity offered by intramolecular bivalent glues can overcome limited affinity of at least one targeting ligand, as illustrated by the weak affinity of the E7820 sulfonamide.

In conclusion, modulating the surface of a target protein by an intramolecular, chemical bridging of two binding sites could outline a generalizable strategy to pharmacologically induce proximity with neo- or intrinsically bound E3 ligases and other cellular effector proteins.

Acknowledgements

We are grateful to all members of the Ciulli and Winter laboratories and to Juraj Konc for experimental advice and helpful discussions. In particular, we thank Hana Imrichova and Florian Andersch for help with analysing flow cytometry based CRISPR screens. We acknowledge the European Synchrotron Radiation Facility (ESRF) for provision of synchrotron radiation facilities, and we would like to thank Max Nanao for assistance and support in using beamline ID23-2. We thank Johannes Zuber and members of the Zuber laboratory at the Research Institute of Molecular Pathology for sharing iCas9 cell lines, reagents and plasmids. We want to thank the Core Facility Flow Cytometry of the Medical University of Vienna for access to flow cytometry instruments and assistance with flow cytometric cell sorting; the CeMM Biomedical Sequencing Facility for NGS sample processing, sequencing and data curation; and Thomas Hannich and the Proteomics Facility of the CeMM Molecular Discovery Platform for access to instruments. We thank Nicholas Larsen at Foghorn Therapeutics for sharing plasmids.

Funding

This work was funded by Eisai and by the pharmaceutical companies supporting the Division of Signal Transduction and Therapy (Boehringer-Ingelheim, GlaxoSmithKline, Merck KaaG) as sponsored research funding to A.C. Funding is also gratefully acknowledged from the European Union's Horizon 2020 research and innovation programme under the Marie Sklodowska-Curie grant agreement No. 101024945 (H2020-MSCA-IF-2020-101024945 DELETER, Marie Skłodowska-Curie Actions Individual Fellowship to A.D.C.). The work of the Ciulli laboratory on targeting E3 ligases and TPD has received funding from the European Research Council (ERC) under the European Union's Seventh Framework Programme (FP7/2007-2013) as a Starting Grant to A.C. (grant agreement ERC-2012-StG-311460 DrugE3CRLs), and the Innovative Medicines Initiative 2 (IMI2) Joint Undertaking under grant agreement no. 875510 (EUbOPEN project). The IMI2 Joint Undertaking receives support from the European Union's Horizon 2020 research and innovation program, European Federation of Pharmaceutical Industries and Associations (EFPIA) companies, and associated partners KTH, OICR, Diamond, and McGill. We acknowledge the University of Dundee CryoEM facility for access to the instrumentation, funded by Wellcome (223816/Z/21/Z), MRC (MRC World Class Laboratories PO 4050845509). CeMM and the Winter laboratory are supported by the Austrian Academy of Sciences. The Winter lab is further supported by funding from the European Research Council (ERC) under the European Union's Horizon 2020 research and innovation program (grant agreement 851478), as well as by funding from the Austrian Science Fund (FWF, projects P32125, P31690 and P7909).

Competing interests

A.C. is a scientific founder, shareholder and advisor of Amphista Therapeutics, a company that is developing targeted protein degradation therapeutic platforms. The Ciulli laboratory receives or has received sponsored research support from Almirall, Amgen, Amphista Therapeutics, Boehringer Ingelheim, Eisai, Merck KaaG, Nurix Therapeutics, Ono

Pharmaceutical and Tocris-Biotechne. A.T. is currently an employee of Amphista Therapeutics. G.E.W. is scientific founder and shareholder of Proxygen and Solgate. The Winter lab received research funding from Pfizer.

Contributions

O.H., M.H. and A.D.C. contributed equally and will be putting their name first on the citation in their CVs. O.H., M.H., A.D.C, G.E.W. and A.C. conceived and planned this project. O.H., M.H. and A.D.C. designed and conducted experiments with help from K.I., T.I. and A.R. O.H., M.H., A.D.C., G.E.W. and A.C. analysed and interpreted original data. K.I., T.I., C.M. and A.T. designed and synthesized compounds. K.H. and M.W. performed and analysed viability-based CRISPR screens with input from M.K. and I.D., A.R. performed and analysed quantitative expression proteomics. A.D.C. performed Cryo-EM imaging, data processing and 3D reconstruction with help from R.S. and M.A.N.; M.A.N., A.C-S., C.C., C.M. and A.T. established critical reagents and methodology. O.H., M.H., A.D.C., G.E.W. and A.C. co-wrote the manuscript with input from all co-authors.

Extended Data

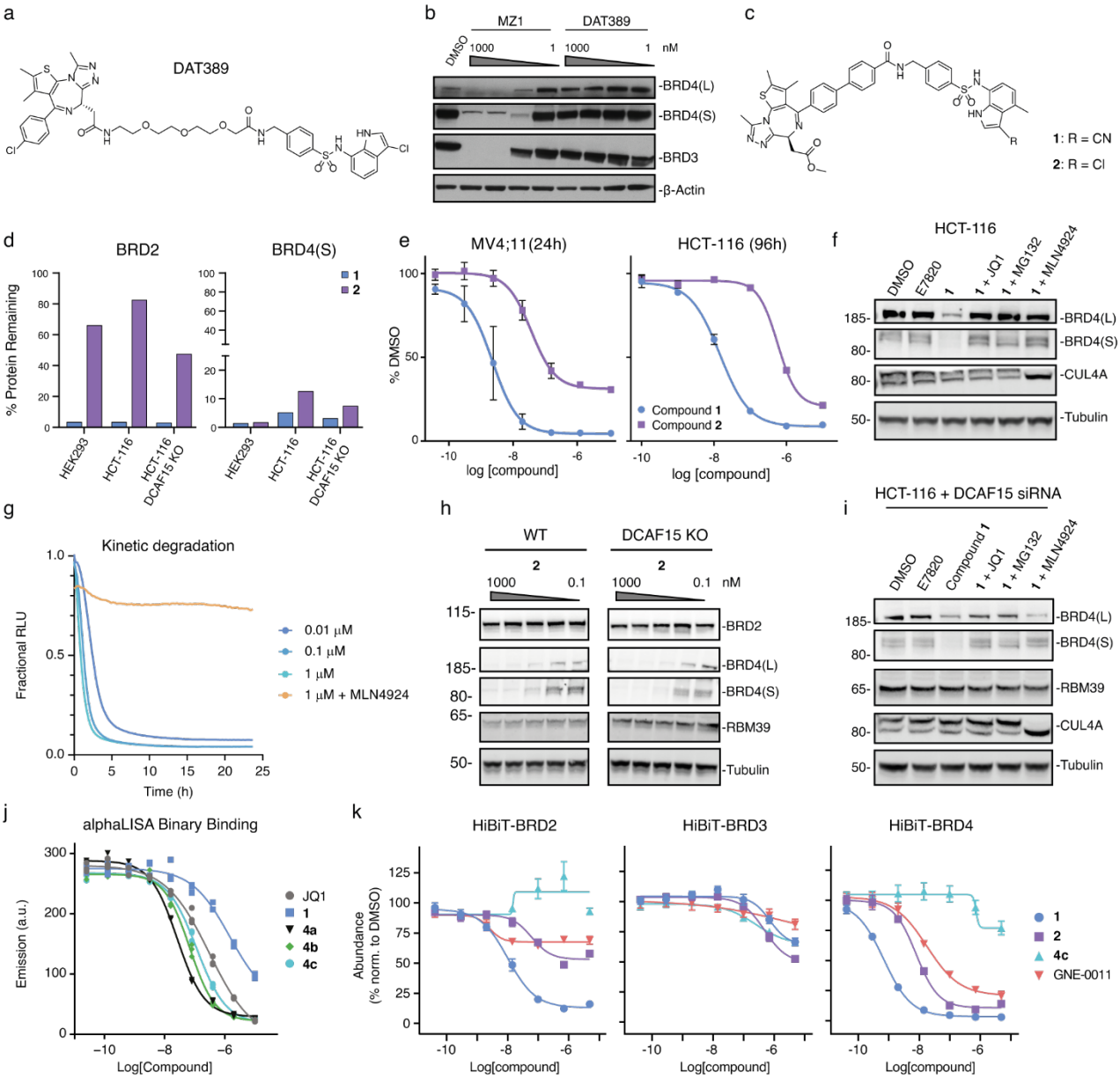

Extended Data Fig. 1: Compounds 1 and 2 degrade BRD2 and BRD4 independent of DCAF15.
a,**b**, Structure (**a**) and BET protein degradation activity (**b**) of sulfonamide-based PROTAC DAT389. HeLa cells were treated with the indicated concentrations of MZ1 or DAT389 for 16 hours and BET protein levels were analysed by immunoblot. **c**, **d**, Structures (**c**) and degradation activities (**d**) of compounds **1** and **2**. BRD2 and BRD4(S) protein remaining after compound treatment in HEK293, HCT-116 WT and DCAF15 KO cells based on immunoblot quantification. Source data, Supplementary Fig. 1a. **e,** Cytotoxicity of compounds **1** and **2**. MV4;11 and HCT-116 cells were treated with increasing concentrations of **1** and **2** for 24 or 96 hours, respectively, and cell viability was assessed via CellTiterGlo assay. Dose-response curves were fitted using non-linear regression fits. Data shown are from n = 2 biological repeats, mean +/- s.d. **f**, In-cell mechanistic evaluation of **1**. HCT-116 cells were treated for 2 hours with E7820 (1 μM) or **1** (10 nM) alone, or after 1 hour pre-treatment with JQ1 (10 μM), MG132 (50 μM) or MLN4924 (3 μM). Western blot representative of n = 3 independent experiments. **g,** NanoBRET kinetic degradation assay. BromoTag-HiBiT-BRD4 knock-in HEK293 cells were treated with compound **1** at indicated concentrations with or without MLN4924 (10 μM) 1-hour pre-

treatment. n = 3 biological repeats. **h,** DCAF15 independent protein degradation. HCT-116 WT and DCAF15 KO cells were treated with increasing concentrations of compound **2** for 6 h and BET protein levels were assessed via immunoblot. Western blots representative of n = 3 independent experiments. **i**, In-cell mechanistic evaluation of **1**. HCT-116 DCAF15 knockdown cells were treated for 2 hours with E7820 (1 μM) or **1** (10 nM) alone, or after 1 hour pre-treatment with JQ1 (10 μM), MG132 (50 μM) or MLN4924 (3 μM). Western blots representative of n = 2 independent experiments. **j**, alphaLISA displacement assay with biotinylated JQ1 probe and His-BRD4^{BD2}. Data shown are from n = 3 technical replicates, mean +/- s.d. **k**, End-point HiBiT protein degradation. HEK293 cells were engineered using CRISPR knock-in of the HiBiT tag at the endogenous BRD2, BRD3 or BRD4 loci, respectively, and were treated with the indicated compounds for 5 h. Levels of HiBiT-tagged proteins were detected via luminescence using the HiBiT lytic detection system. Dose-response curves were fitted using non-linear regression and the data shown are form n = 3 independent repeats, mean +/- s.d.

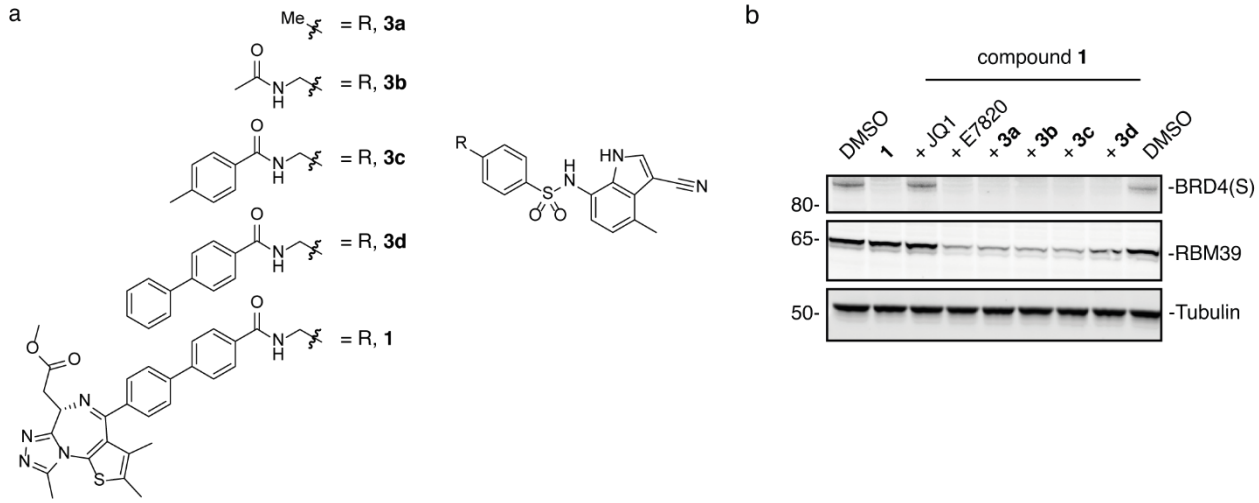

Extended Data Fig. 2: Sulfonamide-containing truncations do not outcompete compound 1.
a, Structures of a sulfonamide-containing truncations based on compound **1**. **b,** Competitive degradation assay. HCT-116 cells were pre-treated for 1 h with compounds **3a-d** (10 μM), followed by 2-hour treatment with compound **1** (10 nM) and immunoblot analysis. Western blot is representative of n = 2 biological replicates.

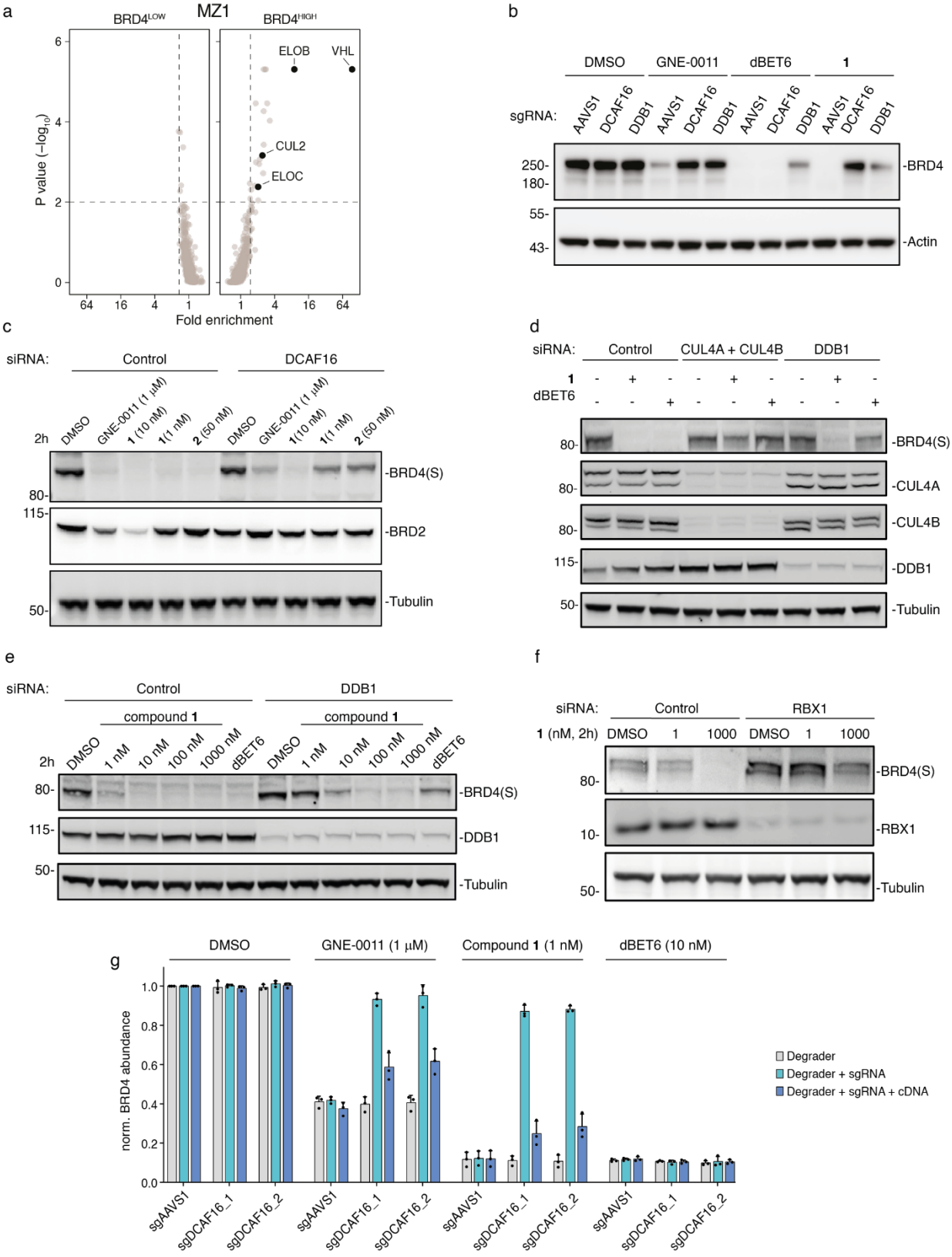

Extended Data Fig. 3: Compound 1 and GNE-0011 degrade BRD2/4 via CRL4^{DCAF16}.
a, MZ1 BRD4-reporter iCas9 CRISPR screen. Average gene-level fold-changes and p-values of BRD4^{HIGH} and BRD4^{LOW} cell populations compared to BRD4^{MID} fraction were calculated using MAGeCK as in Fig. 3b. **b**-**g**,

Immunoblot-based CRISPR/Cas9 screen validation. KBM7 (**b**) or HCT-116 cells (**c**-**f**) were transduced with sgRNA expressing lentivirus (**b**) or transfected with siRNA pools (**c**-**f**) targeting the indicated genes and treated with DMSO, compounds **1** or **2**, GNE-0011 or dBET6 for 2 h (**c**-**f**) or 6 h (**b**) at the indicated concentrations and BET protein levels were analysed via immunoblotting. **g**, DCAF16 knockout/rescue. KBM7 iCas9 BRD4(S)-BFP reporter cells were transduced with lentivirus expressing AAVS1 or two different DCAF16-targeting sgRNAs as well as an sgRNA-resistant DCAF16 expression vector. After 3 days of dox-induced Cas9 expression, cells were treated with DMSO, GNE-0011 (1 μM), compound **1** (1 nM) or dBET6 (10 nM) for 6 h and BRD4-BFP levels analysed via flow cytometry. Data shown for n = 3 biological replicates, mean +/- s.d.

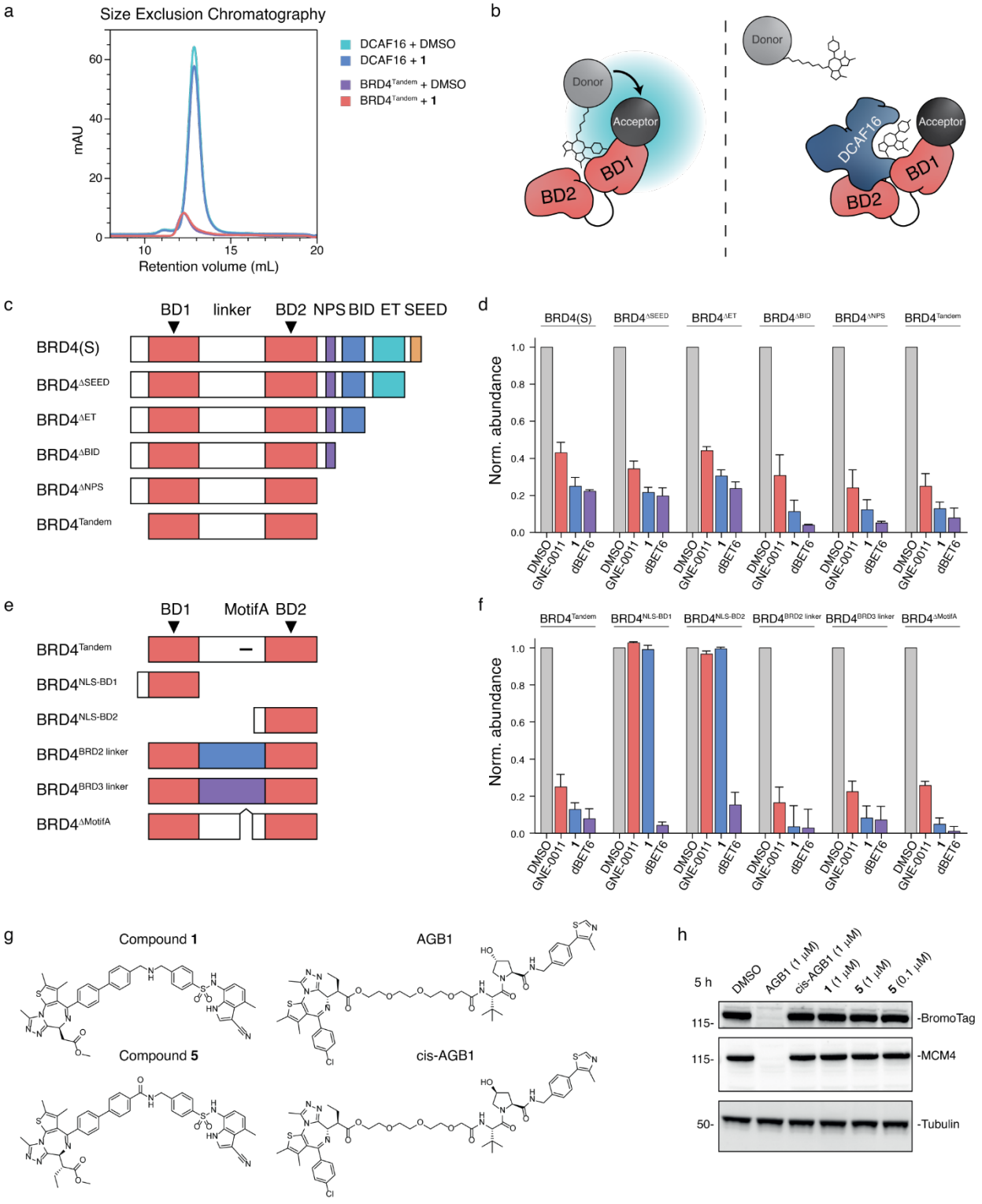

Extended Data Fig. 4: Mechanistic evaluation of compound 1 and GNE-0011.
a, Size exclusion chromatography (SEC) UV chromatogram. DCAF16:DDB1ΔBPB:DDA1 or BRD4^{Tandem} in the with or without excess compound 1 were run on an S200 10/300 column as in Fig. 4a, b. **b**, Schematic representation of alphaLISA displacement assay in Fig. 4c. His-tagged BRD4^{Tandem} is mixed with a biotinylated-JQ1 probe. Binding of the probe to BRD4 bromodomains in the presence of nickel-chelate acceptor beads and streptavidin-europium donor beads induces proximity of donor and acceptor, energy transfer and light emission

(left). Competition of the probe from BRD4^{Tandem} by compound **1** disrupts donor-acceptor proximity and energy transfer, and the presence of DCAF16 further strengthens compound **1** binding over probe binding (positive cooperativity; α > 1; right). **c**-**f**, Protein stability reporter assay. WT or truncated forms of BRD2, BRD3 or BRD4 (**c**, **e**) fused to mTagBFP were stably expressed in KBM7 cells and protein stability after 6-hour treatment with DMSO, GNE-0011 (1 μM), compound **1** (1 nM) or dBET6 (10 nM) was quantified via flow cytometric evaluation of the mTagBFP/mCherry ratio (**d**, **f**) as in Fig. 4e. BD, bromodomain; NPS, N-terminal phosphorylation sites; BID, basic residue-enriched interaction domain; ET, extraterminal domain; SEED, Serine/Glutamic acid/Aspartic acid-rich region; NLS, Nuclear localization signal. Data shown are from n = 3 biological replicates, mean +/- s.d. **g**, **h**, BromoTag degradation. HEK293 cells stably expressing BromoTag-MCM4 were treated for 5 hours with DMSO, BromoTag degrader AGB1 and non-degrader cis-AGB1[28], compound **1**, or 'bumped' analogue compound **5** (**g**) and BromoTag-MCM4 levels were analysed by immunoblotting (**h**). Data representative of n = 2 replicates.

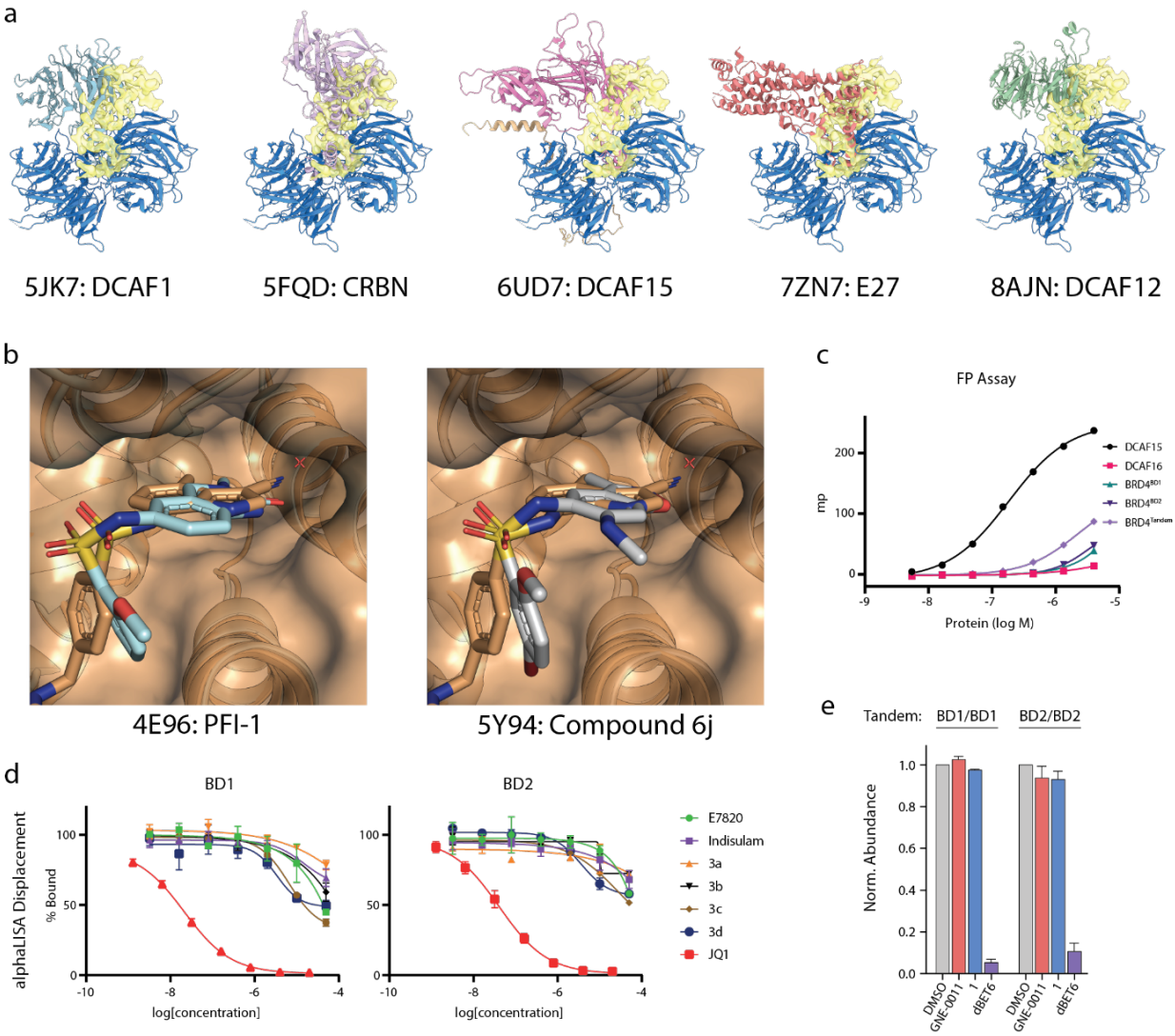

Extended Data Fig. 5: Comparison of substrate receptor-DDB1 binding mode and characterisation of BET-sulfonamide binding

a, Superposition of known substrate receptor-DDB1 complexes (cartoon) and DCAF16 density (transparent surface). **b**, Comparison of binding mode in the acetyl lysine pocket of $BRD4^{BD1}$ (orange surface and cartoon) between compound 1 (orange) and known sulfonamide BET inhibitors PFI-1 (left, light blue) and compound 6j (right, grey). The cyano group of compound 1 overlays close to a conserved water molecule found in both crystal structures and many other published BD1 structures. **c**, FP binary binding assay. Indicated proteins were titrated into 20 nM FITC-sulfonamide probe (from Fig. 3g). Data shown are from n = 3 technical replicates. **d**, alphaLISA displacement assay. Competition of a biotinylated-JQ1 probe following titration of sulfonamide-containing compounds or JQ1 into His-$BRD4^{BD1}$ (left) or His-$BRD4^{BD2}$ (right). Data shown are from n = 2 technical replicates. **e**, Protein stability reporter assay. $BRD4^{Tandem}$ constructs harbouring either two BD1 or two BD2 domains fused by their endogenous linker and connected to mTagBFP were stably expressed in KBM7 cells and protein stability after 6-hour treatment with DMSO, GNE-0011 (1 μM), compound 1 (1 nM) or dBET6 (10 nM) was quantified via flow cytometric evaluation of the mTagBFP/mCherry ratio as in Fig. 4e. Data shown are from n = 3 biological replicates, mean +/- s.d.

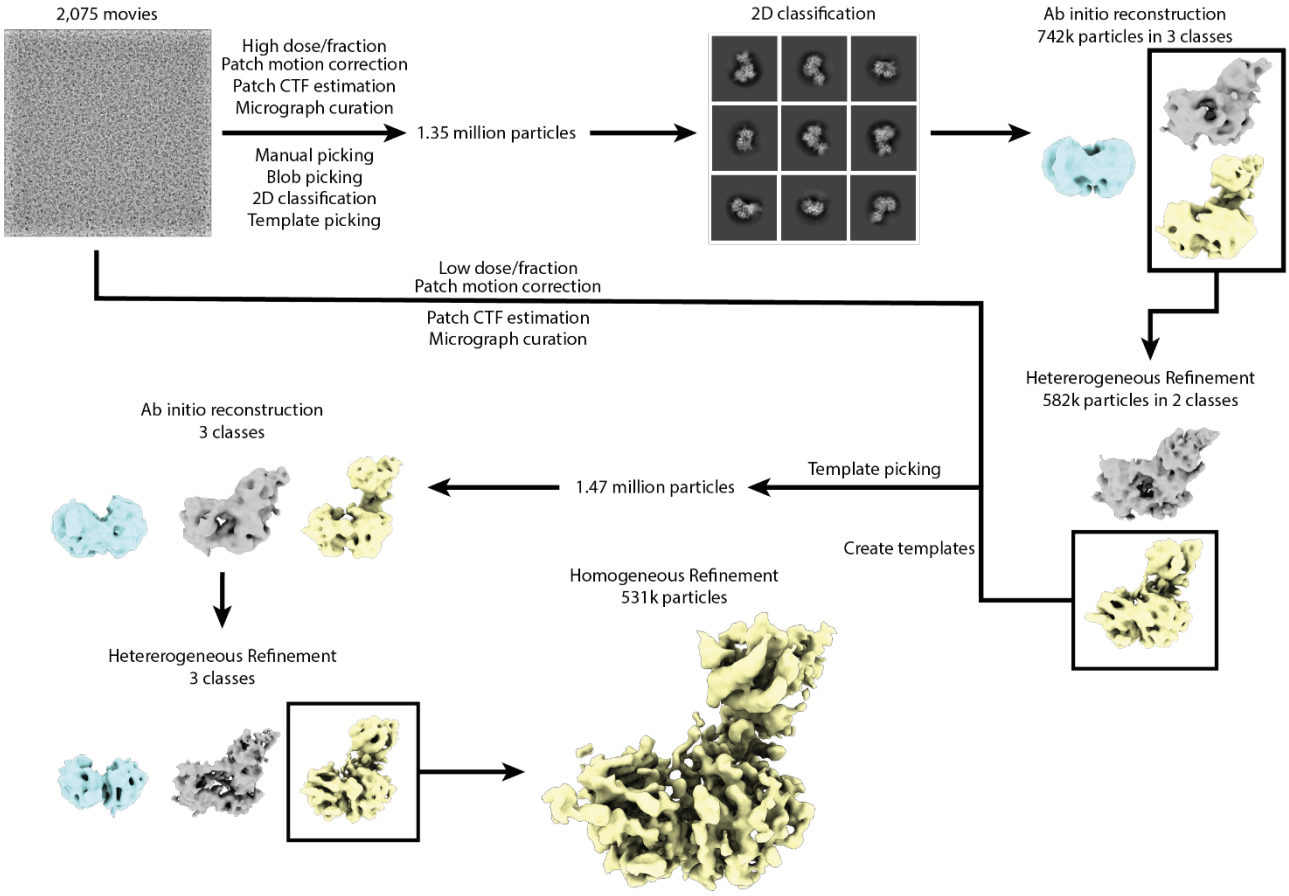

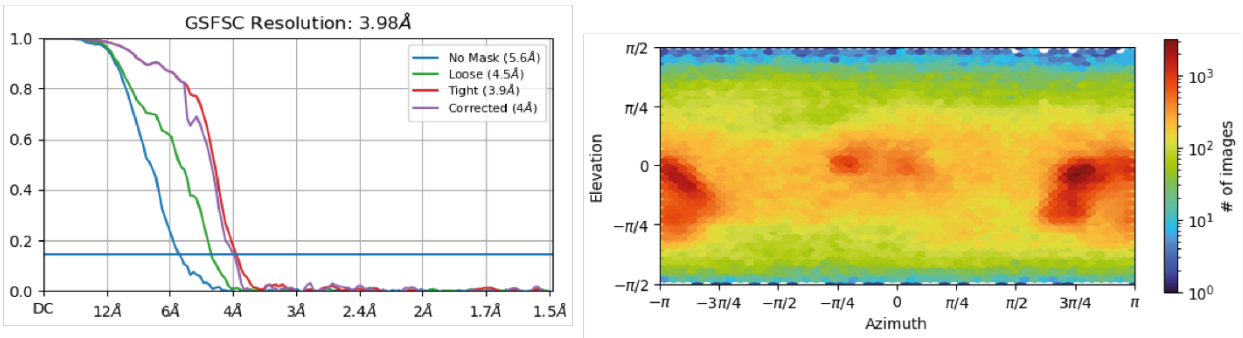

Extended Data Fig. 6: Workflow for cryo-EM data processing with gold-standard Fourier shell correlation at a cutoff of 0.143 and angular distribution plot for the final homogeneous refinement.

Plasmid name	Application
pRRL-SFFV-BRD4(S)-mTagBFP-P2A-mCherry	Protein stability reporter, screen
pRRL-U6-sgRNA-EF1αs-Thy1.1-P2A-NeoR	Screen validation
pRRL-SFFV-FLAG-DCAF16-EF1αs-iRFP670	KO/Rescue
pRRL-SFFV-BRD4(Tandem)-mTagBFP-P2A-mCherry	Protein stability reporter
pRRL-SFFV-BRD4(BD1)-mTagBFP-P2A-mCherry	Protein stability reporter
pRRL-SFFV-BRD4(NLS-BD1)-mTagBFP-P2A-mCherry	Protein stability reporter
pRRL-SFFV-BRD4(BD2)-mTagBFP-P2A-mCherry	Protein stability reporter
pRRL-SFFV-BRD4(NLS-BD2)-mTagBFP-P2A-mCherry	Protein stability reporter
pRRL-SFFV-BRD4(Tandem N140F)-mTagBFP-P2A-mCherry	Protein stability reporter
pRRL-SFFV-BRD4(Tandem N433F)-mTagBFP-P2A-mCherry	Protein stability reporter
pRRL-SFFV-BRD4(Tandem N140F/N433F)-mTagBFP-P2A-mCherry	Protein stability reporter
pRRL-SFFV-BRD2(Tandem)-mTagBFP-P2A-mCherry	Protein stability reporter
pRRL-SFFV-BRD3(Tandem)-mTagBFP-P2A-mCherry	Protein stability reporter
pRRL-SFFV-BRD2-BD1/BRD4-BD2(Tandem)-mTagBFP-P2A-mCherry	Protein stability reporter
pRRL-SFFV-BRD3-BD1/BRD4-BD2(Tandem)-mTagBFP-P2A-mCherry	Protein stability reporter
pRRL-SFFV-BRD4-BD1/BRD2-BD2(Tandem)-mTagBFP-P2A-mCherry	Protein stability reporter
pRRL-SFFV-BRD4-BD1/BRD3-BD2(Tandem)-mTagBFP-P2A-mCherry	Protein stability reporter
pRRL-SFFV-BRD4(Tandem G386E)-mTagBFP-P2A-mCherry	Protein stability reporter
pRRL-SFFV-BRD4(ΔSEED)-mTagBFP-P2A-mCherry	Protein stability reporter
pRRL-SFFV-BRD4(ΔET)-mTagBFP-P2A-mCherry	Protein stability reporter
pRRL-SFFV-BRD4(ΔBID)-mTagBFP-P2A-mCherry	Protein stability reporter
pRRL-SFFV-BRD4(ΔNPS)-mTagBFP-P2A-mCherry	Protein stability reporter
pRRL-SFFV-BRD4(Tandem BRD2-linker)-mTagBFP-P2A-mCherry	Protein stability reporter
pRRL-SFFV-BRD4(Tandem BRD3-linker)-mTagBFP-P2A-mCherry	Protein stability reporter
pRRL-SFFV-BRD4(TandemΔMotifA)-mTagBFP-P2A-mCherry	Protein stability reporter

sgRNA	Sequence (5' to 3')	Application
AAVS1	GCTGTGCCCCGATGCACAC	Screen validation
DCAF16_1	GGACTCCACAAGAGGCCAGA	Screen validation
DCAF16_2	GTTCCAGTTTGGGGACACAA	Screen validation
DDB1	GATGCCTGGTAAGTCAATGC	Screen validation
DCAF15_1	TTGAGGGACACGCACACCCG	Compound **1** MoA
DCAF15_2	ACTCGCATACGGTCAGGTAC	Compound **1** MoA
BRD4_1	TGGGATCACTAGCATGTCTG	HiBiT-Tagging
BRD3	TCGTGGCGGTGGACATCCTC	HiBiT-Tagging
BRD2	TTTGCAGCATCTTGACCGCA	HiBiT-Tagging
BRD4_2	GTGGGATCACTAGCATGTCTG	BromoTag
BRD4_3	GACTAGCATGTCTGCGGAGAG	BromoTag
MCM4_1	GTCCGAGCACTATGTCGTCCC	BromoTag
MCM4_2	GTCCGAGCACTATGTCGTCCC	BromoTag

Extended Data Table 1: Plasmids and sgRNAs used in this study.

Data collection	
Magnification	190,000
Voltage (kV)	200
Detector	Falcon 4i
Electron total dose (e-/Å^2)	12.7
Data Format	EER
Defocus range (μm)	-(1.7-3.2)
Pixel size (Å)	0.74
Exposure time (Sec)	2
Total fractions	18
Dose per fraction (e-/Å^2)	0.69
Reconstruction	
Symmetry imposed	C1
Initial particle images (no.)	1,466,607
Final particle images (no.)	530,879
Map resolution (Å)	4
FSC threshold	0.143
Map resolution range (Å)	4-8
Sharpening B-factor (Å^2)	-210.5

Extended Data Table 2: Summary of cryo-EM data collection conditions and image processing.

Methods

1. Chemistry

Chemicals that are commercially available were purchased from Apollo Scientific, Sigma-Aldrich, Fluorochem, CombiBlocks, TCI, and Enamine and were used without further purification. Liquid chromatography–mass spectrometry (LC-MS) was carried out on a Shimadzu HPLC/MS 2020 equipped with a Hypersil Gold column (1.9 µm, 50 × 2.1 mm2), a photodiode array detector, and an electrospray ionization (ESI) detector. The samples were eluted with a 3 min gradient of 5–95% acetonitrile in water containing 0.1% formic acid at a flow rate of 0.8 mL/min. Flash column chromatography was performed on a Teledyne ISCO Combiflash Companion installed with disposable normal phase RediSep Rf columns (230–400 mesh, 40–63 mm; SiliCycle). Preparative HPLC purification was performed on a Gilson preparative HPLC system equipped with a Waters X-Select C18 column (100 mm × 19 mm and 5 µm particle size) using a gradient from 5 to 95% of acetonitrile in water containing 0.1% formic acid over 10 min at a flow rate of 25 mL/min. Compound characterization using NMR was performed either on a Bruker 500 Ultra shield or on a Bruker Ascend 400 spectrometer. The 1H NMR and 13C NMR reference solvents used are CDCl3-*d1* (δH = 7.26 ppm/δC = 77.16 ppm), CD3OD-*d4* (δH = 3.31 ppm/δC = 49.00 ppm), DMSO-*d6* (δH = 2.50 ppm/δC = 39.52 ppm), or acetone-*d6* (δH = 2.05 ppm/δC = 29.84 ppm). Signal patterns are described as singlet (s), doublet (d), triplet (t), quartet (q), multiplet (m), broad singlet (bs), or a combination of the listed splitting patterns. The coupling constants (*J*) are measured in hertz (Hz).

Synthesis of compound 1

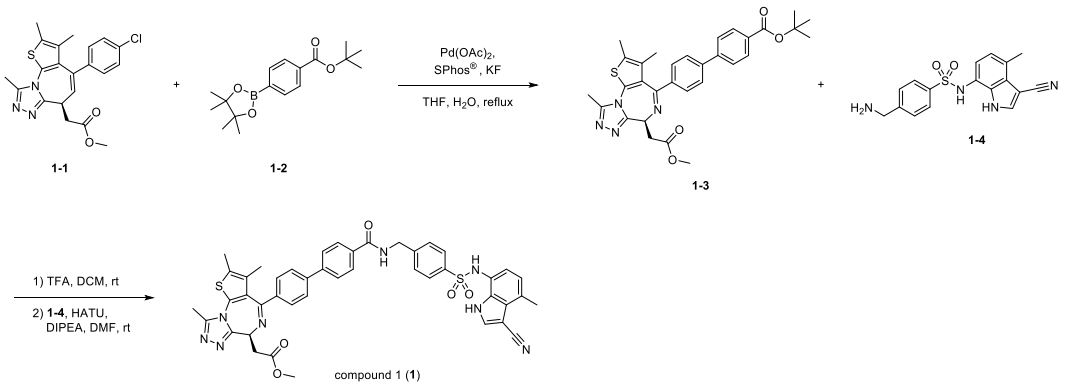

tert-Butyl (S)-4'-(6-(2-methoxy-2-oxoethyl)-2,3,9-trimethyl-6H-thieno[3,2-f][1,2,4]triazolo[4,3-a][1,4]diazepin-4-yl)-[1,1'-biphenyl]-4-carboxylate (**1-3**)

A mixture of methyl (R)-2-(4-(4-chlorophenyl)-2,3,9-trimethyl-6H-thieno[3,2-f][1,2,4]triazolo[4,3-a]azepin-6-yl)acetate (**1-1**) (125.7 mg, 0.30 mmol), 4-(*tert*-Butoxycarbonyl)phenylboronic acid pinacol ester (**1-2**) (101.4 mg, 0.33 mmol, 1.1 eq.), potassium fluoride (52.8 mg, 0.91 mmol, 3.0 eq.), SPhos® (12.4 mg, 0.03 mmol, 0.1 eq.), palladium(II) acetate (6.8 mg, 0.03 mmol, 0.1 eq.), and water (19.6 µl) in THF (1.0 mL) was purged with nitrogen atmosphere then the mixture was stirred at reflux temperature

overnight. The resulted mixture was diluted with excess amount of ethyl acetate, filtered through a celite pad, washed with ethyl acetate, concentrated in vacuo, and then purified by silica gel column chromatography (dichloromethane-methanol) to afford *tert*-butyl (S)-4'-(6-(2-methoxy-2-oxoethyl)-2,3,9-trimethyl-6H-thieno[3,2-f][1,2,4]triazolo[4,3-a][1,4]diazepin-4-yl)-[1,1'-biphenyl]-4-carboxylate (**1-3**) (193.4 mg, quantitative yield.). ^{1}H NMR (500 MHz, $CDCl_3$) δ 8.05 (d, *J* = 8.4 Hz, 2H), 7.63-7.59 (m, 4H), 7.56-7.54 (m, 2H), 4.66 (dd, *J* = 7.8, 6.3 Hz, 1H), 3.79 (s, 3H), 3.72-3.62 (m, 2H), 2.69 (s, 3H), 2.43 (s, 3H), 1.75 (s, 3H), 1.61 (s, 9H). ^{13}C NMR (101 MHz, CD_3OD-*d4*) δ 174.08, 167.99, 167.91, 157.75, 153.06, 146.32, 144.46, 139.95, 134.31, 134.10, 133.41, 133.22, 133.14, 131.89, 131.33, 129.23, 128.93, 83.33, 55.82, 53.31, 38.11, 29.34, 15.29, 13.83, 12.48. LC-MS, ESI$^+$, *m/z* 557.4 $[M+H]^+$.

Methyl (S)-2-(4-(4'-((4-(*N*-(3-cyano-4-methyl-1H-indol-7-yl)sulfamoyl)benzyl)carbamoyl)-[1,1'-biphenyl]-4-yl)-2,3,9-trimethyl-6H-thieno[3,2-f][1,2,4]triazolo[4,3-a][1,4]diazepin-6-yl)acetate (**1**)

To a solution of *tert*-butyl (S)-4'-(6-(2-methoxy-2-oxoethyl)-2,3,9-trimethyl-6H-thieno[3,2-f][1,2,4]triazolo[4,3-a][1,4]diazepin-4-yl)-[1,1'-biphenyl]-4-carboxylate (**1-3**) (57.0 mg, 90 μmol) in dichloromethane (0.5 mL) was added trifluoroacetic acid (0.5 mL) and then the mixture was stirred at room temperature for 4 hours. The resulted mixture was concentrated in vacuo, and then toluene was added thereto. After concentrated in vacuo again, the obtained crude compound, 4-(aminomethyl)-*N*-(3-cyano-4-methyl-1H-indol-7-yl)benzenesulfonamide (**1-4**)[6] (30.8 mg, 90.5 μmol, 1.0 eq.), and *N,N*-diisopropylethylamine (78.8 μl, 452.5 μmol, 5.0 eq.) were mixed in *N*,*N*-dimethylformamide (1.0 mL) and then HATU (61.9 mg, 162.9 μmol, 1.8 eq.) was added to it. After the mixture was stirred at room temperature overnight, the resulted mixture was purified by reverse-phase preparative HPLC (0.1% formic acid in water-acetonitrile) to afford compound 1 methyl (S)-2-(4-(4'-((4-(*N*-(3-cyano-4-methyl-1H-indol-7-yl)sulfamoyl)benzyl)carbamoyl)-[1,1'-biphenyl]-4-yl)-2,3,9-trimethyl-6H-thieno[3,2-f][1,2,4]triazolo[4,3-a][1,4]diazepin-6-yl)acetate (**1**) (26.2 mg, 35% yield). ^{1}H NMR (500 MHz, DMSO-*d6*) δ 11.86 (d, *J* = 2.7 Hz, 1H), 9.90 (s, 1H), 9.14 (t, J = 6.0 Hz, 1H), 8.15 (d, *J* = 3.1 Hz, 1H), 8.00 (d, J = 8.4 Hz, 2H), 7.83-7.79 (m, 4H), 7.69 (d, *J* = 8.4 Hz, 2H), 7.53 (d, *J* = 8.3 Hz, 2H), 7.45 (d, *J* = 8.3 Hz, 2H), 6.77 (d, *J* = 7.8 Hz, 1H), 6.62 (d, 7.8 Hz, 1H), 4.55-4.52 (m, 3H), 3.69 (s, 3H), 3.54-3.43 (m, 2H), 2.62 (s, 3H), 2.56 (s, 3H), 2.43 (s, 3H), 1.69 (s, 3H). ^{13}C NMR (126 MHz, DMSO-*d6*) δ 171.07, 165.87, 163.87, 154.72, 149.89, 144.91, 141.80, 140.90, 137.67, 137.33, 135.14, 133.26, 132.03, 130.71, 130.36, 130.04, 129.84, 129.00, 127.99, 127.54, 127.26, 127.02, 126.76, 126.63, 126.44, 122.40, 120.55, 118.01, 117.29, 84.30, 53.42, 51.51, 42.24, 36.28, 17.56, 14.04, 12.65, 11.21. LC-MS, ESI$^+$, *m/z* 823.1 $[M+H]^+$.

Synthesis of compound 2

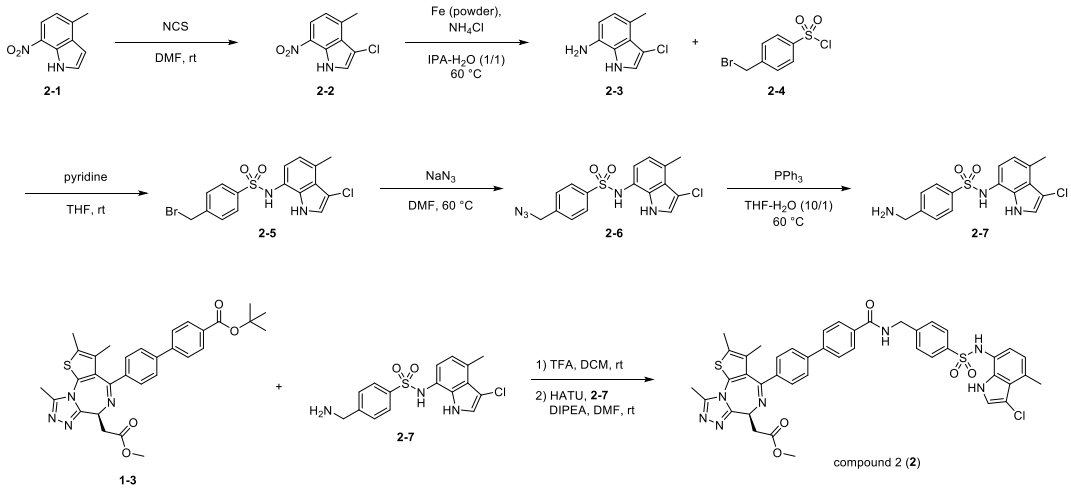

3-Chloro-4-methyl-7-nitro-1H-indole (**2-2**)

A solution of 4-methyl-7-nitro-1H-indole (**2-1**) (1000 mg, 5.68 mmol) in DMF (9.0 mL) was cooled down at 0 °C under nitrogen atmosphere and then a solution of *N*-chlorosuccinimide (909.5 mg, 6.81 mmol, 1.2 eq.) in DMF (3.0 mL) was added thereto slowly at the same temperature. After the completion of the addition, the mixture was gradually warmed up to room temperature and then stirred overnight. To the resulted reaction mixture was added 2 N hydrochloric acid and then the organic was extracted with ethyl acetate. The extract was washed with water and brine, dried over magnesium sulfate, and then concentrated in vacuo. The crude solid was triturated in dichloromethane, collected by filtration, washed with small amount of dichloromethane, and then dried in vacuo to afford 3-chloro-4-methyl-7-nitro-1H-indole (**2-2**) (966.8 mg). The filtrate was combined with 10 g of silica gel, concentrated in vacuo, and then purified by silica gel column chromatography (heptane-ethyl acetate) to afford 3-chloro-4-methyl-7-nitro-1H-indole (**2-2**) (61.9 mg, 1028.7 mg in total, 86% yield). ^{1}H NMR (400 MHz, DMSO-*d6*) δ 12.03 (s, 1H), 8.06 (d, *J* = 8.2 Hz, 1H), 7.61 (d, *J* = 2.8 Hz, 1H), 7.06 (dd, *J* = 8.2, 0.7 Hz, 1H), 2.82 (s, 3H).

3-Chloro-4-methyl-1H-indol-7-amine (**2-3**)

To a suspension of 3-chloro-4-methyl-7-nitro-1H-indole (**2-2**) (500 mg, 2.37 mmol) and ammonium chloride (2.54 g, 47.48 mmol, 20 eq.) in isopropanol (14.2 ml) and water (14.2 ml) was added iron powder (1.33 g, 23.74 mmol, 10 eq.) and then the mixture was stirred at 60 °C for 2.5 hour. After the addition of iron powder (1.33 g, 23.74 mmol, 10 eq.), the mixture was kept stirring for 1 hour. After cooled down, the resulted mixture was filtered through celite pad, washed with ethanol, and then concentrated in vacuo. The obtained solid was dissolved in diethyl ether and 1 N sodium hydroxide aqueous solution and then the organic layer was separated. The obtained organic extract was washed with saturated sodium bicarbonate aqueous solution, water, and brine, and then dried over magnesium sulfate. The residue was dissolved in diethyl ether, mixed with 15 g of silica gel, concentrated in vacuo, and then purified by silica gel column chromatography (heptane-ethyl acetate) to afford 3-chloro-4-methyl-1H-indol-7-amine (**2-3**) (285.1 mg, 67% yield). ^{1}H NMR (400 MHz, DMSO-*d6*) δ 10.82 (s, 1H), 7.34 (d, *J* = 2.5 Hz, 1H), 6.50 (d, *J* = 7.3 Hz, 1H), 6.25 (d, *J* = 7.4 Hz, 1H), 4.92 (s, 2H), 2.53 (s, 3H).

4-(Bromomethyl)-*N*-(3-chloro-4-methyl-1H-indol-7-yl)benzenesulfonamide (**2-5**)
To a solution of 3-chloro-4-methyl-1H-indol-7-amine (**2-3**) (150 mg, 0.83 mmol) and pyridine (201.5 µl, 2.49 mmol, 3.0 eq.) in tetrahydrofuran (3.0 ml) was added 4-(bromomethyl)benzenesulfonyl chloride (**2-4**) (335.7 mg, 1.25 mmol, 1.5 eq.) and then the mixture was stirred at room temperature for 2 hours. The resulted mixture was concentrated in vacuo and then purified by silica gel column chromatography (heptane-ethyl acetate) to afford 4-(bromomethyl)-*N*-(3-chloro-4-methyl-1H-indol-7-yl)benzenesulfonamide (**2-5**) (126.6 mg, 37% yield). ^{1}H NMR (400 MHz, DMSO-*d6*) δ 10.97 (s, 1H), 9.81 (s, 1H), 7.73-7.69 (m, 2H), 7.58-7.56 (m, 2H), 7.38 (d, *J* = 2.8 Hz, 1H), 6.63-6.56 (m, 2H), 4.79-4.71 (m, 2H), 2.59 (s, 3H).

4-(Azidomethyl)-*N*-(3-chloro-4-methyl-1H-indol-7-yl)benzenesulfonamide (**2-6**)
To a solution of 4-(bromomethyl)-*N*-(3-chloro-4-methyl-1H-indol-7-yl)benzenesulfonamide (**2-5**) (126.6 mg, 306.0 µmol) in DMF (2.0 ml) was added sodium azide (29.8 mg, 459.0 µmol, 1.5 eq.) and then the mixture was stirred at 60 °C for 1 hour. The resulted mixture was added to saturated sodium bicarbonate aqueous solution and then the organic was extracted with ethyl acetate. The obtained organic extract was washed with ammonium chloride aqueous solution, water, and brine, dried over magnesium sulfate, and then concentrated in vacuo to afford 4-(azidomethyl)-*N*-(3-chloro-4-methyl-1H-indol-7-yl)benzenesulfonamide (**2-6**) (118.6 mg, quantitative yield). ^{1}H NMR (500 MHz, DMSO-*d6*) δ 10.97 (s, 1H), 9.78 (s, 1H), 7.73 (d, *J* = 8.1 Hz, 2H), 7.49 (d, *J* = 8.0 Hz, 2H), 7.38 (d, *J* = 2.4 Hz, 1H), 6.60 (d, *J* = 7.7 Hz, 1H), 6.54 (d, J = 7.7 Hz, 1H), 4.55 (s, 2H), 3.07 (s, 3H).

4-(Aminomethyl)-*N*-(3-chloro-4-methyl-1H-indol-7-yl)benzenesulfonamide (**2-7**)
To a solution of 4-(azidomethyl)-*N*-(3-chloro-4-methyl-1H-indol-7-yl)benzenesulfonamide (**2-6**) (118.6 mg, 315.6 µmol) in THF (1.0 ml) and water (0.1 ml) was added triphenylphosphine (124.2 mg, 473.4 µmol, 1.5 eq.) and then the mixture was stirred at 60 °C for 1 hour. The resulted mixture was directly purified by reverse-phase column chromatography (0.1% formic acid in water-acetonitrile) to afford 4-(aminomethyl)-*N*-(3-chloro-4-methyl-1H-indol-7-yl)benzenesulfonamide (**2-7**) (8.1 mg, 89% yield). ^{1}H NMR (500 MHz, DMSO-*d6*) δ 11.14 (s, 1H), 8.27 (s, 1H), 7.71 (d, *J* = 8.0 Hz, 2H), 7.48 (d, *J* = 8.0 Hz, 2H), 7.35 (s, 1H), 6.65 (d, *J* = 7.7 Hz, 1H), 6.59 (d, J = 7.7 Hz, 1H), 3.86 (s, 2H), 2.57 (s, 3H).

Methyl (S)-2-(4-(4'-((4-(*N*-(3-chloro-4-methyl-1H-indol-7-yl)sulfamoyl)benzyl)carbamoyl)-[1,1'-biphenyl]-4-yl)-2,3,9-trimethyl-6H-thieno[3,2-f][1,2,4]triazolo[4,3-a][1,4]diazepin-6-yl)acetate (**2**)
To a solution of *tert*-butyl (S)-4'-(6-(2-methoxy-2-oxoethyl)-2,3,9-trimethyl-6H-thieno[3,2-f][1,2,4] triazolo[4,3-a][1,4]diazepin-4-yl)-[1,1'-biphenyl]-4-carboxylate (**1-3**) (20.0 mg, 88.3% purity, 0.03 mmol) in DCM (0.5 mL) was added trifluoroacetic acid (0.5 mL) and then the mixture was stirred at room temperature for 2 hours. The resulted mixture was concentrated in vacuo, and then toluene was added thereto. After concentrated in vacuo again to afford the corresponding carboxylic acid. To a mixture of the carboxylic acid (15.9 mg, 31.8 µmol), 4-(aminomethyl)-*N*-(3-chloro-4-methyl-1H-indol-7-yl)benzenesulfonamide (**2-7**) (24.4 mg, 69.9 µmol, 2.2 eq.), and *N,N*-diisopropylethylamine (27.7 µl, 158.8 µmol, 5 eq.) in DMF (1.5 mL) was added HATU (21.7 mg, 57.2 µmol, 1.8 eq.) and then the mixture was stirred at room temperature overnight. The resulted mixture was purified directly by reverse-phase

preparative HPLC (0.1% formic acid in water-acetonitrile) to afford methyl (S)-2-(4-(4'-((4-(*N*-(3-chloro-4-methyl-1H-indol-7-yl)sulfamoyl)benzyl)carbamoyl)-[1,1'-biphenyl]-4-yl)-2,3,9-trimethyl-6H-thieno[3,2-f][1,2,4]triazolo[4,3-a][1,4]diazepin-6-yl)acetate (**2**) (8.44 mg, 32% yield). ^{1}H NMR (500 MHz, DMSO-*d6*) δ 11.00 (d, *J* = 2.3, 1H), 9.80 (s, 1H), 9.16 (t, *J* = 5.9 Hz, 1H), 8.00 (d, *J* = 8.8 Hz, 2H), 7.81 (t, *J* = 8.8 Hz, 4H), 7.70 (d, *J* = 8.4 Hz, 2H), 7.53 (d, *J* = 8.2 Hz, 2H), 7.44 (d, *J* = 8.4 Hz, 2H), 7.38 (d, *J* = 2.8 Hz, 1H), 6.61-6.58 (m, 2H), 4.54-4.53 (m, 3H), 3.68 (s, 3H), 3.53-3.42 (m, 2H), 2.62 (s, 3H), 2.57 (s, 3H), 2.43 (s, 3H), 1.68 (s, 3H). ^{13}C NMR (126 MHz, DMSO-*d6*) δ 171.13, 165.86, 163.90, 154.76, 149.94, 144.85, 141.82, 140.91, 137.93, 137.36, 133.25, 132.08, 130.72, 130.06, 129.85, 129.05, 128.04, 127.53, 127.03, 126.81, 126.74, 126.68, 123.61, 123.11, 121.05, 120.00, 116.35, 103.92, 53.45, 51.58, 42.24, 36.31, 18.37, 14.13, 12.70, 11.28. LC-MS, ESI^{+}, *m/z* 832.5 [M+H]$^{+}$.

Synthesis of compound 3a

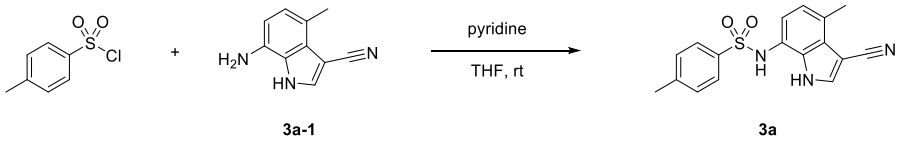

3a-1 3a

To a solution of 7-amino-4-methyl-1H-indole-3-carbonitrile (30 mg, 0.18 mmol) and pyridine (42.5 µl, 0.53 mmol, 3 eq.) in tetrahydrofuran (1 ml) was added 4-toluenesulfonyl chloride (50.1 mg, 0.26 mmol, 1.5 eq.) and then the mixture was stirred at room temperature overnight. The resulted mixture was diluted with DMSO (1 mL), filtered through a membrane filter (0.43 µm), and then purified by reverse-phase preparative HPLC (0.1% formic acid in water-acetonitrile) to afford *N*-(3-cyano-4-methyl-1H-indol-7-yl)-4-methylbenzenesulfonamide (**3a**). ^{1}H NMR (400 MHz, DMSO-*d6*) δ 11.85 (bs, 1H), 9.82 (bs, 1H), 8.15 (s, 1H), 7.58 (d, *J* = 8.3 Hz, 2H), 7.31 (d, *J* = 8.1 Hz, 2H), 6.77 (d, J = 7.7 Hz, 1H), 6.60 (d, *J* = 7.7 Hz, 1H), 2.56 (s, 3H), 2.34 (s, 3H). ^{13}C NMR (101 MHz, DMSO-*d4*) δ 144.87, 138.10, 136.81, 132.13, 131.18, 128.89, 128.59, 128.11, 124.09, 122.37, 119.79, 119.01, 85.98, 22.60, 19.26. LC-MS, ESI^{+}, *m/z* 323.8 [M+H]$^{+}$.

Synthesis of compound 3b

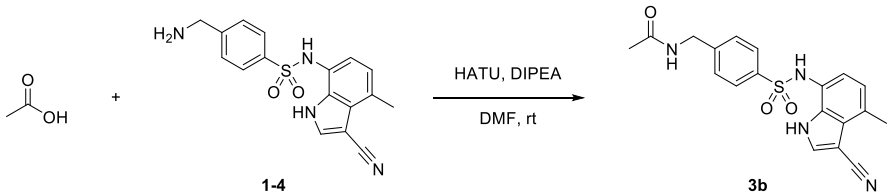

1-4 3b

To a solution of 4-(aminomethyl)-*N*-(3-cyano-4-methyl-1H-indol-7-yl)benzenesulfonamide (**1-4**) (20 mg, 58.8 µmol, 1.0 eq.), acetic acid (5 µl, 452.5 µmol, 5 eq.), and *N,N*-diisopropylethylamine (51.2 µl, 293.8 µmol, 5 eq.) in *N,N*-dimethylformamide (0.5 mL) was

added HATU (40.2 mg, 105.8 μmol, 1.8 eq.) and then the mixture was stirred at room temperature for 6 hours. The resulted mixture was diluted with 0.5 mL of DMSO, filtered through a membrane filter (0.43 μm), and then purified directly by reverse-phase preparative HPLC (0.1% formic acid in water-acetonitrile) to afford *N*-(4-(*N*-(3-cyano-4-methyl-1H-indol-7-yl)sulfamoyl)benzyl)acetamide (**3b**) (3.37 mg, 15% yield). ^{1}H NMR (400 MHz, acetone-*d6*) δ 8.05 (s, 1H), 7.62 (d, *J* = 8.3 Hz, 2H), 7.39 (d, *J* = 8.3 Hz, 2H), 6.78 (d, *J* = 7.7 Hz, 1H), 6.63 (d, *J* = 7.7 Hz, 1H), 4.41 (s, 2H), 2.64 (s, 3H), 1.95 (s, 3H). ^{13}C NMR (101 MHz, acetone-*d6*) δ 171.07, 146.14, 138.80, 135.07, 132.41, 129.81, 128.64, 128.35, 127.96, 123.61, 121.37, 120.96, 100.21, 86.66, 43.08, 22.71, 18.20. LC-MS, ESI^{+}, *m/z* 382.9 [M+H]$^{+}$.

Synthesis of compound 3c

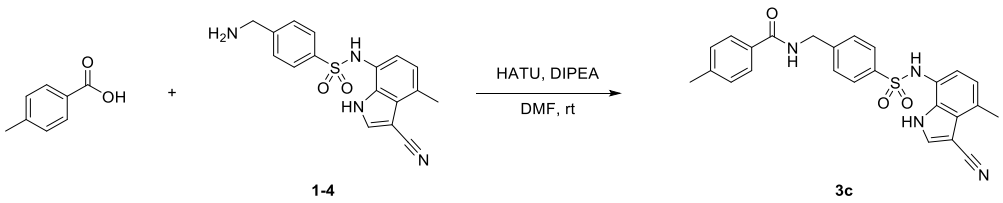

To a solution of 4-(aminomethyl)-*N*-(3-cyano-4-methyl-1H-indol-7-yl)benzenesulfonamide (**1-4**) (30 mg, 79.6 μmol), *p*-toluic acid (13.0 mg, 95.5 μmol, 5 eq.), and *N,N*-diisopropylethylamine (69.3 μl, 398.0 μmol, 5 eq.) in *N,N*-dimethylformamide (0.5 mL) was added HATU (45.4 mg, 119.4 μmol, 1.5 eq.) and then the mixture was stirred at room temperature for 5 hours. The resulted mixture was purified directly by reverse-phase silica gel column chromatography (0.1% formic acid in water-acetonitrile, UV detection). The obtained compound was triturated with dichloromethane. The solid was collected by filtration, washed with dichloromethane, and then dried in vacuo to afford *N*-(4-(*N*-(3-cyano-4-methyl-1H-indol-7-yl)sulfamoyl)benzyl)-4-methylbenzamide (**3c**) (4.77 mg, 13% yield). ^{1}H NMR (500 MHz, acetone-*d6*) δ 11.09 (bs, 1H), 8.87 (bs, 1H), 8.28 (bs, 1H), 8.09 (s, 1H), 7.83 (d, *J* = 8.2 Hz, 2H), 7.65 (d, *J* = 8.4 Hz, 2H), 7.48 (d, *J* = 8.4 Hz, 2H), 7.28 (d, *J* = 8.0 Hz, 2H), 6.80 (dd, *J* = 7.1, 0.7 Hz, 1H), 6.67 (d, *J* = 7.7 Hz, 1H), 4.63 (d, *J* = 6.0 Hz, 2H), 2.64 (s, 3H), 2.37 (s, 3H). ^{13}C NMR (126 MHz, acetone-*d6*) δ 167.36, 146.43, 142.49, 138.64, 135.15, 132.71, 132.44, 129.83, 129.75, 128.67, 128.30, 128.13, 127.90, 123.57, 121.37, 120.96, 117.56, 86.73, 43.43, 21.34, 18.21. LC-MS, ESI^{+}, *m/z* 459.1 [M+H]$^{+}$.

Synthesis of compound 3d

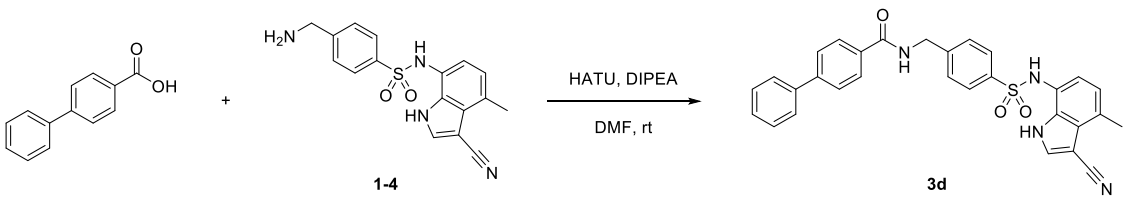

To a solution of 4-(aminomethyl)-*N*-(3-cyano-4-methyl-1H-indol-7-yl)benzenesulfonamide hydrochloride (**28**) (30 mg, 79.6 μmol), 4-phenylbenzoic acid (18.9 mg, 95.5 μmol, 5 eq.), and *N,N*-diisopropylethylamine (69.3 μl, 398.0 μmol, 5 eq.) in *N,N*-dimethylformamide (0.5

mL) was added HATU (45.4 mg, 119.4 μmol, 1.5 eq.) and then the mixture was stirred at room temperature for 5 hours. The resulted mixture was purified directly by reverse-phase silica gel column chromatography (0.1% formic acid in water-acetonitrile). The obtained compound was triturated with dichloromethane. The solid was collected by filtration, washed with dichloromethane, and then dried in vacuo to afford *N*-(4-(*N*-(3-cyano-4-methyl-1H-indol-7-yl)sulfamoyl)benzyl)-[1,1'-biphenyl]-4-carboxamide (**3d**) (3.69 mg, 9% yield). ^{1}H NMR (500 MHz, DMSO-*d6*) δ 11.91 (s, 1H), 9.94 (s, 1H), 9.16 (t, *J* = 6.0 Hz, 1H), 8.16 (s, 1H), 7.99 (d, *J* = 8.5 Hz, 2H), 7.79 (d, *J* = 8.4 Hz, 2H), 7.75-7.73 (m, 2H), 7.68 (d, *J* = 8.4 Hz, 2H), 7.51-7.48 (m, 2H), 7.45 (d, *J* = 8.3 Hz, 2H), 7.41 (t, *J* = 7.4 Hz, 1H), 6.77 (d, *J* = 7.8 Hz, 1H), 6.59 (d, *J* = 7.8 Hz, 1H), 4.55 (d, *J* = 4.6 Hz, 2H), 2.55 (s, 3H). ^{13}C NMR (126 MHz, DMSO-*d6*) δ 165.98, 144.96, 142.93, 139.13, 135.21, 132.79, 130.49, 129.03, 128.07, 127.96, 127.52, 127.06, 126.87, 126.58, 126.47, 122.43, 118.11, 117.38, 84.28, 42.23, 17.64. LC-MS, ESI^{+}, *m/z* 521.1 [M+H]$^{+}$.

Synthesis of compound 4a

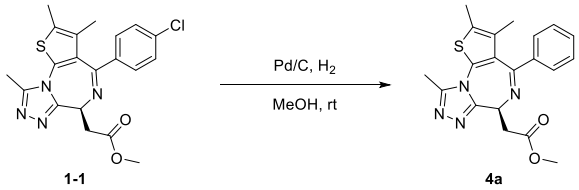

To a solution of methyl (R)-2-(4-(4-chlorophenyl)-2,3,9-trimethyl-6H-thieno[3,2-f][1,2,4]triazolo[4,3-a]azepin-6-yl)acetate (**1-1**) (29.3 mg, 70.6 μmol) in methanol (1.0 mL) was added palladium on carbon (10wt%, 7.5 mg, 7.1 μmol, 0.1 eq.) under nitrogen and then the mixture was stirred under hydrogen (balloon) at room temperature overnight. The resulted mixture was diluted with excess amount of ethyl acetate and then stirred under air at room temperature for 1 hour. The resulted mixture was filtered, washed with ethyl acetate, and then concentrated by nitrogen blow. The crude mixture was suspended in ethyl acetate and small amount of DMSO, washed with saturated ammonium chloride aqueous solution, water, and brine, dried over magnesium sulfate, concentrated in vacuo, and then purified by silica gel column chromatography (dichloromethane-methanol). The obtained fraction which had the desired product was concentrated in vacuo and then purified again by reverse-phase preparative HPLC (0.1% formic acid in water-acetonitrile) to afford methyl (S)-2-(2,3,9-trimethyl-4-phenyl-6H-thieno[3,2-f][1,2,4]triazolo[4,3-a][1,4]diazepin-6-yl)acetate (**4a**) (2.6 mg, 10%) as a white solid. ^{1}H NMR (500 MHz, $CDCl_3$) δ 7.48-7.42 (m, 3H), 7.38-7.35 (m, 2H), 4.66-4.64 (m, 1H), 3.80 (s, 3H), 3.69-3.66 (m, 2H), 2.70 (s, 3H), 2.43 (s, 3H), 1.69 (s, 3H), ^{13}C NMR (126 MHz, $CDCl_3$) δ 172.18, 165.02, 155.48, 149.84, 138.28, 132.10, 131.23, 130.87, 130.51, 130.35, 128.48, 128.43, 53.83, 51.83, 36.80, 14.26, 13.05, 11.83. LC-MS, ESI^{+}, *m/z* 380.7 [M+H]$^{+}$.

Synthesis of compound 4b

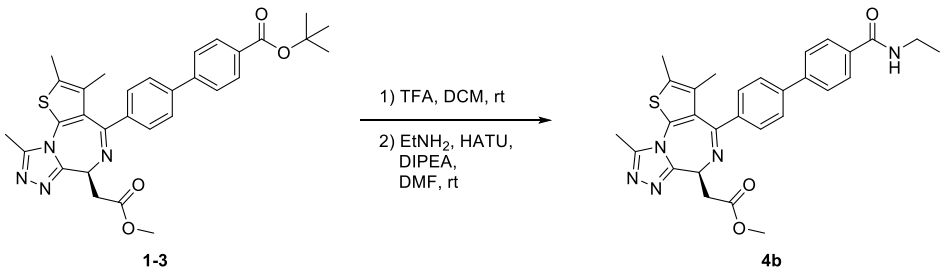

1-3 **4b**

To a solution of *tert*-butyl (S)-4'-(6-(2-methoxy-2-oxoethyl)-2,3,9-trimethyl-6H-thieno[3,2-f][1,2,4] triazolo[4,3-a][1,4]diazepin-4-yl)-[1,1'-biphenyl]-4-carboxylate (**1-3**) (20.0 mg, 88.3% purity, 0.03 mmol) in DCM (0.5 mL) was added trifluoroacetic acid (0.5 mL) and then the mixture was stirred at room temperature for 2 hours. The resulted mixture was concentrated in vacuo, and then toluene was added thereto. After concentrated in vacuo again to afford the corresponding carboxylic acid. To the mixture of the carboxylic acid, 2 M ethylamine in THF (49.9 µl, 99.9 µmol, 2.0 eq.), and *N,N*-diisopropylethylamine (43.5 µl, 250 µmol, 5.0 eq.) in *N,N*-dimethylformamide (1.0 mL) was added HATU (28.5 mg, 74.9 µmol, 1.5 eq.) and then the mixture was stirred at room temperature overnight. The resulted mixture was purified directly by reverse-phase preparative HPLC (0.1% formic acid in water-acetonitrile) to afford methyl (S)-2-(4-(4'-(ethylcarbamoyl)-[1,1'-biphenyl]-4-yl)-2,3,9-trimethyl-6H-thieno[3,2-f][1,2,4]triazolo[4,3-a][1,4]diazepin-6-yl)acetate (**4b**) (4.9 mg, 19% yield) as a white solid. ^{1}H NMR (400 MHz, CD_3OD-*d4*) δ 7.91 (d, *J* = 8.4, 2H), 7.77-7.72 (m, 4H), 7.56 (d, *J* = 8.2 Hz, 2H), 4.64 (t, *J* = 7.2 Hz, 1H), 4.50 (s, 1H), 3.78 (s, 3H), 3.56 (d, *J* = 7.2 Hz, 2H), 3.43 (q, *J* = 7.2 Hz, 2H), 2.71 (s, 3H), 2.47 (s, 3H), 1.75 (s, 3H), 1.24 (t, *J* = 7.2 Hz, 3H). ^{13}C NMR (101 MHz, CD_3OD-*d4*) δ 173.20, 169.60, 167.08, 156.87, 152.17, 144.24, 143.66, 138.90, 135.20, 133.40, 133.22, 132.35, 132.26, 130.43, 128.93, 128.25, 128.11, 54.91, 52.41, 37.20, 35.87, 14.90, 14.38, 12.92, 11.57. LC-MS, ESI$^+$, *m/z* 528.6 $[M+H]^+$.

Synthesis of compound 4c

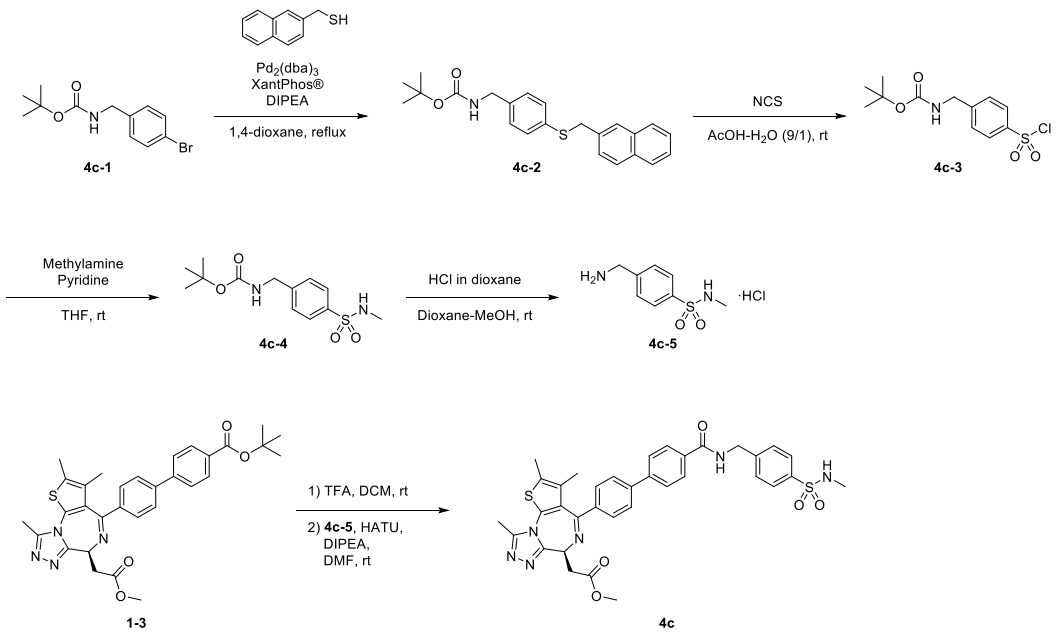

<u>*tert*-Butyl (4-((naphthalen-2-ylmethyl)thio)benzyl)carbamate (**4c-2**)</u>
To a mixture of *tert*-butyl bromobenzylcarbamate (**4c-1**) (500 mg, 1.75 mmol), naphthalen-2-ylmethanethiol (334.9 mg, 1.92 mmol, 1.1 eq.), tris(dibenzylideneacetone)dipalladium(0) (80.0 mg, 0.09 mmol, 0.05 eq.), XantPhos® (101.1 mg, 0.17 mmol, 0.1 eq.) was added DIPEA (608.7 µl, 3.49 mmol, 2.0 eq.) and 1,4-dioxane (10 ml) under nitrogen and then the mixture was stirred at 100 °C for 8 hours. The resulted mixture was concentrated in vacuo and then purified by silica gel column chromatography (heptane-ethyl acetate) to afford *tert*-butyl (4-((naphthalen-2-ylmethyl)thio)benzyl)carbamate (**4c-2**) (583.6 mg, 88% yield). ^{1}H NMR (400 MHz, $CDCl_3$) δ 7.81-7.73 (m, 3H), 7.67 (s, 1H), 7.47-7.44 (m, 3H), 7.28 (d, *J* = 8.2 Hz, 2H), 7.15 (d, *J* = 7.9 Hz, 2H), 4.76 (bs, 1H), 4.25 (s, 4H), 1.45 (s, 9H). ^{13}C NMR (101 MHz, $CDCl_3$) δ 155.96, 137.56, 135.24, 135.04, 133.46, 132.75, 130.55, 128.44, 128.11, 127.83, 127.79, 127.53, 127.08, 126.28, 125.96, 79.70, 44.40, 39.72, 28.54. LC-MS, ESI$^-$, *m/z* 377.9 [M-H]$^-$.

<u>*tert*-Butyl (4-(chlorosulfonyl)benzyl)carbamate (**4c-3**)</u>
To a solution of *tert*-butyl (4-((naphthalen-2-ylmethyl)thio)benzyl)carbamate (**4c-2**) (250 mg, 659 µmol) in acetic acid (9.0 ml) and water (1.0 ml) was added *N*-chlorosuccinimide (439.8 mg, 3294 µmol, 5.0 eq.) and then the mixture was stirred at room temperature for 1.5 hours. The resulted mixture was added to water and then the organic was extracted with toluene. The organic layer was washed with water and brine, dried over magnesium sulfate, and then purified by silica gel column chromatography (heptane-ethyl acetate) to afford *tert*-butyl (4-(chlorosulfonyl)benzyl)carbamate (**4c-3**) (57.6 mg, 29% yield). ^{1}H NMR (400 MHz, $CDCl_3$) δ 7.98 (d, *J* = 8.3 Hz, 2H), 7.52 (d, *J* = 8.3 Hz, 2H), 5.08 (bs, 1H), 4.42-4.41 (m, 2H), 1.46 (s, 9H). ^{13}C NMR (101 MHz, $CDCl_3$) δ 155.99, 147.73, 143.36, 128.30, 127.53, 80.43, 44.25, 28.50. LCMS was only detected as sulfonic acid form: LC-MS, ESI$^-$, *m/z* 285.8 [M-Cl +O]$^-$.

<u>*tert*-Butyl (4-(*N*-methylsulfamoyl)benzyl)carbamate (**4c-4**)</u>

To a solution of *tert*-butyl (4-(chlorosulfonyl)benzyl)carbamate (**4c-3**) (22.1 mg, 72.3 μmol) and pyridine (17.5 μl, 217 μmol, 3.0 eq.) in tetrahydrofuran (1.0 ml) was added 2.0 M methylamine in THF (72.3 μl, 145 μmol, 2.0 eq.) and then the mixture was stirred at room temperature overnight. After the addition of 2.0 M methylamine in THF (72.3 μl, 145 μmol, 2.0 eq.), the mixture was stirred for 2 hours. The resulted mixture was added to water and then the organic was extracted with toluene. The organic layer was washed with water and brine, dried over magnesium sulfate, and then purified by silica gel column chromatography (heptane-ethyl acetate) to afford *tert*-butyl (4-(*N*-methylsulfamoyl)benzyl)carbamate (**4c-4**) (17.6 mg, 81% yield). ^{1}H NMR (400 MHz, CD_3OD-*d4*) δ 7.78 (d, *J* = 6.4 Hz, 2H), 7.46 (d, *J* = 6.4 Hz, 2H), 4.29 (s, 2H), 2.5 (s, 3H), 1.42 (s, 9H). ^{13}C NMR (101 MHz, $CDCl_3$) δ 155.83, 147.62, 143.12, 128.12, 127.31, 80.23, 44.04, 28.31. LC-MS, ESI$^+$, *m/z* 299.6 $[M+H]^+$.

4-(Aminomethyl)-*N*-methylbenzenesulfonamide hydrochloride (**4c-5**)

To a solution of *tert*-butyl (4-(*N*-methylsulfamoyl)benzyl)carbamate (**4c-4**) (17.6 mg, 58.6 μmol) in 1,4-dioxane (293.0 μl) was added 4 M hydrogen chloride in 1,4-dioxane (293.0 μl, 1172 μmol, 20 eq.) and then the mixture was stirred at room temperature for 3.5 hours. After the addition of 4 M hydrogen chloride in 1,4-dioxane (293.0 μl, 1172 μmol, 20 eq.) and methanol (293.0 μl), the mixture was stirred for 2 hours. The resulted mixture was concentrated in vacuo and then used for next reaction without further purification.

Methyl (S)-2-(4-(4'-(ethylcarbamoyl)-[1,1'-biphenyl]-4-yl)-2,3,9-trimethyl-6H-thieno[3,2-f][1,2,4]triazolo[4,3-a][1,4]diazepin-6-yl)acetate (**4c**)

To a solution of *tert*-butyl (S)-4'-(6-(2-methoxy-2-oxoethyl)-2,3,9-trimethyl-6H-thieno[3,2-f][1,2,4]triazolo[4,3-a][1,4]diazepin-4-yl)-[1,1'-biphenyl]-4-carboxylate (**1-3**) (18.2 mg, 36.4 μmol) in DCM (0.5 mL) was added trifluoroacetic acid (0.5 mL) and then the mixture was stirred at room temperature for 2 hours. The resulted mixture was concentrated in vacuo, and then toluene was added thereto. After concentrated in vacuo again to afford the corresponding carboxylic acid. To a mixture of the carboxylic acid, 4-(aminomethyl)-*N*-methylbenzenesulfonamide hydrochloride (**4c-5**) (13.8 mg, 58.2 μmol, 1.6 eq.), and *N,N*-diisopropylethylamine (31.7 μl, 182 μmol, 5.0 eq.) in *N,N*-dimethylformamide (1.0 mL) was added HATU (24.9 mg, 65.4 μmol, 1.5 eq.) and then the mixture was stirred at room temperature overnight. After the addition of HATU (24.9 mg, 65.4 μmol, 1.5 eq.) and *N,N*-diisopropylethylamine (31.7 μl, 182 μmol, 5.0 eq.), the mixture was stirred for 2 hours. The resulted mixture was added to ammonium chloride aqueous solution and then the organic was extracted with ethyl acetate. The obtained organic extract was washed with brine, dried over magnesium sulfate, concentrated in vacuo, and then purified by silica gel column chromatography (dichloromethane-methanol). The obtained compound was purified again by reverse-phase preparative HPLC (0.1% formic acid in water-acetonitrile) to afford methyl (S)-2-(4-(4'-(ethylcarbamoyl)-[1,1'-biphenyl]-4-yl)-2,3,9-trimethyl-6H-thieno[3,2-f][1,2,4]triazolo[4,3-a][1,4]diazepin-6-yl)acetate (**4c**) (6.76 mg, 27% yield). ^{1}H NMR (400 MHz, CD_3OD-*d4*) δ 8.00-7.98 (m, 2H), 7.84-7.79 (m, 4H), 7.77-7.75 (m, 2H), 7.59-7.58 (m, 4H), 4.70 (s, 2H), 4.66 (t, J = 7.2 Hz, 1H), 4.52 (s, 1H), 3.79 (s, 3H), 3.58 (d, *J* = 7.2 Hz, 2H), 2.73 (s, 3H), 2.53 (s, 3H), 2.49 (s, 3H), 1.76 (s, 3H). ^{13}C NMR (101 MHz, CD_3OD-*d4*) δ 171.78, 168.40, 165.71, 155.44, 150.81, 144.09, 143.18, 142.16, 137.96, 137.56, 133.22, 132.02, 131.84, 130.90, 130.84, 129.07, 127.72, 127.68, 127.07, 126.89, 126.84, 53.48, 51.03, 42.71, 35.75, 27.80, 13.01, 11.53, 10.19. LC-MS, ESI$^+$, *m/z* 683.5 $[M+H]^+$.

Synthesis of compound 5

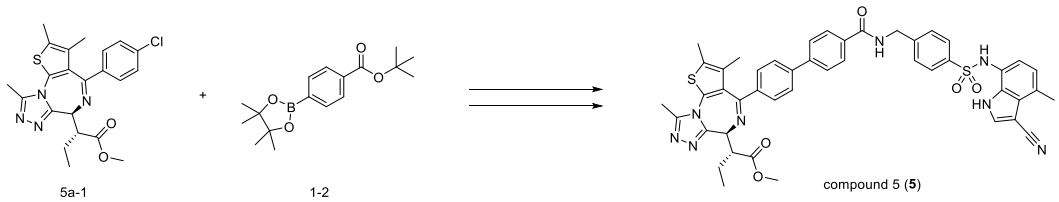

Compound 5 was synthesized according to the same procedure with **compound 1** using **5a-1**[28] instead of **1-1** .^{1}H NMR (500 MHz, CD_3OD-*d4*) δ 8.00-7.95 (m, 2H), 7.92 (s, 1H), 7.83-7.34 (m, 4H), 7.69-7.62 (m, 2H), 7.56-7.45 (m, 4H), 6.75 (m, 1H), 6.52 (m, 1H), 4.66 (s, 2H), 4.30 (d, *J* = 11.0 Hz, 1H), 3.90 (s, 3H), 3.87 (dd, *J* = 10.9, 3.7 Hz, 1H), 2.73 (s, 3H), 2.66 (s, 3H), 2.50 (s, 3H), 2.10 (m, 1H), 1.77 (s, 3H), 1.71 (m, 1H), 1.06 (t, *J* = 7.45 Hz, 3H). LC-MS, ESI$^+$, *m/z* 851.0 $[M+H]^+$.

Synthesis of DAT389

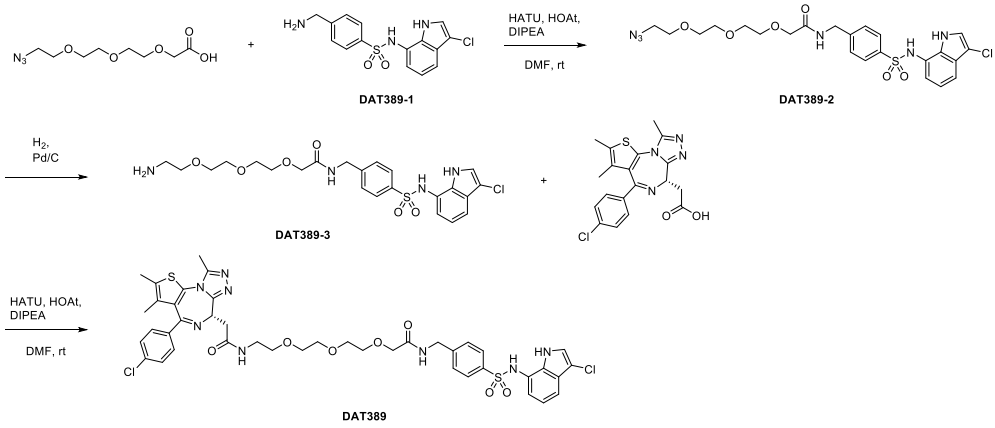

2-(2-(2-(2-Azidoethoxy)ethoxy)ethoxy)-*N*-(4-(*N*-(3-chloro-1H-indol-7-yl)sulfamoyl)benzyl)acetamide (**DAT389-2**)

To a solution of 4-(aminomethyl)-*N*-(3-chloro-1H-indol-7-yl)benzenesulfonamide (19.7 mg, 0.059 mmol), 2-[2-[2-(2-azidoethoxy)ethoxy]ethoxy]acetic acid (16.4 mg, 0.070 mmol, 1.2 eq.) (**DAT-389-1**)[10], *N,N*-diisopropylethylamine (50 µl, 0.29 mmol, 5 eq.) and 1-hydroxy-7-azabenzotriazole (6.3 mg, 0.046 mmol, 0.8 eq.) in DMF (0.5 mL) was added 1-[bis(dimethylamino)methylene]-1H-1,2,3-triazolo[4,5-b]pyridinium 3-oxid hexafluorophosphate (24.5 mg, 0.065 mmol, 1.1 eq.) at room temperature. The reaction was stirred for 1 hour. The crude mixture was then purified with reverse-phase column chromatography (0.1% formic acid in acetonitrile-water) to give 2-(2-(2-(2-azidoethoxy)ethoxy)ethoxy)-*N*-(4-(*N*-(3-chloro-1H-indol-7-yl)sulfamoyl)benzyl)acetamide (**DAT-389-2**) (19.0 mg, 0.035 mmol, 59% yield). ^{1}H NMR (400 MHz, CD_3OD-*d4*) δ 7.70-7.65 (m, 2H), 7.43-7.37 (m, 2H), 7.34 (dd, *J* = 8.0, 1.0 Hz, 1H), 7.27 (s, 1H), 6.92 (dd, *J* = 7.6, 7.6 Hz, 1H), 6.71 (dd, *J* = 7.6, 0.8 Hz, 1H), 4.50 (s, 2H), 4.08 (s, 2H), 3.74-3.66 (m, 4H), 3.63-3.57 (m, 2H), 3.57-3.52 (m, 4H), 3.30 (t, *J* = 5.1 Hz, 2H). ^{13}C NMR (101 MHz, CD_3OD-*d4*) δ 173.09, 145.37, 139.50, 131.96, 128.78, 128.63, 1128.25, 123.24, 123.18, 120.95, 119.10,

116.78, 106.29, 72.05, 71.44, 71.42, 71.36, 71.23, 70.97, 51.68, 42.94. LC-MS, ESI^+, *m/z* 551.2 $[M+H]^+$.

2-(2-(2-(2-Aminoethoxy)ethoxy)ethoxy)-*N*-(4-(*N*-(3-chloro-1H-indol-7-yl)sulfamoyl)benzyl)acetamide (**DAT389-3**)

To a solution of 2-(2-(2-(2-azidoethoxy)ethoxy)ethoxy)-*N*-(4-(*N*-(3-chloro-1H-indol-7-yl)sulfamoyl)benzyl)acetamide (19.0 mg, 0.035 mmol) in MeOH (3.0 mL) was added 10% Pd/C (2.0 mg). The reaction mixture was degassed under reduced pressure and filled with H_2 gas. After being stirred at room temperature for 2 hours, the mixture was filtered, and concentrated. The product was used in the next reaction without further purifications.

(S)-*N*-(4-(*N*-(3-Chloro-1H-indol-7-yl)sulfamoyl)benzyl)-2-(2-(2-(2-(4-(4-chlorophenyl)-2,3,9-trimethyl-6H-thieno[3,2-f][1,2,4]triazolo[4,3-a][1,4]diazepin-6-yl)acetamido)ethoxy)ethoxy)ethoxy)acetamide (**DAT389**)

To a solution of 2-(2-(2-(2-aminoethoxy)ethoxy)ethoxy)-*N*-(4-(*N*-(3-chloro-1H-indol-7-yl)sulfamoyl)benzyl)acetamide (0.035 mmol), (S)-2-(4-(4-chlorophenyl)-2,3,9-trimethyl-6H-thieno[3,2-f][1,2,4]triazolo[4,3-a][1,4]diazepin-6-yl)acetic acid (14.0 mg, 0.035 mmol, 1.0 eq.), *N,N*-diisopropylethylamine (13.5 µl, 0.10 mmol, 3.0 eq.), and 1-hydroxy-7-azabenzotriazole (4.6 mg, 0.035 mmol, 1.0 eq.) in DMF (0.5 mL) was added 1-[bis(dimethylamino)methylene]-1H-1,2,3-triazolo[4,5-b]pyridinium 3-oxid hexafluorophosphate (13 mg, 0.035 mmol, 1.0 eq.) at room temperature. The reaction was allowed to stir for 1 hour. Then the mixture was purified with reverse-phase preparative HPLC chromatography (0.1% formic acid in acetonitrile-water) to give (S)-*N*-(4-(*N*-(3-chloro-1H-indol-7-yl)sulfamoyl)benzyl)-2-(2-(2-(2-(2-(4-(4-chlorophenyl)-2,3,9-trimethyl-6H-thieno[3,2-f][1,2,4]triazolo[4,3-a][1,4]diazepin-6-yl)acetamido)ethoxy)ethoxy)ethoxy)acetamide (**DAT389**) (10.1 mg, 0.011 mmol, 32% yield). ^1H NMR (400 MHz, CD_3OD-*d4*) δ 7.58-7.57 (m, 2H), 7.46-7.38 (m, 4H), 7.33-7.29 (m, 3H), 7.25 (s, 1H), 6.89 (t, *J* = 7.7 Hz, 1H), 6.70 (dd, *J* = 7.53, 0.77 Hz, 1H), 4.66 (dd, *J* = 8.8, 5.5 Hz, 1H), 4.45 (s, 2H), 4.08 (s, 2H), 3.74-3.67 (m, 4H), 3.64-3.61 (m, 2H), 3.60-3.53 (m, 4H), 3.49-3.30 (m, 4H), 2.69 (s, 3H), 2.46 (s, 3H), 1.69 (s, 3H). ^{13}C NMR (106 MHz, CD_3OD-*d4*) δ 173.9, 167.1, 157.9, 153.1, 146.2, 140.5, 139.0, 138.9, 134.4, 134.1, 132.92, 132.89, 132.8, 132.2, 130.7, 129.7, 129.4, 129.1, 124.3, 124.1, 121.9, 119.9, 117.5, 107.2, 72.9, 72.4, 72.3, 72.2, 72.1, 71.5, 56.1, 43.9, 41.4, 39.7, 15.3, 13.8, 12.5. LC-MS, ESI^+, *m/z* 906.9 $[M+H]^+$.

2. Biology

Plasmids and oligonucleotides

The design and construction of the human CRL-focused sgRNA library used for BRD4 stability screens, lentiviral sgRNA expression vectors used for single gene knockouts, as well as viral vectors used for the engineering of inducible Cas9 cell lines have been described previously[18,19]. For the engineering of the fluorescent protein stability reporters, BRD4(S) (Twist Bioscience), BRD2 (Addgene plasmid # 65376) or BRD3 (Addgene plasmid # 65377; both gifts from Kyle Miller[53]) was cloned into a pRRL lentiviral vector, fused to 3x V5-tags and mTagBFP, and coupled to mCherry for normalization. For knockout/rescue studies, DCAF16 open reading frame cDNA (Twist Bioscience) was synonymously mutated to remove the sgRNA protospacer adjacent motif and seed sequence, coupled to a FLAG-Tag and cloned into a pRRL lentiviral vector expressing iRFP670 for flow cytometric detection. All plasmids and sgRNAs used in this study are shown in Extended Data Table 1, and the CRL-focused sgRNA libraries used for FACS-based and viability-based CRISPR/Cas9 screens, are shown in Supplementary Table 1 and Supplementary Table 3, respectively.

Cell culture

HEK293(T) and HCT-116 cell lines, originally sourced from ATCC, were provided by the MRC PPU reagents facility at the University of Dundee. HEK293, Lenti-X 293T lentiviral packaging cells (Clontech) and HCT-116 were cultured in DMEM (Gibco) supplemented with 10% fetal bovine serum (FBS; Thermo Fisher), 100 U/ml penicillin/streptomycin (Thermo Fisher) and 2 mM L-glutamine (Thermo Fisher). MV4;11 and KBM7 cells were cultured in IMDM (Gibco), supplemented with the same additives as above. All cell lines were grown in a humidified incubator at 37ºC and 5% CO_2 and routinely tested for mycoplasma contamination.

Lentivirus production and transduction

Semiconfluent Lenti-X cells were co-transfected with lentiviral plasmids, the lentiviral pCMVR8.74 helper (Addgene plasmid # 22036) and pMD2.G envelope (Addgene plasmid # 12259; both gifts from Didier Trono) plasmids using polyethylenimine (PEI) transfection (PEI MAX® MW 40,000, Polysciences) as previously described. Virus containing supernatant was clarified by centrifugation. Target cells were infected at limiting dilutions in the presence of 4 μg ml^{-1} of polybrene (Santa Cruz Biotechnology).

CRISPR/Cas9 DCAF15 KO cell line generation

DCAF15 KO cell line was generated using HCT-116 cells via ribonuclear protein (RNP) transfection using gRNAs targeting both exon 2 and exon 4 (IDT) (Extended Data Table 1), spCas9 Nuclease V3 (IDT) and TransIT-X2® (Mirus Bio). Following initial transfection for 48

hours, cells were trypsinized and re-plated in 96-well plates at low density and allowed to grow for > 2 weeks. Single colonies were then isolated and expanded, and later verified for DCAF15 KO via western blotting using an optimised RBM39 degradation assay as well as via genomic DNA sequencing (Supplementary Fig. 1).

CRISPR/Cas9 HiBiT and BromoTag knock-in cell line generation

HiBiT BRD2, BRD3 and BRD4 cell lines were generated via RNP transfection of (IDT), single-stranded DNA oligonucleotides as the ssODN donor templates (IDT), spCas9 (Sigma Aldrich) and target-specific gRNA (IDT) (Extended Data Table 1). HEK293 cells were resuspended in buffer R (ThermoFisher), along with the RNP complex and ssODN template, which were then subsequently electroporated using a 10 µL neon electroporation cuvette tip (ThermoFisher). Immediately following electroporation, cells were added to pre-warmed DMEM supplemented with 10% (v/v) FBS (100 U/ml penicillin/streptomycin additionally added for BromoTag cell lines only). Edited pools were analysed for HiBiT insertion by assaying for luminescence on a PHERAstar spectrophotometer (BMG Labtech) 48–72 h post-electroporation. Successful knock-in of HiBiT three days post-electroporation was first established using Promega's HiBiT lytic assay on the mixed cell population. Following identification of luminescent signal these cells underwent single cell sorting using an SH800 cell sorter (Sony Biotechnology). Single cells were sorted into 3 × 96 well plates per experiment in 200 µL of 50% filtered preconditioned media from healthy cells and 50% fresh DMEM. After two weeks, all visible colonies were expanded, validated using Promega's HiBiT lytic assay and subsequently frozen down.

BromoTag cell lines were generated in HEK293 cells via simultaneous transfection of two vectors at a 4:1 reagent: DNA ratio with FuGENE 6 (Promega). The first vector was a pMK-RQ vector containing 500 bp homology arms on either side of either an eGFP-IRES-BromoTag or eGFP-IRES-HiBiT-BromoTag sequence for integration into MCM4 and BRD4, respectively (Extended Data Table 1). The second vector was a custom pBABED vector harbouring a U6-sgRNA, Cas9 and puromycin expression cassettes. MRC-PPU CRISPR services constructed these plasmids at the University of Dundee. Following transfection, cells were repeatedly washed with PBS and then treated with one µg/ml of puromycin over a week before FACS sorting. Single cell clones were generated by FACS sorting of single GFP^+ cells using an SH800 cell sorter and sorting between 2-10 × 96 well plate in 200 µL of 50% filtered preconditioned media from healthy cells and 50% fresh.

siRNA-mediated knockdown

Cells were transfected for 48-hours using ON-TARGETplus SMARTPool siRNAs for DCAF15, DCAF16, DDB1, RBX1, CUL4A, and CUL4B (all from Dharmacon) and RNAiMAX (Invitrogen) following the manufacturer's instructions, with 35 pmol of siRNA per well in 6-well plates. When using targeting 2 genes, half the amount of siRNA was used for each gene.

Cell viability assay

MV4;11, HCT-116 or KBM7 cells were plated in 96-well plates at a density of $0.5x10^6$ (MV4;11 and HCT-116) or $0.1x10^6$ (KBM7) cells/ml in 50 µl cell suspension per well. The following day, 2x stocks of compounds were added for a final volume of 100 µl. Cells were treated for 24 (MV4;11), 72 (KBM7) or 96 (HCT-116) hours in a humidified incubator at 37ºC and 5% CO_2. CellTiter-Glo (G7570, Promega) or CellTiter-Glo® 2.0 reagent (G924A, Promega) was then added to the plates per manufacturer instructions, before shaking the plate for 3-20 minutes at 300 rpm and measuring the luminescence using a PHERAstar (BMG Labtech) or VICTOR X3 (Perkin Elmer) multilabel plate reader. The results were normalised to DMSO controls and analysed using Graphpad Prism (v9.3.1 or v9.5.0) to derive EC_{50} values by 4-parameter non-linear regression curve fitting or interpolation of a sigmoidal standard curve.

Degradation assays and western blotting

HEK293 and HCT-116 cells were plated in 6-well plates at varying densities ($0.2\text{-}0.6x10^6$ cells/ml) depending on experimental set up. In all experiments, media was changed prior to compound treatment. Stock solutions of all compounds were prepared in DMSO at a concentration of 10 mM and stored at -20ºC. Working dilutions were made fresh using DMEM media and added dropwise to 6-well plates. For competition assays cells were plated in 6-well plates and pre-treated with 10 µM of the competition compounds, 3 µM MLN4924 or 50 µM MG132 for 1 hour, before treating with PROTAC **1** at 10nM or PROTAC **2** at 100 nM for 2 hours. The six-well plates were incubated at 37ºC and 5% CO_2 for the duration of the experiment.

For all experiments, cells were washed once with ice-cold PBS before lysing for 15 minutes on ice with RIPA buffer supplemented with Benzonase (Sigma or 70746, Millipore) and cOmplete™, EDTA-free Protease Inhibitor Cocktail (11873580001, Roche). Following centrifugation, lysates were used for protein concentration determined using the Pierce™ BCA Protein Assay (23225, Fisher Scientific) and typically 30 µg of lysate was prepared using 4x LDS sample buffer (Thermo Fisher) and 10% 2-Mercaptoethanol or 50 mM dithiothreitol (DTT) and loaded per lane of NuPAGE 4-12% bis-tris gels (Thermo Fisher). Proteins were transferred to nitrocellulose membranes, blocked for 1 hour in 5% milk TBS-T at room temperature, before incubating with primary antibodies overnight. The following primary antibodies were used: BRD2 (no. Ab139690, Abcam), BRD3 (no. Ab50818, Abcam), BRD4 (E2A7X, no. 13440, Cell Signaling Technology and no. Ab128874, Abcam), BromoTag (no. NBP3-17999, Novus Biologicals), CUL4A (no. A300-738A, Bethyl Laboratories), CUL4B (no. 12916-1-AP, Proteintech), DDB1 (no. A300-462A, Bethyl Laboratories), MCM4 (no. ab4459, Abcam) RBM39 (no. HPA001591, Atlas Antibodies), RBX1 (D3J5I, no. #11922, Cell Signalling Technology), β-Actin (AC-15, no. A5441, Sigma-Aldrich), α-Tubulin (DM1A, no. T9026, Sigma-Aldrich). Membranes were then washed in TBS-T and incubated with fluorescent or HRP-conjugated secondary antibodies for 1 hour at room temperature, before further washes and imaging on a ChemiDoc Touch imaging system (Bio-Rad). Secondary antibodies used were HRP anti-rabbit IgG (7074, Cell Signaling Technology), HRP anti-mouse IgG (7076, Cell Signaling Technology), IRDye®

680RD anti-mouse (no. 926-68070, Li-Cor), IRDye® 800CW anti-rabbit (no. 926-32211, Li-Cor), StarBright™ blue 520 goat anti-mouse (no. 12005866, Biorad) and hFABTM rhodamine anti-tubulin (no. 12004165, Biorad).

HiBiT degradation assays

Endogenously tagged HiBiT cells were plated in 96-well plates (PerkinElmer) at a density of $0.5x10^6$ cells/ml, with 50 µl of cell suspension per well. The following day, 2x stocks of compounds were added for a final volume of 100 µl. Cells were treated for 5 or 6 hours before lysing using the HiBiT lytic assay buffer (Promega) per manufacturer instructions. Plates were then read on a BMG Pherastar® plate reader for luminescence detection. Treated wells were normalised to a DMSO-only control and analysed using GraphPad Prism 9 via fitting of non-linear regression curves for extraction of DC_{50} and D_{MAX} values.

Kinetic ubiquitination and degradation assays

For kinetic ubiquitination assays, HiBiT-tagged 293 cells were initially seeded in 6-well plates at a density of $8x10^6$ cells/ml in 2 ml volume. After 5 hours, LgBiT and Halo-Ub cDNA (Promega) were transfected using FuGENE HD (Promega) with 1 µg of each plasmid at a 3:1 transfection reagent:plasmid ratio. The following day, cells were trypsinized and re-suspended in phenol-red free OptiMEM (Gibco) supplemented with 4% FBS and seeded in 96-well plates at a density of $3.5x10^5$ cells/ml in the presence or absence of 0.1 mM HaloTag NanoBRET™ ligand (Promega). Following overnight incubation, media was removed from the wells and replaced with 90 µl OptiMEM (4% FBS) with a 1:100 dilution of Vivazine substrate. The plate was then at 37°C for a further hour before 10X stocks of experimental compounds were added and the plate was read on a GloMAX® Discover microplate reader (Promega) in kinetic mode for NanoBRET ratio metric (460 nM donor and 618 nm acceptor emissions) signal detection for 6 hours, with measurements taken every 3-5 minutes. Data was processed by subtracting NanoBRET ligand-free controls before plotting NanoBRET signal versus time in GraphPad Prism 9.

Kinetic degradation assays were performed as previously described[54], using the HiBiT-tagged cells with exogenous LgBiT transfection the same as described above for the kinetic ubiquitination assays. Endurazine substate was used (1:100) and incubated for 2.5 hours at 37°C prior to 10X compound addition, with luminescence measurements taken using the same GloMAX® Discover microplate reader (Promega) every 15 minutes for 24 hours. Data were normalised to DMSO-only controls and plotted for luminescence signal versus time in GraphPad Prism 9.

FACS-based CRISPR/Cas9 BRD4 stability screens

For pooled FACS-based CRISPR–Cas9 BRD4 protein stability screens, a CRL-focused sgRNA library[19] was lentivirally packaged using polyethylenimine (PEI MAX® MW 40,000,

Polysciences) transfection of Lenti-X cells and the lentiviral pCMVR8.74 helper (Addgene plasmid # 22036) and pMD2.G envelope (Addgene plasmid # 12259; both gifts from Didier Trono) plasmids. The virus containing supernatant was cleared of cellular debris by filtration through a 0.45-µm PES filter and used to transduce KBM7 BRD4-BFP reporter cells harbouring a doxycycline inducible Cas9 allele at a multiplicity of infection (MOI) of 0.05 and 1,000-fold library representation. Library-transduced cells were selected with G418 (1 mg ml^{-1}, Gibco) for 14 days, expanded and Cas9 expression was induced with DOX (0.4 µg ml^{-1}, PanReac AppliChem).

3 days after Cas9 induction, 25 million cells per condition were treated with DMSO (1:1000), MZ1 (10 nM), compound 1 (1 nM) or GNE-0011 (1 µM) for 6 hours in two biological replicates. Cells were washed with PBS, stained with Zombie NIR™ Fixable Viability Dye (1:1000, BioLegend) and APC anti-mouse CD90.1/Thy-1.1 antibody (1:400, BioLegend) in the presence of Human TruStain FcX™ Fc Receptor Blocking Solution (1:400, BioLegend), and fixed with 0.5 mL methanol-free paraformaldehyde 4% (Thermo Scientific™ Pierce™) for 30 min at 4 ºC, while protected from light. Cells were washed with, and stored in FACS buffer (PBS containing 5% FBS and 1 mM EDTA) at 4 ºC over night. The next day, cells were strained trough a 35 µm nylon mesh and sorted on a BD FACSAria™ Fusion (BD Biosciences) using a 100 µm nozzle. Aggregates, dead (ZombieNIR positive), Cas9-negative (GFP) and sgRNA library-negative (Thy1.1-APC) cells were excluded, and the remaining cells were sorted based on their BRD4-BFP and mCherry levels into BRD4HIGH (8-10% of cells), BRD4MID (25-30%) and BRD4LOW (8-10%) fractions. For each sample, cells corresponding to at least 1,500-fold library representation were sorted per replicate.

Next-generation sequencing (NGS) libraries of sorted cell fractions were prepared as previously described[18]. In brief, genomic DNA was isolated by cell lysis (10 mM Tris-HCl, 150 mM NaCl, 10 mM EDTA, 0.1% SDS), proteinase K treatment (New England Biolabs) and DNAse-free RNAse digest (Thermo Fisher Scientific), followed by two rounds of phenol extraction and 2-propanol precipitation. Isolated genomic DNA was subjected to several freeze–thaw cycles before nested polymerase chain reaction (PCR) amplification of the sgRNA cassette.

Barcoded NGS libraries for each sorted population were generated using a two-step PCR protocol using AmpliTaq Gold (Invitrogen. The resulting PCR products were purified using Mag-Bind® TotalPure NGS beads (Omega Bio-tek) and amplified in a second PCR introducing the standard Illumina adapters. The final Illumina libraries were bead-purified, pooled and sequenced on a HiSeq 3500 platform (Illumina).

Screen analysis was performed as previously described[18]. Briefly, sequencing reads were quantified using the crispr-process-nf Nextflow workflow, available at https://github.com/ZuberLab/crispr-process-nf/tree/566f6d46bbcc2a3f49f51bbc96b9820f408ec4a3. For statistical analysis, we used the crispr-mageck-nf Nextflow workflow, available at https://github.com/ZuberLab/crispr-mageck-nf/tree/c75a90f670698bfa78bfd8be786d6e5d6d4fc455. To calculate gene-level

enrichment, the sorted populations (BRD4HIGH or BRD4LOW) were compared to the BRD4MID populations in MAGeCK (0.5.9)[27], using median normalized read counts.

Viability-based CRISPR/Cas9 screen

The ubiquitin/Nedd8 system CRISPR-KO library (Supplementary Table 3) was generated using the covalently-closed-circular-synthesized (3Cs) technology, as previously described[55,56]. The library contained 3,347 gRNAs cloned under the U6 promoter in a modified pLentiCRISPRv2-puromycin vector containing a modified gRNA scaffold sequence starting with GTTTG. Each gene was represented by 4 gRNAs selected with the Broad Institute CRISPick tool[57-59]. Additionally, the library included a set of essential genes, non-targeting as well as AAVS1-targeting control sgRNAs.

HCT-116 cells were transduced with the ubiquitin/Nedd8 system lentiviral CRISPR-Cas9 library at an MOI 0.5 and a coverage of 500. Cells were selected with 1 μg/ml puromycin for 12 days. Eight million selected cells per condition were then plated in T175 flasks. Cells were treated with DMSO or compound **1** (58 nM), corresponding to 4 times the IC50 value for 3 days, followed by replating and treatment for additional 3 days. After a total of 6 days of treatment, cells were trypsinized, washed three times with PBS, followed by genomic DNA isolation. Sequencing libraries were prepared via PCR as previously described[56] and purified via GeneJET Gel Extraction Kit (Thermo Fisher Scientific).

Raw sequencing data were demultiplexed with bcl2fastq v2.20.0.422 (Illumina) to generate raw fastq files. To determine the abundance of individual gRNAs per samples, the fastq files were trimmed using cutadapt 2.8 to retain only the putative gRNA sequences. These sequences were then aligned to the original gRNA library with Bowtie 2.3.0 and only perfect matches were counted. Statistical analysis was performed via MAGeCK[27], using median or total read count normalization and removal of gRNAs with zero counts in the control samples. Genes with a LFC > 1 or < -1 and a p-value < 0.01 were labelled as significantly depleted or enriched hits.

Flow-cytometric BRD4 reporter assay

KBM7 iCas9 cells were transduced with lentivirus expressing WT, mutated or truncated versions of SFFV-BRD4(S)-mTagBFP-P2A-mCherry to generate stable reporter cell lines. For evaluation of reporter degradation, cells were treated with DMSO (1:1000), GNE-0011 (1 μM), compound **1** (1 nM) or dBET6 (10 nM) for 6 hours before flow cytometry analysis on an LSRFortessa (BD Biosciences).

To quantify the influence of genetic perturbation on compound-induced reporter degradation, stable BRD4(S) or BRD4^{Tandem} reporter cell lines were transduced with a lentiviral sgRNA (pLenti-U6-sgRNA-IT-EF1αs-Thy1.1-P2A-NeoR) and/or transgene expression vector (pRRL-SFFV-3xFLAG-DCAF16-EF1αs-iRFP670) to 30-50% transduction

efficiency. Cas9 expression was induced with docycycline (0.4 µg ml^{-1}) for 3days, followed by 6 hours of degrader treatment. Cells were stained for sgRNA expression with an APC conjugated anti-mouse -CD90.1/Thy1.1 antibody (#202526, Biolegend; 1:400) and Human TruStain FcX Fc receptor blocking solution (#422302, Biolegend; 1:400) for 5 minutes in FACS buffer (PBS containing 5% FBS and 1 mM EDTA) at 4°C. Cells were washed and resuspended in FACS buffer and analyzed on an LSRFortessa (BD Biosciences.

Flow cytometric data analysis was performed in FlowJo v10.8.1. BFP and mCherry mean fluorescence intensity (MFI) values for were normalized by background subtraction of the respective values from reporter-negative KBM7 wild type cells. BRD4 abundance was calculated as the ratio of background subtracted BFP to mCherry MFI, and is displayed normalized to DMSO treated, sgRNA/cDNA double negative cells.

Quantitative proteomics

For unbiased identification of degrader target proteins, 50x10^6 KBM7 iCas9 cells per condition were treated with DMSO (1:1000), compound **1** (1 nM), GNE-0011 (1 µM) or dBET6 (10 nM) for 6 hours in biological triplicates. Cells were harvested via centrifugation, washed three times in ice-cold PBS and snap-frozen in liquid nitrogen. Cell pellet were lysed in 500 µl of freshly prepared lysis buffer (50 mM HEPES pH 8.0, 2% SDS, 1 mM PMSF and protease inhibitor cocktail (Sigma-Aldrich)). Samples incubated at RT for 20 minutes before heating to 99 °C for 5 min. DNA was sheared by sonication using a Covaris S2 high performance ultrasonicator. Cell debris was removed by centrifugation at 16,000 × g for 15 min at 20 °C. Supernatant was transferred to fresh tubes and protein concentration determined using the BCA protein assay kit (Pierce Biotechnology). Filter-aided sample preparation (FASP) was performed using a 30 kDa molecular weight cutoff centrifugal filters (Microcon 30, Ultracel YM-30, Merck Millipore) as previously described[60]. In brief, 200 µg of total protein per sample was reduced by the addition of DTT to a final concentration of 83.3 mM, followed by incubation at 99°C for 5 minutes. Samples were mixed with 200 µL freshly prepared 8 M urea in 100 mM Tris-HCl (pH 8.5) (UA-solution) in the filter unit and centrifuged at 14.000 × g for 15 min at 20 °C to remove SDS. Residual SDS was washed out by a second wash step with 200 µL UA. Proteins were alkylated with 100 µl of 50 mM iodoacetamide in the dark for 30 min at RT. Thereafter, three washes were performed with 100 µl of UA solution, followed by three washes with 100 µl of 50 mM TEAB buffer (Sigma-Aldrich). Proteolytic digestion was performed using trypsin (1:50) overnight at 37°C. Peptides were recovered using 40 µL of 50 mM TEAB buffer followed by 50 µL of 0.5 M NaCl. Peptides were desalted using the Pierce™ Peptide Desalting Spin Columns (Thermo Scientific). TMTpro 16plex Label Reagent Set was used for labeling according to the manufacturer (Pierce,). After the labeling reaction was quenched, the samples were pooled, the organic solvent removed in a vacuum concentrator, and the labeled peptides purified by C18 solid phase extraction (SPE).

For offline fractionation via reverse phase (RP) HPLC at high pH as previously described, tryptic peptides were re-buffered in 10 mM ammonium formate buffer (pH 10). Peptides were

separated into 96 time-based fractions on a Phenomenex C18 RP column (150 × 2.0 mm Gemini-NX, 3 µm C18 110Å, Phenomenex) using an Agilent 1200 series HPLC system fitted with a binary pump delivering solvent at 50 µL/min. Acidified fractions were consolidated into 36 fractions via a concatenated strategy as previously described[61]. After removal of solvent in a vacuum concentrator, samples were reconstituted in 0.1% TFA prior to LC-MS/MS analysis.

Mass spectrometry analysis was performed on an Orbitrap Fusion Lumos Tribrid mass spectrometer coupled to a Dionex Ultimate 3000 RSLCnano system (via a Nanospray Flex Ion Source (all ThermoFisher Scientific) interface and operated via Xcalibur Version 4.3.73.11 and Tune 3.4.3072.18. Peptides were loaded onto a trap column (PepMap 100 C18, 5 µm, 5 × 0.3 mm, ThermoFisher Scientific) at a flow rate of 10 µL/min using 0.1% TFA as loading buffer. After loading, the trap column was switched in-line with an Acclaim PepMap nanoHPLC C18 analytical column (2.0 µm particle size, 75µm IDx500mm, # 164942, ThermoFisher Scientific). The column temperature was maintained at 50 °C. Mobile phase A consisted of 0.4% formic acid (FA) in water, and mobile phase B consisted of 0.4% FA in a mixture of 90% acetonitrile and 10% water. Separation was achieved using a four-step gradient over 90 min at a flow rate of 230 nL/min. In the liquid junction setup, electrospray ionization was enabled by applying a voltage of 1.8 kV directly to the liquid being sprayed, and non-coated silica emitter was used. The mass spectrometer was operated in a data dependent acquisition (DDA) mode using a maximum of 20 dependent scans per cycle. Full MS1 scans were acquired in the Orbitrap with a scan range of 400 - 1600 m/z and a resolution of 120,000 at 200m/z. Automatic gain control (AGC) was set to ‘standard’ and a maximum injection time (IT) of 50 ms was applied. MS2 spectra were acquired in the Orbitrap at a resolution of 50,000 at 200 m/z with a fixed first mass of 100 m/z. To achieve maximum proteome coverage, a classical tandem MS approach was chosen instead of the available synchronous precursor selection (SPS)-MS3 approach. To minimize TMT ratio compression effects by interference of contaminating co-eluting isobaric peptide ion species, precursor isolation width in the quadrupole was set to 0.5 Da and an extended fractionation scheme applied. Monoisotopic peak determination was set to ‘peptides’ with inclusion of charge states between 2 and 5. Intensity threshold for MS2 selection was set to 2.5×10^4. Higher energy collision induced dissociation (HCD) was applied with a normalized collision energy (NCE) of 34%. Normalized AGC was set to 200% with a maximum injection time of 86 ms. Dynamic exclusion for selected ions was 90 s.

The acquired raw data files were processed using Proteome Discoverer v.2.4.1.15, via TMT16plex quantification method. Sequest HT database search engine and the Percolator validation software node were used to remove false positives with FDR 1% at the peptide and protein level. All MS/MS spectra were searched against the human proteome (Canonical, reviewed, 20 304 sequences) and appended known contaminants and streptavidin, with a maximum of two allowable miscleavage sites. The search was performed with full tryptic digestion with or without deamidation on amino acids asparagine, glutamine, and arginine. Methionine oxidation and protein N-terminal acetylation, as well as methionine loss and protein N-terminal acetylation with methionine loss were set as variable

modifications, while carbamidomethylation of cysteine residues and tandem mass tag (TMT) 16-plex labeling of peptide N termini and lysine residues were set as fixed modifications. Data were searched with mass tolerances of ±10 ppm and ±0.025 Da for the precursor and fragment ions, respectively. Results were filtered to include peptide spectrum matches with Sequest HT cross-correlation factor (Xcorr) scores of ≥1 and high peptide confidence assigned by Percolator. MS2 signal-to-noise (S/N) values of TMTpro reporter ions were used to calculate peptide/protein abundance values. Peptide spectrum matches with precursor isolation interference values of ≥70% and average TMTpro reporter ion S/N ≤10 were excluded from quantification. Both unique and razor peptides were used for TMT quantification. Correction of isotopic impurities was applied.

Data were normalized to total peptide abundance and scaled “to all average”. Abundances were compared to DMSO treated cells and protein ratios were calculated from the grouped protein abundances using an ANOVA hypothesis test. Adjusted p-values were calculated using the Benjamini-Hochberg method. Proteins with less than three unique peptides detected were excluded from downstream analysis.

Protein construction, expression and purification

His_6-BRD4 bromodomain 1 ($BRD4^{BD1}$) (amino acids 44-178) and His_6-BRD4 bromodomain 2 ($BRD4^{BD2}$) (amino acids 333-460) were expressed in *Escherichia coli* (*E. Coli)* BL21(DE3) at 18ºC for 20 hours using 0.2 mM IPTG and purified as described previously[23]. Briefly, N-terminally His_6-tagged $BRD4^{BD1}$ and $BRD4^{BD2}$ were purified by Ni-affinity chromatography and SEC. His_6 tag cleavage and reverse Ni-affinity was performed for some applications, for others the tag was left on.

His_6-SUMO-$BRD4^{Tandem}$ (residues 1-463) was prepared as previously described[54]. Briefly, protein was expressed in *E. coli* BL21(DE3) sequentially by nickel affinity on a HisTrap HP 5 mL column (GE Healthcare), His_6 tag cleavage by SENP1 reverse nickel-affinity, cation exchange on a HiTrap SP HP 5 mL column, and size exclusion on a HiLoad 16/600 Superdex 200 pg column. Concentrated protein in 20 mM HEPES pH 7.5, 100 mM sodium chloride, 1 mM TCEP was aliquoted and flash frozen in LN2 then stored at -80°C.

His_{10}-3C-$BRD4^{Tandem}$ was cloned into pRSF-DUET with N-terminal 10xHis-HRV3C and modified pGEX4T1 with 10xHis-GST-TEV at the N-terminus. His_{10}-3C-$BRD4^{Tandem}$ was expressed in *E. coli* BL21(DE3), with IPTG induction (0.35 mM) at OD_{600} ~0.8, and grown overnight at 18°C. Cells were harvested by centrifugation, resuspended in IMAC buffer A (25mM Sodium Phosphate, 500 mM NaCl, 80 mM imidazole, 1 mM TCEP, pH 7.5), and lysed at 15,000 psi using a CF1 Cell Disruptor (Constant Systems). The lysate was cleared by spinning at 19,000 rpm for 30 min at 4 °C, syringe filtered using a 0.45 µm filter. The lysate was loaded on to a 5 ml His-Trap HP column (Cytiva) and washed for 25 cv in IMAC buffer A, and eluted with 100% IMAC buffer B (25mM Sodium Phosphate, 500 mM NaCl,

450 mM imidazole, 1 mM TCEP, pH 7.5). The elution was dialyzed against (25 mM TRIS, 250 mM NaCl, 1 mM TCEP, pH 7.0) overnight at 4 °C in 3,500 MWCO SnakeSkin (Thermo Fisher). $BRD4^{Tandem}$ (residues 42-460) was then concentrated in 10,000 MWCO Amicon centrifugal filter unit (Merck Millipore) and loaded on a 16/600 Superdex 75 SEC column (GE LifeSciences) pre-equilibrated in SEC buffer (20 mM HEPES, 250 mM NaCl, 0.5 mM TCEP, pH 7.5). Fractions containing pure $BRD4^{Tandem}$ were confirmed by SDS-PAGE and concentrated to 50 µM using a 10,000 MWCO Amicon and protein aliquots were stored at -80 °C until use.

For Cryo-EM, His_{12}-GST-TEV-$BRD4^{Tandem}$ (residues 43-459) expression in *E. coli* BL21(DE3) cells was induced at OD_{600} = 2 with 0.5 mM IPTG at 20°C for 16 hours. Cells were harvested by centrifugation and resuspended in 50 mM HEPES pH 7.5, 500 mM NaCl, 20 mM Imidazole, 0.5 mM TCEP (10 mL/g pellet weight) supplemented with DNAse and 1 cOmplete EDTA-free Protease Inhibitor Cocktail tablet (Roche) per 2 L of culture. Cells were lysed at 30 kpsi using a CF1 Cell Disruptor (Constant Systems Ltd) and lysate was clarified by centrifugation. Lysate was filtered through a BioPrepNylon Matrix Filter (BioDesign) then incubated with 1 mL Ni-NTA resin per litre culture for 1 hour. The lysate-resin slurry was poured into a Bio-Rad Econo-column and resin was washed with buffer (50 mM HEPES pH 7.5, 150 mM NaCl, 20 mM Imidazole, 0.5 mM TCEP). Bound protein was eluted with high imidazole buffer (50 mM HEPES pH 7.5, 150 mM NaCl, 500 mM Imidazole, 0.5 mM TCEP) then incubated with 1 mL glutathione agarose resin per litre culture for 30 mins. The mixture was poured into an Econo-column and resin was washed with buffer (20 mM HEPES pH 7.5, 150 mM NaCl, 0.5 mM TCEP). TEV protease was added to the resin slurry for on-bead cleavage and the column was incubated overnight on a roller at 4°C. Protein was eluted from the column then concentrated and run on a HiLoad 16/600 Superdex 75 pg column. Fractions containing protein were pooled, concentrated and aliquoted then flash frozen in LN2 then stored at -80°C until use.

DCAF15Δpro with N-terminal His6-TEV-Avi tag, DDB1ΔBPB (residues 396-705 replaced with a GNGNSG linker), and full-length DDA1 coding sequences were cloned into a pFastBacDual vector. Bacmid was generated using the Bac-to-Bac baculovirus expression system (Thermo Fisher Scientific). Baculovirus was generated via an adapted single-step protocol[62,63]. Briefly, bacmid (1 µg/mL culture volume) was mixed with 2 µg PEI 25K (Polysciences, Inc.) per µg bacmid in 200 µL warm PBS and incubated at RT for 30 mins. The mixture was added to a suspension culture of Sf9 cells at 1 x 10^6 cells/mL in Sf-900™ II SFM (Gibco) and incubated at 27°C with shaking at 110 rpm. Viral supernatant (P0) was harvested after 4-6 days. For expression, *Spodoptera* frugiperda cells (Sf9) were grown to densities between 1.9-3.0 x 10^6 cells/mL in Sf-900™ II SFM (Gibco) and infected with a total virus volume of 1% per 1 x 10^6 cells/mL. Cells were incubated at 27°C in 2 L Erlenmeyer flasks (~500 mL culture/flask) with shaking at 110 rpm for 48 hours. Cells were spun at 1,000 x g for 10 mins and supernatant was discarded. Pellets were resuspended in lysis buffer (50 mM HEPES pH 7.5, 200 mM NaCl, 2 mM TCEP) with magnesium chloride (to 2 mM), benzonase (to 1 µg/mL) and cOmplete EDTA-free Protease Inhibitor Cocktail (Roche, 2 tablets/L initial culture volume). The suspension was frozen and stored at -80°C, and then thawed. Cell suspensions were sonicated and lysates were centrifuged at 40,000 rpm for 30

mins. The supernatant was incubated with 1.5 mL Ni-NTA agarose resin (Qiagen) on a roller at 4°C for 1.5 hour. The lysate-resin slurry was loaded into a glass bench top column. Supernatant was allowed to flow through then the resin was washed with wash buffer (50 mM HEPES pH 7.5, 200 mM NaCl, 2 mM TCEP, 20 mM imidazole). Bound protein was eluted with elution buffer (50 mM HEPES pH 7.5, 200 mM NaCl, 2 mM TCEP, 500 mM imidazole). TEV protease was added to protein and dialyzed with buffer (50 mM HEPES pH 7.5, 200 mM NaCl, 2 mM TCEP). Cleaved protein was run over 1.5 mL Ni-NTA agarose resin and the flow through and washes with binding buffer were collected and pooled. Protein was diluted with buffer (25 mM HEPES pH 7.5, 2 mM TCEP) to adjust the NaCl concentration to 50 mM, then loaded onto a HiTrap Q HP 5 mL column (Cytiva). The column was washed with IEX buffer A and bound protein was eluted with a 0-100% IEX buffer B (25 mM HEPES pH 7.5, 1 M NaCl, 2 mM TCEP) gradient. Fractions containing protein were pooled and concentrated to ~1-2 mL then run on 16/600 Superdex 200 pg column in GF buffer (25 mM HEPES pH 7.5, 300 mM NaCl, 1 mM TCEP). Fractions containing the purified protein complex were pooled, concentrated and aliquoted then flash frozen in LN2 for storage at -80°C.

The coding sequence for full-length DCAF16 with a TEV-cleavable N-terminal His_6-tag was cloned into a pFastBacDual vector under the control of the polh promoter. Coding sequences for full-length DDB1 or DDB1ΔBPB (residues 396-705 replaced with a GNGNSG linker) and full-length DDA1 were cloned into a pFastBacDual vector under the control of polh and p10 promoters, respectively. Bacmid was generated using the Bac-to-Bac baculovirus expression system (Thermo Fisher Scientific). Baculovirus was generated as described above and viral supernatant (P0) was harvested after 5-7 days. For expression, *Trichoplusia ni* High Five cells were grown to densities between 1.5-2 x 10^6 cells/mL in Express Five™ SFM (Gibco) supplemented with 18 mM L-glutamine and infected with a total virus volume of 1% per 1 x 10^6 cells/mL, consisting of equal volumes of DCAF16 and DDB1+DDA1 baculoviruses. Cells were incubated at 27°C in 2 L erlenmeyer flasks (~600-650 mL culture/flask) with shaking at 110 rpm for 72 hours. Cells were spun at 1,000 x g for 20 mins and supernatant was discarded. Pellets were resuspended in 25 mL binding buffer (50 mM HEPES pH 7.5, 300 mM NaCl, 1 mM TCEP), flash frozen in LN2 and stored at -80°C. Pellets were thawed and diluted with binding buffer to ~100 mL/L original culture volume. Tween-20 (to 1% (v/v)), magnesium chloride (to 2 mM), benzonase (to 1 µg/mL) and cOmplete EDTA-free Protease Inhibitor Cocktail (Roche, 2 tablets/L initial culture volume) were added to the cell suspension and stirred at RT for 30 mins. Cell suspensions were sonicated and lysates were centrifuged at 23,000 rpm for 60 mins. Supernatants were filtered through 0.45 µm filters then incubated with 2 mL cobalt agarose resin on a roller at 4°C for 1 hour. The lysate-resin slurry was loaded into a glass bench top column. Supernatant was allowed to flow through then the resin was washed with wash buffer (50 mM HEPES pH 7.5, 300 mM NaCl, 1 mM TCEP, 0.05% (v/v) Tween-20). Bound protein was eluted with elution buffer (50 mM HEPES pH 7.5, 300 mM NaCl, 1 mM TCEP, 0.05% (v/v) Tween-20, 400 mM imidazole) and run on a 26/10 HiPrep Desalting column (Cytiva) in binding buffer to remove imidazole. TEV protease was added to protein and incubated for 2 hours at RT then 4°C overnight. Cleaved protein was run over 0.25 mL cobalt agarose resin

and the flow through and washes with binding buffer were collected and pooled. Protein was exchanged into ion exchange (IEX) buffer A (50 mM HEPES pH 7.5, 50 mM NaCl, 1 mM TCEP) on a 26/10 HiPrep Desalting column then loaded onto a HiTrap Q HP 5 mL column (Cytiva). The column was washed with IEX buffer A and bound protein was eluted with a 0-100% IEX buffer B (50 mM HEPES pH 7.5, 1 M NaCl, 1 mM TCEP) gradient. Fractions containing protein were pooled and concentrated to ~1-2 mL then run on 16/600 Superdex 200 pg column in GF buffer (20 mM HEPES pH 7.5, 150 mM NaCl, 1 mM TCEP). Fractions containing the purified protein complex were pooled, concentrated and aliquoted then flash frozen in LN2 for storage at -80°C.

Sulfo-Cy5 NHS ester labelling

Sulfo-Cy5 NHS ester (Lumiprobe) was prepared to a final concentration of 800 µM in DMF before combining with DCAF16-DDB1ΔBPB-DDA1 (100 µM) and sodium bicarbonate (100 mM). The solution was protected from light and shaken for 1 hour at RT. The solution was spun down at 15,000 x g for 5 mins then run on a Superdex 200 10/300 gl column (Cytiva) to remove free dye and aggregated protein. Fractions containing the sulfo-Cy5-labelled DCAF16-DDB1ΔBPB-DDA1 were pooled and concentrated, the degree of labelling (DOL) was calculated to be 109%. Labelled protein was aliquoted then flash frozen in LN2 and stored at -80°C.

Fluorescence polarisation (FP) assay

Stock solutions of reaction components including DCAF15Δpro-DDB1ΔBPB-DDA1, DCAF16-DDB1ΔBPB-DDA1, 6xHis BRD4^{BD1}, 6xHis BRD4^{BD2}, BRD4^{Tandem} (residues 43-459), and FITC-sulfonamide probe[7] were prepared in FP assay buffer (25 mM HEPES pH 7.5, 300 mM NaCl, 1.0 mM TCEP). DCAF15Δpro-DDB1ΔBPB-DDA1, DCAF16-DDB1ΔBPB-DDA1, BRD4^{BD1}, BRD4^{BD2}, and BRD4^{Tandem} were titrated 1/3 in FP assay buffer. Components were added to Corning™ 384-Well Solid Black Polystyrene Microplates to a final volume of 15 uL. Final concentration of 20 nM for FITC-sulfonamide probe was used while DCAF15Δpro-DDB1ΔBPB-DDA1, DCAF16-DDB1ΔBPB-DDA1, BRD4^{BD1}, 6xHisBRD4^{BD2}, and BRD4^{Tandem} were titrated from 4 uM to 5.5 nM. Background subtraction was performed with 20 nM FITC-sulfonamide probe but not protein constructs. Components were mixed by spinning down plates at 50 x g for 1 min and the plate was covered and incubated at RT for 1 hour, and then the plate was read on a PHERAstar FS (BMG LABTECH) with fluorescence excitation and emission wavelengths (λ) of 485 and 520 nm, respectively, with a settling time of 0.3 s.

AlphaLISA displacement assay

The alphaLISA assays were performed as described previously[54] using 6xHis $BRD4^{BD1}$, 6xHis$BRD4^{BD2}$ or 10xHis $BRD4^{Tandem}$ and the biotinylated JQ1 probe. Assay conditions in the present work used were as follows: 100 nM bromodomain protein, 10 nM Bio-JQ1 probe, 25 ug/ml acceptor (nickel chelate) and donor (anti-his europium) (both from Perkin Elmer). All components were diluted to working concentrations in alphaLISA buffer (50 mM HEPES, 100 mM NaCl, 0.1% BSA, 0.02% CHAPS, pH 7.5). Bromodomain protein was co-incubated with test compounds using 384-well in AlphaPlates (PerkinElmer) in the absence or presence of DCAF16 (1 μM) for 1 hour, before adding the acceptor and donor beads simultaneously in a low light environment and incubating the pate at RT for a further hour. The plate was then read on a BMG Pherastar® equipped with an alphaLISA module. Data were normalised to a DMSO control and expressed as % bound vs log[concentration] of compound and analysed by non-linear regression, with extraction of binding affinity values (IC_{50}) from the curves. Where applicable, K_D values were calculated from a titration of bromodomain protein on the same assay plate alone into the probe, as described previously[64].

TR-FRET proximity assay

Stock solutions of reaction components including sulfo-Cy5-labelled DCAF16-DDB1ΔBPB-DDA1, His_6-$BRD4^{BD1}$, His_{10}-$BRD4^{BD2}$, His_{10}-$BRD4^{Tandem}$, compound **1** and LANCE Eu-W1024 Anti-6xHis donor (PerkinElmer) were prepared in TR-FRET assay buffer (20 mM HEPES pH 7, 100 mM NaCl, 1 mM TCEP, 0.05% Tween-20). Sulfo-Cy5-labelled DCAF16-DDB1ΔBPB-DDA1 was titrated ¼ in TR-FRET assay buffer. Components were added to PerkinElmer OptiPlate-384 (white) to a final well volume of 15 μL. Final concentrations of 200 nM for BRD4 constructs and 1 μM for compound **1** were used, while Sulfo-Cy5-labelled DCAF16-DDB1ΔBPB-DDA1 was titrated from 5 μM to 19.5 nM. LANCE Eu-W1024 Anti-6xHis donor and DMSO concentrations were kept constant across the plate at 2 nM and 0.5%, respectively. Background subtraction was performed with using concentration matched samples containing sulfo-Cy5-labelled DCAF16-DDB1ΔBPB-DDA1 but not BRD4. Assays were run with technical duplicates with two experimental repeats. Components were mixed by spinning down plates at 50 x g for 1 min and plates were covered and incubated at RT for 2 hours. Plates were read on a PHERAstar FS (BMG LABTECH) with fluorescence excitation and dual emission wavelengths (λ) of 337 and 620/665 nm, respectively with an integration time between 70 – 400 μs. Data were processed in GraphPad Prism, curve fitting for compound **1** curve was performed by setting the maximum as DMSO-only 5 μM sulfo-Cy5-labelled DCAF16-DDB1ΔBPB-DDA1 datapoint.

Analytical size exclusion chromatography

DCAF16:DDB1ΔBPB:DDA1, $BRD4^{Tandem}$ (residues 1-463), $BRD4^{BD1}$ (His_6 tag removed), $BRD4^{BD2}$ (His_6 tag removed), and compound **1** were incubated alone and in various combinations in 20 mM HEPES pH 7, 150 mM NaCl, 1 mM TCEP, 2% DMSO. Final concentrations used for Fig. 4a and Extended Fig. 4a were 10 μM DCAF16:DDB1ΔBPB:DDA1, 5 μM $BRD4^{Tandem}$, 25 μM compound **1** in 250 μL reaction

volumes. Final concentrations used for Fig. 4b were 5 μM DCAF16:DDB1ΔBPB:DDA1, 5 μM $BRD4^{Tandem}$, 5 μM $BRD4^{BD1}$, 5 μM $BRD4^{BD2}$, 12.5 μM compound **1** in 200 μL reaction volumes. Mixtures were incubated on ice for 50 minutes then run on a Superdex 200 10/300 gl column in 20 mM HEPES pH 7, 150 mM NaCl, 1 mM TCEP.

Cryo-EM sample and grid preparation

Protein complexes for cryo-EM were prepared by first co-incubating $BRD4^{Tandem}$ (res 43-459) with compound **1** in 20 mM HEPES pH 7.5, 50 mM NaCl, 0.5 mM TCEP-HCl, 2% (v/v) DMSO for 10 mins at RT. DCAF16:DDB1ΔBPB:DDA1 complex was added to the mixture to give final concentrations of 14 μM $BRD4^{Tandem}$, 14 μM DCAF16:DDB1ΔBPB:DDA1 and 35 μM compound **1** in a final reaction volume of 200 μL and incubated on ice for 50 mins. The sample was loaded onto a 10/300 Superdex 200 gl column in 20 mM HEPES pH 7.5, 50 mM NaCl, 0.5 mM TCEP-HCl. Due to incomplete complex formation and to avoid monomeric proteins, only the earliest eluting fraction containing the ternary complex was taken and concentrated to 4.8 μM. The complex was vitrified in liquid ethane using Vitrobot Mark IV (Thermo Fisher Scientific). Quantifoil R1.2/1.3 Holey Carbon 400 mesh gold grids (Electron Microscopy Sciences) were glow discharged for 60 s with a current of 35 mA under vacuum using a Quorum SC7620. The complex (3.5 μL) was dispensed onto the grid, allowed to disperse for 10 s, blotted for 3.5 s using blot force 3, then plunged into liquid ethane using a Vitrobot Mark IV (Thermo Fisher Scientific) with the chamber at 4°C and 100% humidity.

Cryo-EM data acquisition

Cryo-EM data were collected on a Glacios transmission electron microscope (Thermo-Fisher) operating at 200 keV. Micrographs were acquired using a Falcon4i direct electron detector, operated in electron counting mode. Movies were collected at 190,000 x magnification with the calibrated pixel size of 0.74 Å/pixel on the camera. Images were taken over a defocus range of –3.2 μm to -1.7 μm with a total accumulated dose of 12.7e−/$Å^2$ using single particle EPU (Thermo Fisher Scientific, version 3.0) automated data software. A total of 2,075 movies were collected in EER format and after cleaning up for large motion and poor CTF a total of 1,896 movies were used for further processing. A summary of imaging conditions and image processing is presented in Extended Data Table 2.

Cryo-EM image processing

Movies were imported into cryosparc v4.1.2[65] and the EER movie data was fractionated into 8 fractions to give a dose of 1.59 e−/$Å^2$ per fraction. Movies were processed using patch motion correction and CTF correction then manually curated to remove suboptimal micrographs. Manual picking of 153 particles was performed on 20 micrographs, which were used for blob tuner with minimum and maximum diameters of 70 and 130 Å, respectively. 12,579 particles were picked by blob tuner, extracted with a box size of 324 pix (240 Å) and run through initial 2D classification. Good classes with diverse views were selected and used as templates for template picking on all movies. Picks were inspected and curated, and 1.35 million particles were extracted with box size 324 pix and used for 2D classification. Particles from the well-resolved, diverse classes were used for ab-initio reconstruction with 3 classes.

One class contained primarily empty DDB1ΔBPB and a second class contained biased views upon testing of the particle set with 2D re-classification, leading to smeared maps. The third class unambiguously contained density corresponding to DDB1ΔBPB, two bromodomains, and density likely corresponding to DCAF16 between them. Particles belonging to the third class were run sequentially through heterogenous refinement yielding a map into which DDB1ΔBPB and 2 bromodomains could be placed with confidence. To improve the resolution, movies were re-imported in cryosparc and fractionated into 18 fractions to give a lower dose of ~0.7 e/Å^2 per fraction. Fifty templates for particle picking were generated using the create templates job with the input map from the previous heterogeneous refinement. The templates were used in the template picker to pick particles from the curated movies. Picks were curated with thresholds of NCC score > 0.4, local power >342 and <809, resulting in ~1.47 million particles that were extracted with a box size of 324 pix and used for ab-initio reconstruction with 3 classes. This produced similar results to the first ab-initio job and all classes were subjected to a heterogeneous refinement. The map and particles (530,879) from the best class were used for homogenous refinement with a static mask created in ChimeraX[66]. This produced a map with a gold-standard Fourier shell correlation (GSFSC) resolution of 3.98 Å at cutoff 0.143. The workflow, angular distribution plot and GSFSC curve are presented in Extended Data Fig. 6.

Cryo-EM model building

The unsharpened half-maps from cryosparc were auto-sharpened in Phenix[67] and used for density modification in Resolve Cryo-EM[68] with a modest resolution improvement measured by FSCref over the sharpened full map from cryosparc. Visual inspection revealed improved map quality in comparison to the cryosparc sharpened map. DDB1ΔBPB, BRD4^{BD1} and BRD4^{BD2} extracted from PDB entries 5FQD[41], 3MXF[69] and 6DUV, respectively, were manually placed into the map in coot[70] by rigid body fitting. Correct placement of each bromodomain was aided by manual inspection of residues Asn93 and Gly386 in equivalent positions in the ZA loops of BD1 and BD2, respectively. In one bromodomain, this position was facing solvent while in the other it was at a protein-protein interface with density corresponding to DCAF16. Given that mutation of Gly386 to Glu prevents degradation of BRD4 by compound **1** (Fig. 3i), BD2 was placed in the position where Gly386 was adjacent to the DCAF16 density. Both bromodomains were joined onto a single chain designation. Initial restraints for compound **1** were generated using a SMILES string with eLBOW[71], then run through the GRADE webserver (Grade2 v1.3.0). Compound **1** was fit into density by overlaying the JQ1 moiety with its known binding mode in either the BRD4^{BD1} or BRD4^{BD2}. Positioning the ligand in BD2 was compatible with electron density, whereas positioning in BD1 caused a clash with DCAF16 due to the rigid linker. The structure was refined with rounds of model building in coot and refinement with Phenix real-space refinement[72]. Figures were generated in ChimeraX and The PyMOL Molecular Graphics System, Version 2.5.2, Schrödinger, LLC.

References

1 Bekes, M., Langley, D. R. & Crews, C. M. PROTAC targeted protein degraders: the past is prologue. *Nat Rev Drug Discov* **21**, 181-200, doi:10.1038/s41573-021-00371-6 (2022).

2 Hanan, E. J. *et al.* Monomeric Targeted Protein Degraders. *J Med Chem* **63**, 11330-11361, doi:10.1021/acs.jmedchem.0c00093 (2020).

3 Hanzl, A. & Winter, G. E. Targeted protein degradation: current and future challenges. *Curr Opin Chem Biol* **56**, 35-41, doi:10.1016/j.cbpa.2019.11.012 (2020).

4 Cowan, A. D. & Ciulli, A. Driving E3 Ligase Substrate Specificity for Targeted Protein Degradation: Lessons from Nature and the Laboratory. *Annu Rev Biochem* **91**, 295-319, doi:10.1146/annurev-biochem-032620-104421 (2022).

5 Han, T. *et al.* Anticancer sulfonamides target splicing by inducing RBM39 degradation via recruitment to DCAF15. *Science* **356**, doi:10.1126/science.aal3755 (2017).

6 Uehara, T. *et al.* Selective degradation of splicing factor CAPERalpha by anticancer sulfonamides. *Nat Chem Biol* **13**, 675-680, doi:10.1038/nchembio.2363 (2017).

7 Bussiere, D. E. *et al.* Structural basis of indisulam-mediated RBM39 recruitment to DCAF15 E3 ligase complex. *Nat Chem Biol* **16**, 15-23, doi:10.1038/s41589-019-0411-6 (2020).

8 Du, X. *et al.* Structural Basis and Kinetic Pathway of RBM39 Recruitment to DCAF15 by a Sulfonamide Molecular Glue E7820. *Structure* **27**, 1625-1633 e1623, doi:10.1016/j.str.2019.10.005 (2019).

9 Faust, T. B. *et al.* Structural complementarity facilitates E7820-mediated degradation of RBM39 by DCAF15. *Nat Chem Biol* **16**, 7-14, doi:10.1038/s41589-019-0378-3 (2020).

10 Zoppi, V. *et al.* Iterative Design and Optimization of Initially Inactive Proteolysis Targeting Chimeras (PROTACs) Identify VZ185 as a Potent, Fast, and Selective von Hippel-Lindau (VHL) Based Dual Degrader Probe of BRD9 and BRD7. *J Med Chem* **62**, 699-726, doi:10.1021/acs.jmedchem.8b01413 (2019).

11 Coomar, S. & Gillingham, D. G. Exploring DCAF15 for reprogrammable targeted protein degradation. *bioRxiv*, 542506, doi:10.1101/542506 (2019).

12 Li, L. *et al.* In vivo target protein degradation induced by PROTACs based on E3 ligase DCAF15. *Signal Transduct Target Ther* **5**, 129, doi:10.1038/s41392-020-00245-0 (2020).

13 Zhou, X. L. *et al.* A comprehensive review of BET-targeting PROTACs for cancer therapy. *Bioorg Med Chem* **73**, 117033, doi:10.1016/j.bmc.2022.117033 (2022).

14 Ohba, K. *et al.* Sulfonamide or Sulfinamide Compound Having Effect of Inducing BRD4 Protein Degradation and Pharmaceutical Use Thereof. WO2021157684 (2021).

15 Blake, R. A. *et al.* Preparation of tert-Butyl(S)-2-(4-(Phenyl)-6H-thieno[3,2-f][1,2,4]triazolo[4,3-a][1,4]-diazepin-6-yl)acetate Derivatives and Related Compounds as Bromodomain BRD4 Inhibitors for the Treatment of Cancer. WO2020055976 (2020).

16 Dragovich, P., Thomas, P., Blake, R. A. & Wertz, I. Chemical Inducers of Degradation and Methods of Use. WO2020086858 (2020).

17 Winter, G. E. *et al.* BET Bromodomain Proteins Function as Master Transcription Elongation Factors Independent of CDK9 Recruitment. *Mol Cell* **67**, 5-18 e19, doi:10.1016/j.molcel.2017.06.004 (2017).
18 de Almeida, M. *et al.* AKIRIN2 controls the nuclear import of proteasomes in vertebrates. *Nature* **599**, 491-496, doi:10.1038/s41586-021-04035-8 (2021).
19 Mayor-Ruiz, C. *et al.* Rational discovery of molecular glue degraders via scalable chemical profiling. *Nat Chem Biol* **16**, 1199-1207, doi:10.1038/s41589-020-0594-x (2020).
20 Zengerle, M., Chan, K. H. & Ciulli, A. Selective Small Molecule Induced Degradation of the BET Bromodomain Protein BRD4. *ACS Chem Biol* **10**, 1770-1777, doi:10.1021/acschembio.5b00216 (2015).
21 Dai, X. *et al.* Prostate cancer-associated SPOP mutations confer resistance to BET inhibitors through stabilization of BRD4. *Nat Med* **23**, 1063-1071, doi:10.1038/nm.4378 (2017).
22 Zhang, P. *et al.* Intrinsic BET inhibitor resistance in SPOP-mutated prostate cancer is mediated by BET protein stabilization and AKT-mTORC1 activation. *Nat Med* **23**, 1055-1062, doi:10.1038/nm.4379 (2017).
23 Gadd, M. S. *et al.* Structural basis of PROTAC cooperative recognition for selective protein degradation. *Nat Chem Biol* **13**, 514-521, doi:10.1038/nchembio.2329 (2017).
24 Roy, M. J. *et al.* SPR-Measured Dissociation Kinetics of PROTAC Ternary Complexes Influence Target Degradation Rate. *ACS Chem Biol* **14**, 361-368, doi:10.1021/acschembio.9b00092 (2019).
25 Lu, G. *et al.* UBE2G1 governs the destruction of cereblon neomorphic substrates. *Elife* **7**, doi:10.7554/eLife.40958 (2018).
26 Mayor-Ruiz, C. *et al.* Plasticity of the Cullin-RING Ligase Repertoire Shapes Sensitivity to Ligand-Induced Protein Degradation. *Mol Cell* **75**, 849-858 e848, doi:10.1016/j.molcel.2019.07.013 (2019).
27 Li, W. *et al.* MAGeCK enables robust identification of essential genes from genome-scale CRISPR/Cas9 knockout screens. *Genome Biol* **15**, 554, doi:10.1186/s13059-014-0554-4 (2014).
28 Bond, A. G. *et al.* Development of BromoTag: A "Bump-and-Hole"-PROTAC System to Induce Potent, Rapid, and Selective Degradation of Tagged Target Proteins. *J Med Chem* **64**, 15477-15502, doi:10.1021/acs.jmedchem.1c01532 (2021).
29 Le-Trilling, V. T. K. *et al.* Structural mechanism of CRL4-instructed STAT2 degradation via a novel cytomegaloviral DCAF receptor. *EMBO J*, e112351, doi:10.15252/embj.2022112351 (2023).
30 Pla-Prats, C., Cavadini, S., Kempf, G. & Thoma, N. H. Recognition of the CCT5 di-Glu degron by CRL4(DCAF12) is dependent on TRiC assembly. *EMBO J*, e112253, doi:10.15252/embj.2022112253 (2023).
31 Wu, Y. *et al.* The DDB1-DCAF1-Vpr-UNG2 crystal structure reveals how HIV-1 Vpr steers human UNG2 toward destruction. *Nat Struct Mol Biol* **23**, 933-940, doi:10.1038/nsmb.3284 (2016).
32 Fish, P. V. *et al.* Identification of a chemical probe for bromo and extra C-terminal bromodomain inhibition through optimization of a fragment-derived hit. *J Med Chem* **55**, 9831-9837, doi:10.1021/jm3010515 (2012).
33 Zhang, M. *et al.* Structure-Based Discovery and Optimization of Benzo[d]isoxazole Derivatives as Potent and Selective BET Inhibitors for Potential Treatment of

Castration-Resistant Prostate Cancer (CRPC). *J Med Chem* **61**, 3037-3058, doi:10.1021/acs.jmedchem.8b00103 (2018).

34 Zaware, N. & Zhou, M. M. Bromodomain biology and drug discovery. *Nat Struct Mol Biol* **26**, 870-879, doi:10.1038/s41594-019-0309-8 (2019).

35 Waring, M. J. *et al.* Potent and selective bivalent inhibitors of BET bromodomains. *Nat Chem Biol* **12**, 1097-1104, doi:10.1038/nchembio.2210 (2016).

36 Tanaka, M. *et al.* Design and characterization of bivalent BET inhibitors. *Nat Chem Biol* **12**, 1089-1096, doi:10.1038/nchembio.2209 (2016).

37 Tan, X. *et al.* Mechanism of auxin perception by the TIR1 ubiquitin ligase. *Nature* **446**, 640-645, doi:10.1038/nature05731 (2007).

38 Ito, T. *et al.* Identification of a primary target of thalidomide teratogenicity. *Science* **327**, 1345-1350, doi:10.1126/science.1177319 (2010).

39 Kronke, J. *et al.* Lenalidomide induces ubiquitination and degradation of CK1a in del(5q) MDS. *Nature* **523**, 183-U102, doi:10.1038/nature14610 (2015).

40 Kronke, J. *et al.* Lenalidomide causes selective degradation of IKZF1 and IKZF3 in multiple myeloma cells. *Science* **343**, 301-305, doi:10.1126/science.1244851 (2014).

41 Petzold, G., Fischer, E. S. & Thoma, N. H. Structural basis of lenalidomide-induced CK1alpha degradation by the CRL4(CRBN) ubiquitin ligase. *Nature* **532**, 127-130, doi:10.1038/nature16979 (2016).

42 Sievers, Q. L. *et al.* Defining the human C2H2 zinc finger degrome targeted by thalidomide analogs through CRBN. *Science* **362**, doi:10.1126/science.aat0572 (2018).

43 Slabicki, M. *et al.* The CDK inhibitor CR8 acts as a molecular glue degrader that depletes cyclin K. *Nature* **585**, 293-297, doi:10.1038/s41586-020-2374-x (2020).

44 Slabicki, M. *et al.* Small-molecule-induced polymerization triggers degradation of BCL6. *Nature* **588**, 164-168, doi:10.1038/s41586-020-2925-1 (2020).

45 Vogel, C., Bashton, M., Kerrison, N. D., Chothia, C. & Teichmann, S. A. Structure, function and evolution of multidomain proteins. *Curr Opin Struct Biol* **14**, 208-216, doi:10.1016/j.sbi.2004.03.011 (2004).

46 Zhou, X., Hu, J., Zhang, C., Zhang, G. & Zhang, Y. Assembling multidomain protein structures through analogous global structural alignments. *Proc Natl Acad Sci U S A* **116**, 15930-15938, doi:10.1073/pnas.1905068116 (2019).

47 Zhang, X., Crowley, V. M., Wucherpfennig, T. G., Dix, M. M. & Cravatt, B. F. Electrophilic PROTACs that degrade nuclear proteins by engaging DCAF16. *Nat Chem Biol* **15**, 737-746, doi:10.1038/s41589-019-0279-5 (2019).

48 Shergalis, A. G. *et al.* CRISPR Screen Reveals BRD2/4 Molecular Glue-like Degrader via Recruitment of DCAF16. *ACS Chem Biol*, doi:10.1021/acschembio.2c00747 (2023).

49 Cao, S. *et al.* Defining molecular glues with a dual-nanobody cannabidiol sensor. *Nat Commun* **13**, 815, doi:10.1038/s41467-022-28507-1 (2022).

50 Ishida, T. & Ciulli, A. E3 Ligase Ligands for PROTACs: How They Were Found and How to Discover New Ones. *SLAS Discov* **26**, 484-502, doi:10.1177/2472555220965528 (2021).

51 Garcia-Seisdedos, H., Empereur-Mot, C., Elad, N. & Levy, E. D. Proteins evolve on the edge of supramolecular self-assembly. *Nature* **548**, 244-247, doi:10.1038/nature23320 (2017).

52 Zhang, X., Thielert, M., Li, H. & Cravatt, B. F. SPIN4 Is a Principal Endogenous Substrate of the E3 Ubiquitin Ligase DCAF16. *Biochemistry* **60**, 637-642, doi:10.1021/acs.biochem.1c00067 (2021).
53 Gong, F. *et al.* Screen identifies bromodomain protein ZMYND8 in chromatin recognition of transcription-associated DNA damage that promotes homologous recombination. *Genes Dev* **29**, 197-211, doi:10.1101/gad.252189.114 (2015).
54 Imaide, S. *et al.* Trivalent PROTACs enhance protein degradation via combined avidity and cooperativity. *Nat Chem Biol* **17**, 1157-1167, doi:10.1038/s41589-021-00878-4 (2021).
55 Wegner, M. *et al.* Circular synthesized CRISPR/Cas gRNAs for functional interrogations in the coding and noncoding genome. *Elife* **8**, doi:10.7554/eLife.42549 (2019).
56 Diehl, V. *et al.* Minimized combinatorial CRISPR screens identify genetic interactions in autophagy. *Nucleic Acids Res* **49**, 5684-5704, doi:10.1093/nar/gkab309 (2021).
57 Doench, J. G. *et al.* Optimized sgRNA design to maximize activity and minimize off-target effects of CRISPR-Cas9. *Nat Biotechnol* **34**, 184-191, doi:10.1038/nbt.3437 (2016).
58 Sanson, K. R. *et al.* Optimized libraries for CRISPR-Cas9 genetic screens with multiple modalities. *Nat Commun* **9**, 5416, doi:10.1038/s41467-018-07901-8 (2018).
59 Chen, B. *et al.* Dynamic imaging of genomic loci in living human cells by an optimized CRISPR/Cas system. *Cell* **155**, 1479-1491, doi:10.1016/j.cell.2013.12.001 (2013).
60 Wisniewski, J. R., Zougman, A., Nagaraj, N. & Mann, M. Universal sample preparation method for proteome analysis. *Nat Methods* **6**, 359-362, doi:10.1038/nmeth.1322 (2009).
61 Wang, Y. *et al.* Reversed-phase chromatography with multiple fraction concatenation strategy for proteome profiling of human MCF10A cells. *Proteomics* **11**, 2019-2026, doi:10.1002/pmic.201000722 (2011).
62 Roest, S. *et al.* Transfection of insect cell in suspension for efficient baculovirus generation. *MethodsX* **3**, 371-377, doi:10.1016/j.mex.2016.04.011 (2016).
63 Scholz, J. & Suppmann, S. A new single-step protocol for rapid baculovirus-driven protein production in insect cells. *BMC Biotechnol* **17**, 83, doi:10.1186/s12896-017-0400-3 (2017).
64 Van Molle, I. *et al.* Dissecting fragment-based lead discovery at the von Hippel-Lindau protein:hypoxia inducible factor 1alpha protein-protein interface. *Chem Biol* **19**, 1300-1312, doi:10.1016/j.chembiol.2012.08.015 (2012).
65 Punjani, A., Rubinstein, J. L., Fleet, D. J. & Brubaker, M. A. cryoSPARC: algorithms for rapid unsupervised cryo-EM structure determination. *Nat Methods* **14**, 290-296, doi:10.1038/nmeth.4169 (2017).
66 Pettersen, E. F. *et al.* UCSF ChimeraX: Structure visualization for researchers, educators, and developers. *Protein Sci* **30**, 70-82, doi:10.1002/pro.3943 (2021).
67 Liebschner, D. *et al.* Macromolecular structure determination using X-rays, neutrons and electrons: recent developments in Phenix. *Acta Crystallogr D Struct Biol* **75**, 861-877, doi:10.1107/S2059798319011471 (2019).
68 Terwilliger, T. C., Ludtke, S. J., Read, R. J., Adams, P. D. & Afonine, P. V. Improvement of cryo-EM maps by density modification. *Nat Methods* **17**, 923-927, doi:10.1038/s41592-020-0914-9 (2020).
69 Filippakopoulos, P. *et al.* Selective inhibition of BET bromodomains. *Nature* **468**, 1067-1073, doi:10.1038/nature09504 (2010).

70 Emsley, P. & Cowtan, K. Coot: model-building tools for molecular graphics. *Acta Crystallogr D Biol Crystallogr* **60**, 2126-2132, doi:10.1107/S0907444904019158 (2004).

71 Moriarty, N. W., Grosse-Kunstleve, R. W. & Adams, P. D. electronic Ligand Builder and Optimization Workbench (eLBOW): a tool for ligand coordinate and restraint generation. *Acta Crystallogr D Biol Crystallogr* **65**, 1074-1080, doi:10.1107/S0907444909029436 (2009).

72 Afonine, P. V. *et al.* Real-space refinement in PHENIX for cryo-EM and crystallography. *Acta Crystallogr D Struct Biol* **74**, 531-544, doi:10.1107/S2059798318006551 (2018).